2015

Algorithm Development of a Multi-Section Crop Detection System for a Corn Head

Keith Joseph Lensing
Iowa State University

Algorithm development of a multi-section crop detection system for a corn head

by

Keith Joseph Lensing

A thesis submitted to the graduate faculty
in partial fulfillment of the requirements for the degree of
MASTER OF SCIENCE

Major: Agricultural Engineering

Program of Study Committee:
Matthew Darr, Major Professor
Brian Steward
Steven Hoff

Iowa State University
Ames, Iowa
2015

TABLE OF CONTENTS

LIST OF FIGURES

LIST OF TABLES

LIST OF EQUATIONS

ACKNOWLEDGEMENTS

I would like to thank Deere and Company for providing the funding for this research. I would like to thank my major professor, Dr. Matthew Darr, for providing me with this opportunity, as well as the guidance to complete my degree. I would also like to thank Dr. Steven Hoff and Dr. Brian Steward for their guidance through my academic journey and their willingness to serve on my program of study committee.

I am sincerely thankful to all of my colleagues who assisted me in the development of this project through technical support and setup of tests. I am specifically grateful to Brad Kruse, Robert McNaull, Levi Powell and Junsu Shin for their many hours of assistance. Without all of your help this project would not have been possible.

Finally, I would like to thank my family and friends for be so supportive of my goals and understanding of the time put forth. Without the love and encouragement received the work that I have completed would have no meaning. I am forever grateful of all the things that you have done and continue to do.

Most of all, I would like to thank God for the opportunity to challenge and better prepare myself for this journey in life.

ABSTRACT

Over the next several decades the need for grain-based commodities will increase, due mostly to the demand for grain in developing countries and grain-based biofuels. To meet the increase in demand additional grain-based commodities will come from two likely sources: current land used for production and land yet to be developed. Increased spatial resolution of crop production is one way producers can grow more crops without more land development. If farmland productivity can be monitored on a smaller scale, producers can begin to implement better site-specific management decision at a higher resolution, such as variable-rate nitrogen application. The development of high resolution yield mapping techniques would provide producers the ability to evaluate if additional grain could be produced.

Currently, yield mapping technology provides an average yield value for a discrete harvested area. Average yield values are the summation of grain harvested by a number of row units across a corn-head. The harvested area is a function of the number of row units on a corn-head. The primary goal of this research was to develop an ear detection system that could predict the number of ears that entered individual row units. By generating ear count prediction for individual row units, harvested grain could be spatially allocated across multiple section of the corn-head to produce higher resolution yield maps.

Preliminary testing showed that the developed ear detection system could produce ear count predictions that were strongly correlated with the number of ears that entered individual row units of the corn-head. The ear detection system used accelerometers mounted to the two deck-plates of the row unit. Deck-plates would remove ears from stalks as a field of corn was harvested. Accelerometers were able to measure a shock impulse produced on deck-plate as an ear was removed from a stalk. Controlled field testing validated the functionality of the ear detection system and produced R^2 values as high as 0.877. Uncontrolled harvest data was used to successfully validate the ear detection system as a future enhancement to current yield monitoring technology.

CHAPTER 1: GENERAL INTRODUCTION

1.1 Project Description

Over the next several decades the need for grain-based commodities will increase, due mostly to the demand for grain in developing countries and grain-based biofuels. According to the 2008 Agricultural Outlook from the Food and Agricultural Organization of the United Nations, global meat consumption rates will expand by 55 to 310 metric tons/year (21.5% increase), while biofuels expand by 28 to 67 billion liters/year (71.8% increase) over the next decade (Edgerton, 2009). This additional demand will become a major factor in food and energy security around the world.

To meet the increase in demand additional grain-based commodities will come from two likely sources: the current land used for production and the land yet to be developed. Most information suggests that a combination of the two sources will be needed. Additionally, continual advancements in technology can lead the way and minimize the additional land that is required. Of the land in current production, the majority has adopted numerous technological advances over the past century to reach the current level of yields. It is unrealistic to assume that this rate of increase in yield can be maintained into the future. From a simple economic standpoint, there will be a limit to the maximum yield for a given economic situation. In the future, incremental increases in yield will come in a reduced size or at a higher cost. With increases in input costs, growers will find it necessary to have the ability to measure land productivity on a smaller scale. This ability to measure variations in yield throughout a field is called yield monitoring and will ensure that investment in technology is still economically feasible.

This research project focuses on the current technology behind corn-based yield monitoring and methods that can improve redistribution of current yield data to more localized areas of a corn-head. With the redistribution of yield data, higher resolution yield maps could be achieved. These maps would better depict the underlying variations in yield that current technology missed. The goal of the project was to develop core sensing technologies to evaluate economic feasibility of inputs on a more spatially localized scale.

CHAPTER 2: LITERATURE REVIEW

2.1 Combine Operation

Modern combines that harvest corn use an attached corn-head to operate several simultaneous functions. These functions allow for continuous harvest and flow of crop into a combine to be processed. Initially, individual rows are fed into assemblies called row-units. Here, ears of corn are detached from stalks and gathered on an individual row basis. The flow of ears is further gathered across the entire corn-head and is fed into the combine.

Figure 1: John Deere Combine with a 16 Row Corn-head
Image Source: (Deere & Company, 2015)

A row-unit is comprised of several key components: the corn-head frame, deck-plates (fixed and adjustable), gathering-chain assemblies, stalk rolls and snout-covers. The corn-head frame is the supporting structure for the mechanically driven ear collection systems. This main structure extends across the rows of corn that are being harvested. From the front of the main structure extends individual row-unit frames, these frames extend forward between each row of corn. Fixed and adjustable deck-plates are installed on top of each row-unit frame. Each deck-plate is attached to the row-unit frame by bolted chain-guide assemblies. As a fixed deck-plate is bolted to a row-unit frame it will be held stationary. As an adjustable deck-plate is bolted to a row-unit frame it can still be moved by a hydraulically driven lever arm. This feature is controlled from inside the combine cab and sets the harvest spacing between fixed and adjustable deck-plates. Chain guide assemblies are comprised of a gathering chain, mounting bracket, chain-guide and chain-tensioner. Gathering chains circulate on around two revolving sprockets,

of which the back sprocket is mechanically driven. Gathering chains are further supported by the mounting bracket, chain-guide and chain-tensioner. These components provide direction, support and tension to the gathering chain. Above these assemblies are snout covers which can be lower to cover row-units from debris as corn is harvested (Figure 2).

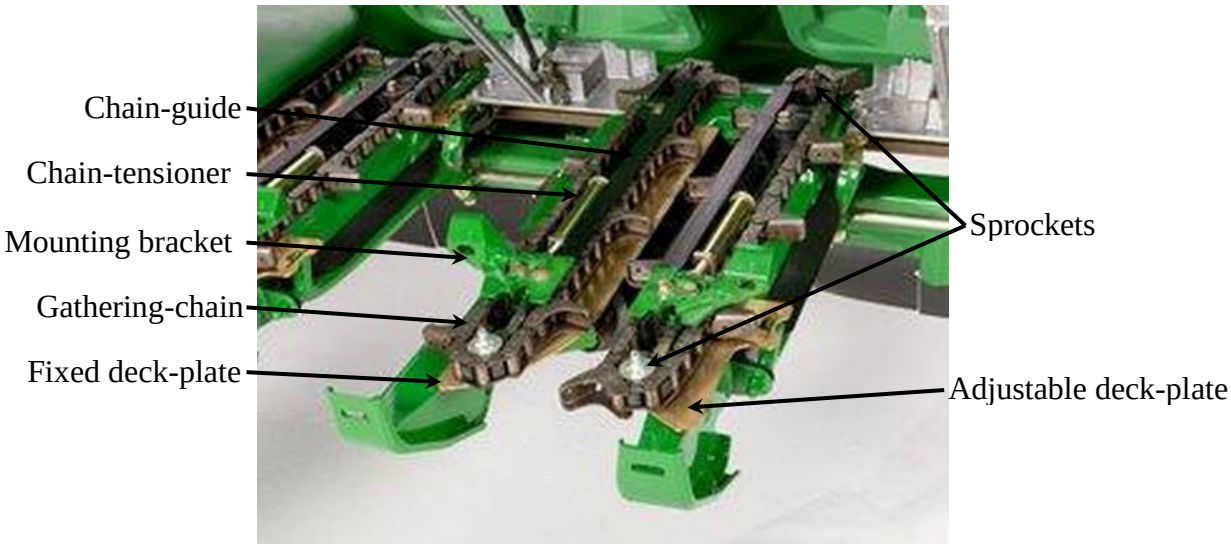

Figure 2: Corn-head Row Unit Assembly
Image Source: (Deere & Company, 2015)

When a corn stalk is fed into an individual row-unit it is first engaged by a pair of gathering-chains, a chain-link assembly that rides on top of each deck-plate and has additional protruding nodes that are used to direct stalks and gather ears. As each gathering-chain rotates in oppose directions they generate a force that guides each stalk between a pair of deck-plates towards the back of the corn-head. This process is in preparation to remove an ear from its stalk. Deck-plates are spaced just far enough apart for an individual stalk to pass between them.

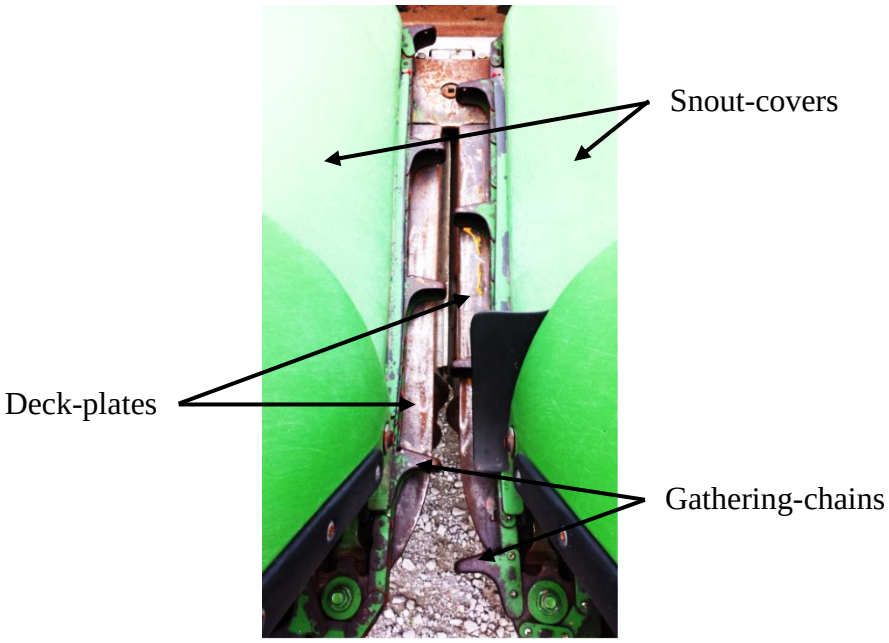

Figure 3: Row Unit of a Corn-head

As a stalk moves between the deck-plates it is engaged by a pair of stalk rolls, a cylindrical component with protruding knives, which accelerates the stalk downward relative to the corn-head. Each stalk roll is located directly below a corresponding deck-plate and rotates in oppose directions to generate a downward force on each stalk it engages.

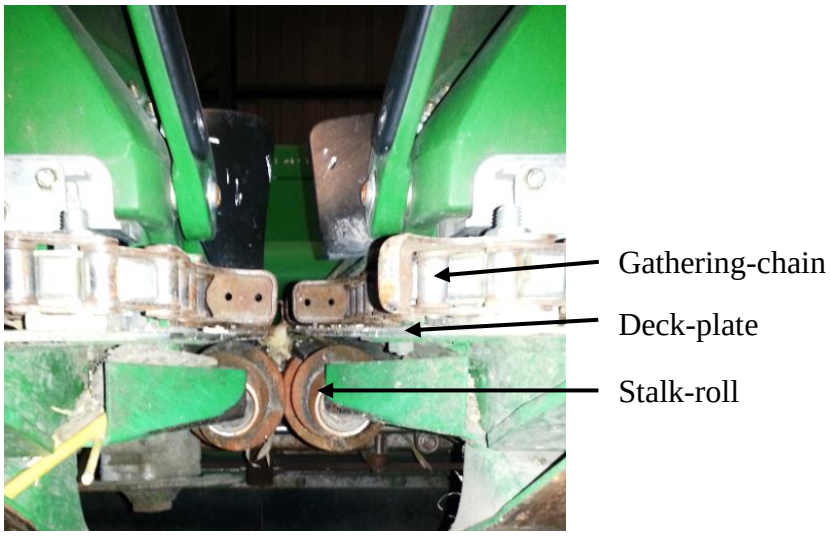

Figure 4: Front View of an Individual Row-Unit of a Corn-head

Any ear that is attached to a corn stalk will become dislodged as stalks are accelerated downward between a pair of deck-plates. Ideally, corn stalks are pulled through the deck-plates while ears are gathered and directed towards the back of the corn-head by the gathering-chains.

As ears from individual rows reach the back of the corn-head they are guided by a cross-auger to the feeder-house of the combine. At the feeder-house, ears and any additional stalks enter the combine to be separated into clean grain and crop material. Clean grain flows by yield monitoring components and arrives in a grain tank. Material other than grain is separated and discharged out the back of the combine.

2.2 Principles of a Yield Monitor

In the early 1990's, Allen Myers, a pioneer in the precision agriculture field, developed the first widely successful yield monitor (Myers, 1991). In grain harvesting, a yield monitor is a system that generates yield information for a harvested area. Instantaneous yield information is displayed in the combine cab while harvesting a single pass. Yield maps are the consolidation of large amounts of yield information about spatially referenced locations. Grain producers use both types of information to understand yield variation across a field and drive site-specific management decisions.

Key components of a yield monitor includes: a mass flow sensor, moisture sensor, DGPS (differential global positioning system) receiver and task computer/user interface (Figure 5). All components are synchronized to generate, collect and present yield information in a map style format.

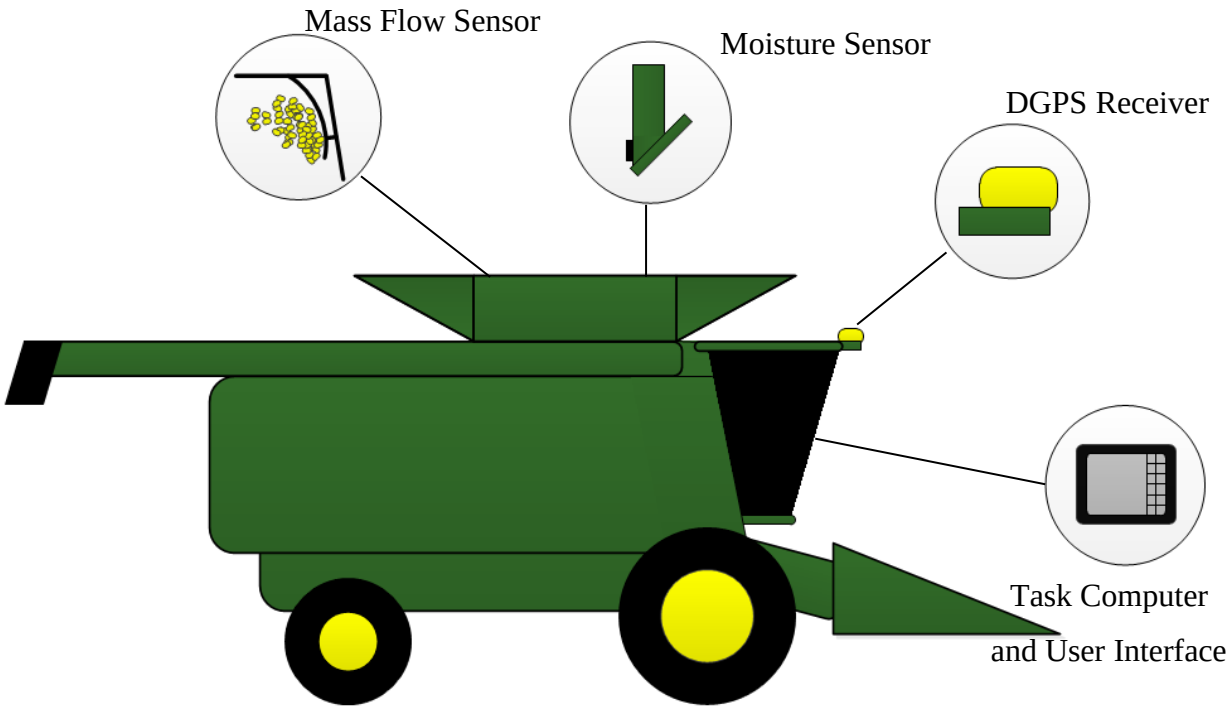

Figure 5: Graphical Abstract of a Yield Monitor System

2.2.1 Grain Mass Flow Sensors

Grain mass flow sensors measure instantaneous mass flow rate of grain through a combine without full interruption of the grain stream. There are several types of mass flow sensors, they include: impact sensors, optical sensors, radiation sensors and load cells. In this section impact plates, optical sensors and radiation sensors will be discussed. These sensors are the most common sensors among original equipment manufacturers.

2.2.1.1 Impact Plate

Impact plates are the most common mass flow sensors among original equipment manufacturers of combine harvesters. An impact plate is a vertically mounted scale at the top of clean grain elevator of a combine. This devices measures an impulse force of the grain stream as grain is thrown against it. An electrical output proportional to the force that the impact plate measures is later adjusted to account for changes in conveyor and grain speed. Clean grain is measured as it is thrown against an impact plate by mechanically driven conveyor (Figure 6).

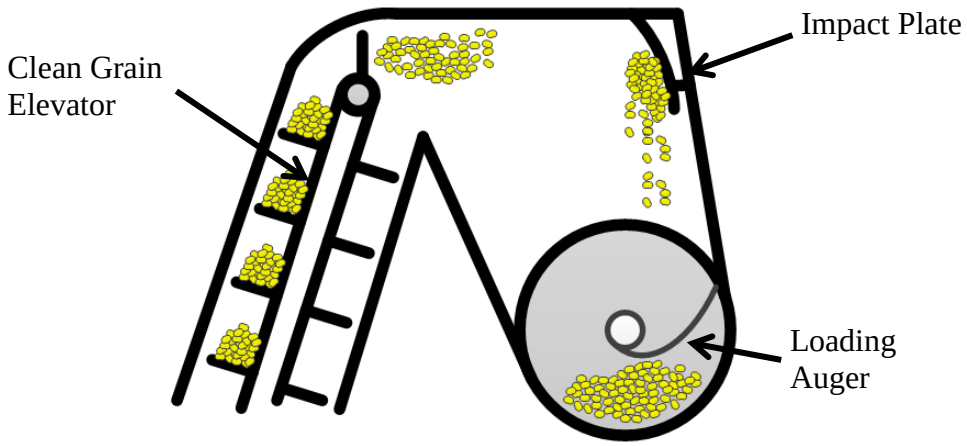

Figure 6: Impact Plate at the Top of a Clean Grain Elevator

Grain mass flow rate is calculated with a calibration characteristic which is different for different grain types and moisture content (Myers, 1991). This mass flow rate measurement can be used to find an average grain yield of an area. A rate at which an area is harvested can be calculated by multiplying vehicle speed and combine swath width. Integrating grain mass flow rate over an area rate of harvest produces an average yield per a unit of area.

2.2.1.2 Optical Sensor

A second method to measure grain mass flow rate is an optical sensor. These sensors use emitter/detector pairs that use a specific wavelength of light. These wavelengths are outside the visible spectrum of light that an eye can see to not disrupt the function of the sensor. For this application, an emitter emits a beam of light with a prescribed wavelength towards it paired detector. A detector detects the presence of the beam of light and outputs a voltage signal, high if a beam is present and low if it is not. For this application, sensor pairs are strategically placed on either side of the clean grain elevator. The volume of grain on each paddle can be calculated from elevator speed, area of a paddle and the duration of time the voltage signal spent in a low state (Figure 7).

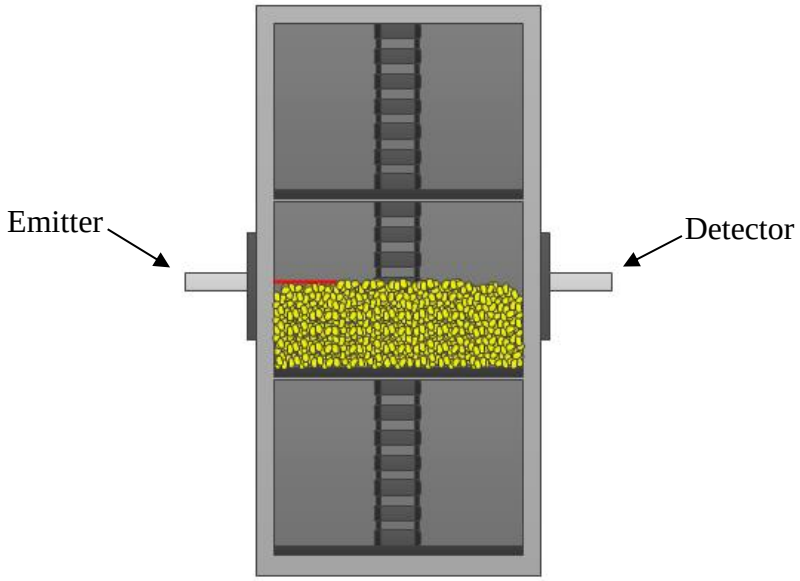

Figure 7: Optical Sensor inside a Clean Grain Elevator

2.2.1.3 Radiation Sensor

A third method to measure grain mass flow rate is a radiation sensor. This method is similar to an optical sensor in that it has a source and sensor. As grain flows between the radiation source and sensor, some radiation is absorbed by grain and is taken down stream. In lower grain flow rates, higher radiation intensity is measured by the sensor. Similarly, in higher flow rates a reduced amount of radiation intensity is measured. For these reasons radiation sensors have been successfully calibrated to calculate mass flow rate of grain.

2.2.2 Grain Moisture Sensor

Grain crops such as corn can significantly vary in moisture content throughout a field. An effective yield monitor system must be able to measure and correct grain volumes to a marketable weigh based on variation in grain moisture measurements. Grain moisture measurements use capacitive sensors and systems are very similar between combines. A capacitive sensor detects differences in voltage between two conductive surfaces. These conductive surfaces are separated from each other by some distance. Differences in voltage are directly related to dielectric constants of material in the proximity of both conductive surfaces. As different materials enter the surrounding area, an electric field between conductive surfaces is disturbed. The voltage differences between the two conductive surfaces will adjust with respect to material dielectric properties, in this case moisture content.

Most original equipment manufacturers install grain moisture sensor on the clean grain elevator for the easy access to clean grain flow. Two holes are added to the clean grain elevator for sensor installation. One hole is added to the side as clean grain travels up the elevator and another hole is added to the side where empty paddles travel down. As grain travels up the elevator, kernels fall through the first hole into a measurement chamber of the moisture sensor. A proximity sensor detects when the chamber is full. This sequences the capacitive sensor to take a moisture measurement. Once complete an auger is used to empty the grain sample through the second hole where empty paddles travel downward. This sequence continually repeats itself to obtain moisture measurements as a field is harvested.

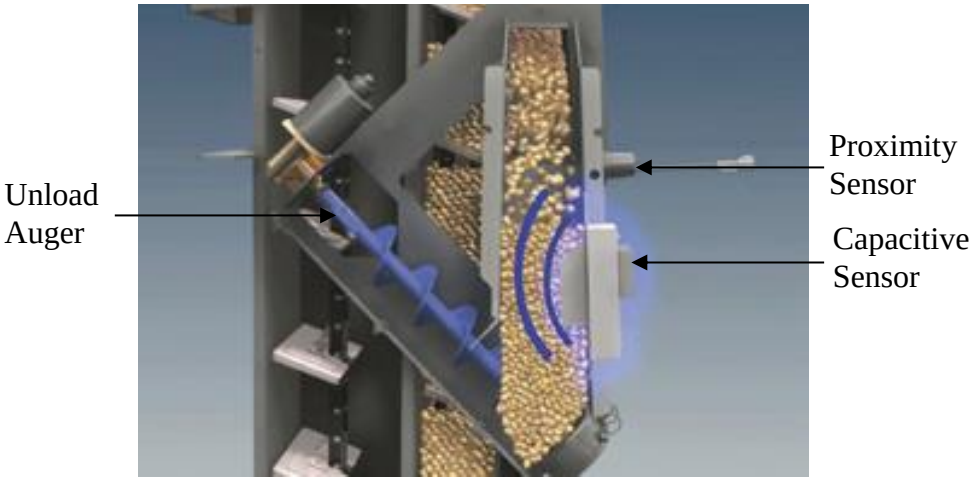

Figure 8: Moisture Sensor
Image Source: (CNH Industrial, 2015)

2.2.3 DGPS Receiver

DGPS (differential global positioning system) receiver uses a network of GPS (global positioning system) satellites and ground-based reference stations to acquire position information about the location of a receiver. A receiver interprets satellite information that it receives and outputs GPS coordinates. These coordinates can be recorded and interpreted by the yield monitor to tell the current location of a combine (Figure 9). With modern farm practices, DGPS receivers have become a common piece of equipment on many farms.

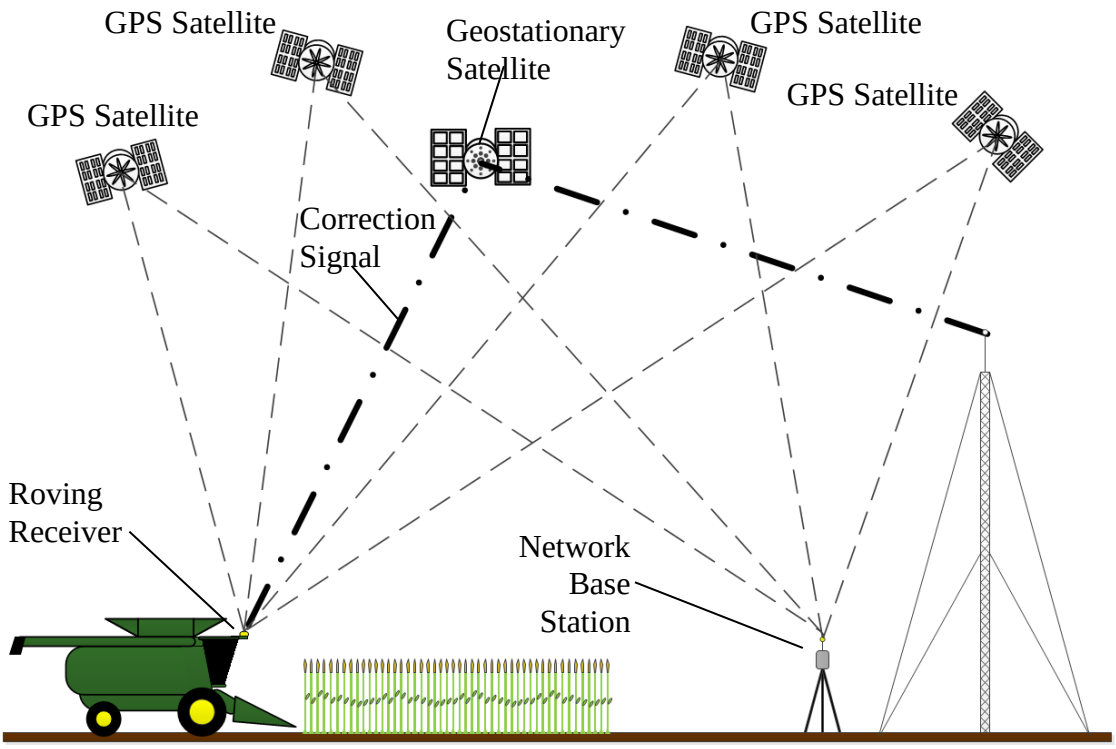

Figure 9: Graphical Abstract of DGPS Network

2.2.4 User Interface

User interfaces acts as a bridge between the yield monitor system and an operator. It performs several tasks; it receives input parameters from the user, provides data storage, and presents yield data. User interfaces allow users to provide initial input parameters about physical a system. Input parameters include examples such as combine head swath width and a combine head height set point. These parameters, such as effective swath width, are used to estimate the amount of area that was harvested over a specific path and allows for accurate calculation of yield data.

Operators can view instantaneous yield data on a display, all while data is also being stored in non-volatile memory. Transfer of this data to a personal computer has shifted to industry standards such as compact memory cards, flash drives, and telemetrics. Once data is retrieved, it can be further processed into yield maps with additional software and used in site-specific management decisions.

2.2.5 Task Controller

A task controller performs computational routines necessary to produce yield data. As a combine harvests corn a signal from the mass flow sensor is used with a sensor calibration to calculate mass flow rate. With the moisture sensor signal mass flow rate can be adjusted to marketable grain moisture content. This mass flow rate measurement can then be used to find average grain yield of an area. First, vehicle speed is acquired from a speed sensor or DGPS coordinates. Then an area rate of harvest can be calculated by multiplying vehicle speed and combine swath width. Integrating marketable grain mass flow rate over an area rate of harvest produces an average yield per a unit of area. This process is used to generate individual yield map pixels. Each pixel stores spatial and yield information, green as high yield and red as low yield (Figure 10).

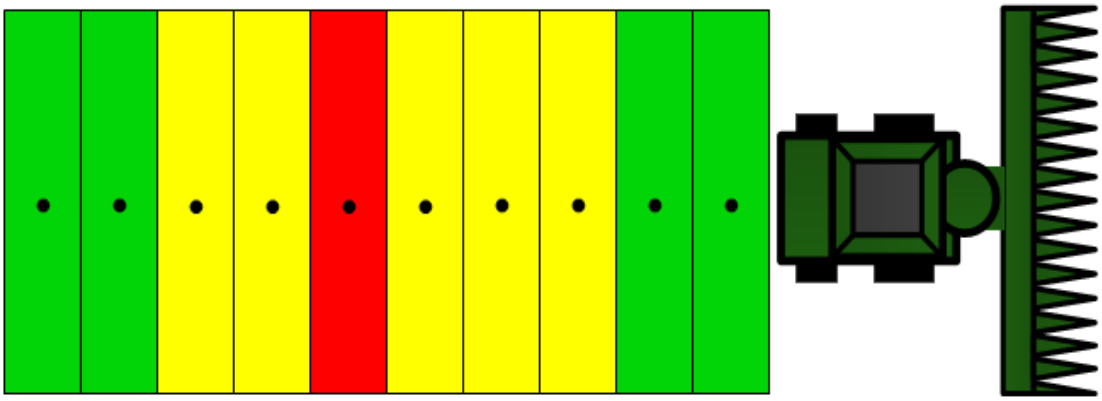

Figure 10: Visualization of Individual Pixels of a Yield Map

Spatial information is the size and geographical coordinate of a specific area. Yield information is an average yield in marketable grain volume over a specific area. Yield maps are the convolution of both types of information.

Once a significant area of a field has been harvested pixels can be collected in the form of a yield map. Yield maps are a spatial representation of the variation in yield over a harvested area. These maps offer growers insight on areas of a field that underperform relative to another (Figure 11).

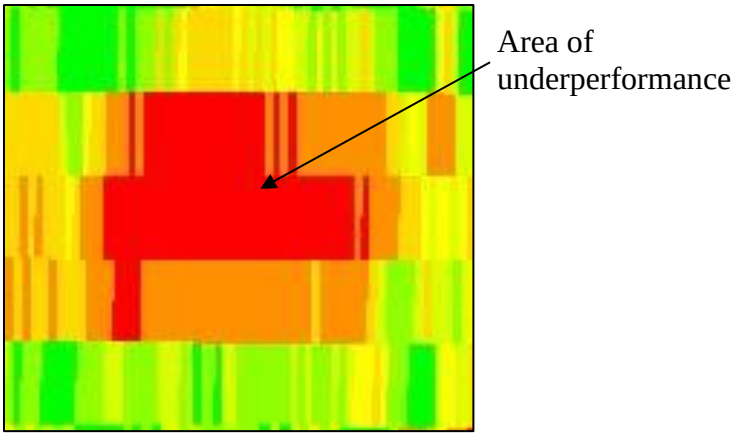

Figure 11: Actual Yield Map

This additional knowledge can be used to drive better management practices in the next growing season. A yield map from a single year does not provide sufficient information on the prediction of long-term yield trends. With long-term yield data, growers can become more effective in evaluation of the productivity and profitability of farmland (Casady, et. al.). Long-term, high-accuracy yield data is an essential part to meet the future demand of grain-based commodities.

2.2.6 Yield Monitor Calibration Methods

The goal of yield monitor calibration is to match the response of a yield monitor to different grain flow rates that are experienced while harvesting. Yield monitors are calibrated as individual grain test loads are harvested at different grain flow rates. As a combine harvests, the yield monitor predicts a grain weight for each test load. After each test load is harvested, grain is unloaded from the combine on to a grain cart to weigh the test load. Actual weights of the test loads are entered into the yield monitor and are used with predicted grain weights to adjust the yield monitor prediction curve. Some yield monitors are capable of being calibrated with a single test load, but various between manufacturers. If the yield monitor has a nonlinear response to different grain flow rates, multiple calibration loads should be taken at to get a more accurate measurement (Nielsen, 2010). It is best practice to consult a yield monitor owner's manual on how and when to calibrate. Most manuals would suggest that a yield monitor should be calibrated multiple times throughout a harvest season.

2.3 Advancements in Yield Monitor Technology

Since the development of the yield monitor systems there has been many attempts to further advance the technology. A common example would include compensation of vehicle dynamics in a mass flow measurement. With changes in terrain, such as varying pitch and roll, there are changes in orientation of the impact plate and the stream of grain that collides with the impact plate. In a relevant study, it was found that variations in terrain produced errors in mass flow rate measurements and that a predictive linear model could correct flow rates to reduce these errors (Fulton, et. al., 2009). These types of advancements focus on improvements in the accuracy of sensor measurements. This technique has provided enhancements in data quality, but has done minimal in the redistribution of data to more localized areas.

Over the past 25, years corn-heads have grown in size. In 1990, the largest corn-head produced by John Deere with row spacing of 30 inches was an 8 row corn-head, model number 843. In 2015, the largest corn-head produced by John Deere with row spacing of 30 inches was a 16 row corn-head, model number 616C. Over this time period, commercially available corn-heads have doubled in size and greatly increased harvest capabilities. It is important note that as swath widths of corn-heads grew, so did the pixel size of the data that yield monitors produced. An increase in pixel size, has had a negative effect on the resolution of yield maps. With a larger pixel size fewer pixels are needed for a defined area, this implies that the resolution of an average yield map has decreased over time (Figure 12).

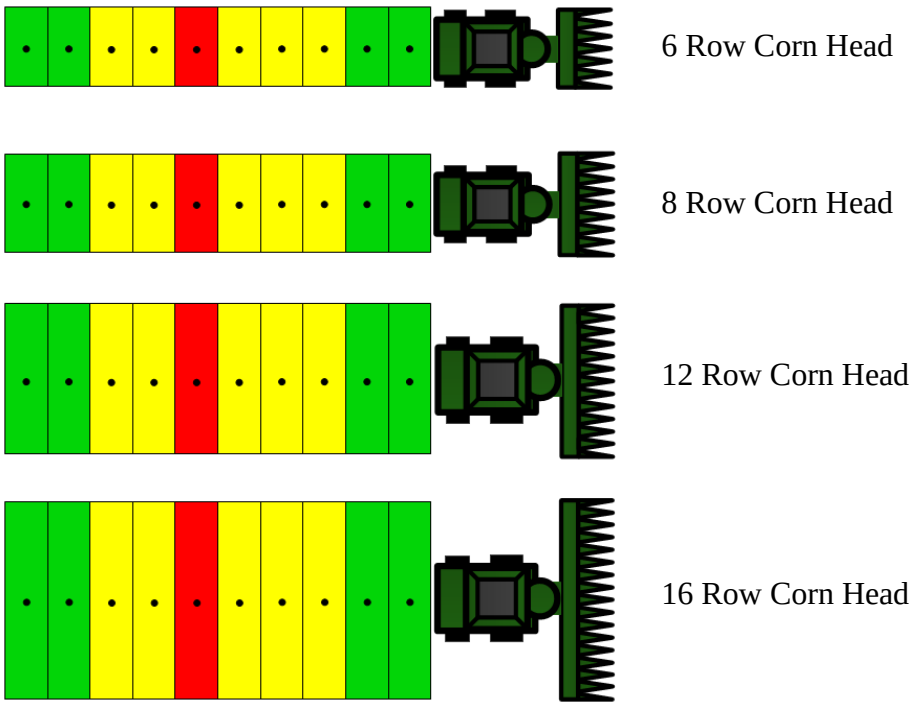

Figure 12: Increase in Yield Map Pixel Size as an Increase in Swath Width

It is evident that modern grain harvest equipment will not reduce in size in the future. To overcome the reduction in yield map resolution issue, an additional subsystem is needed to account for where yield data came from across the swath width of a corn-head. This subsystem would allow for accurate redistribution of data to correct geographical location. Several methods including deconvolution of yield data, remote sensing and plant population monitoring are further discussed in the following sections.

2.3.1 Deconvolution of Yield Data

Convolution is a descriptive word that describes something that is twisted or intertwined. As for mathematics, convolution describes the overlap in the area of two functions as one function is shifted over another. Both definitions describe something that comes from multiple parts. Deconvolution is a process to simplify a complex system into individual elements. For an application in grain yield monitors, deconvolution would be the separation of a stream of grain from a mass flow rate measurement into individual streams from each row. A relevant study on deconvolution methods in yield data found "a trade-off between adequately correcting the yield signal and amplifying inherent errors (Whelan et. al., 2000)." Results further suggested that yield

data could be located on a spatially reduced scale, but with a trade-off of an increase in the coefficient of variation from 10.8% to 19.6% (Whelan et. al., 2000).

2.3.2 Remote Sensing

With the advent of aviation and satellites, remote sensing has become important in monitoring different aspects of geographical locations, such as farmland productivity. Remote sensing techniques have shown promise in monitoring crop health with the introduction of multispectral cameras. This technology can capture a normalized difference vegetation index (NDVI) image, which depicts the amount of vegetative material throughout an area. These images have become of interest in yield mapping research for the ability to provide supplemental information to correct yield maps on a more fine-scale. Fine resolution can be achieved from an NVDI image with 25cm resolution when compared to an actual yield map generated with a 40ft swath width (Figure 13).

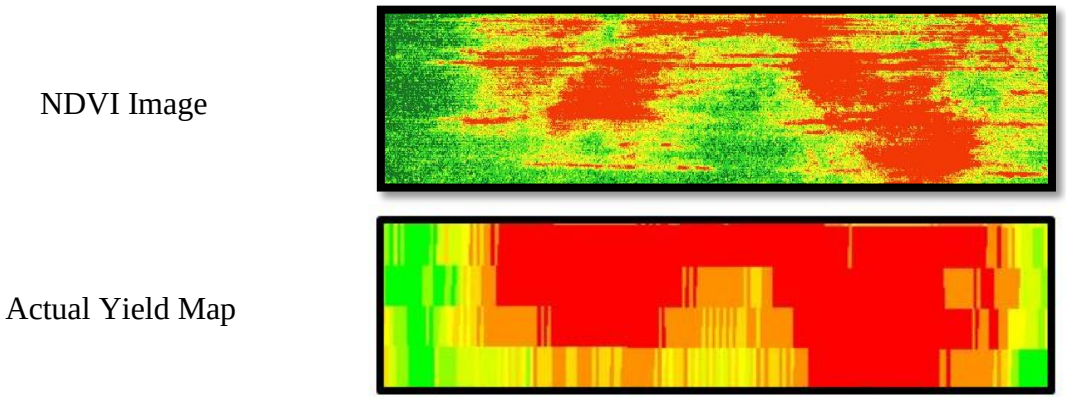

Figure 13: NDVI vs. Yield Map Comparison

A major goal of aerial-based remote sensing is to provide a non-contact solution that can drive site-specific management decisions for smaller areas of a field. Several studies have used multispectral cameras to produce NDVI images for various growth stages of corn plants. These studies have associated variations in plant health and corn yields with crop biomass, leaf area index (LAI) and crop canopy reflectance. Some research has found high correlation (0.92) between NDVI images and grain yield (Shanahan, et al., 2001). “Less emphasis has been given to geostatistical techniques that predict yield by utilizing yield monitor data in combination with remotely sensed imaginary as secondary information to account for spatial auto and cross-

correlation (Dobermann et. al., 2004).” Correlation values as high as 0.933 were found for this technique and opportunities for improvement were identifed as “(i) minimizing the spatial mismatch between yield monitor records and remote sensing data, (ii) improving VI (vegetative index) for yield estimation, and (iii) identifying crop-specific optimal dates for image acquisition (Dobermann et. al., 2004).”

From the correlation methods above, it is important to discuss what affects multispectral remote sensing will have on the future of site-specific agriculture. In a relevant journal article, several plausible applications for the technology were discussed: anomaly detection of crop variations within a field, correlation of spectral responses to specific variables, and converting spectral response to quantitative units to be integrated into physically based growth models of crops (Barnes, et. al., 1996). Development of these methods will continue as aerial-based multispectral imaginary becomes more commercially available at higher resolutions. Overall, this technology has made significant advancements and possesses the potential of becoming commercially adopted for site-specific agriculture applications.

2.3.3 Plant Population Monitoring

Selection of an optimum plant population can depend on several factors such as hybrids, moisture stress level and soil fertility; all of which can have a major impact on yield (Farnham, 2015). After an optimum plant population is selected, producers want to ensure the selection performs. Plant population monitoring can identify the location and spacing of plants. With these measurements, producers can begin to predict yield potential and necessary fertilizer application rates. Several plant population monitoring systems have shown promise in the detection of corn plants through various growth stages. These systems are discussed below.

On-machine vision techniques have had successful application in areas such as part recognition, machine control, and robotics. These applications have led to studies of machine vision for precision agriculture, particularly in the field of plant recognition. With the use of an on-machine digital camera, plant-counting algorithms have successfully achieved R^2 values greater than 0.90 when correlated manual counted values. These tests were conducted at speeds of 1 m s^{-1} through various test treatments of corn plants at V3 and V4 growth stages (Shrestha et. al., 2003). On-machine vision has shown it can provided plant emergence information at lower speeds. When compared to multispectral aerial imaginary, on-machine vision may find it difficult to economically monitor plant health for a full growth season on a commercial scale.

Laser measurement techniques have been around for decades and have found successful implementation in consumer products such as distance rangefinders for hunting and construction applications. Similar applications have been at the center of precision agriculture. In a relevant study, a corn stalk identification system found the location of stalks in V8 and V10 growth stages. This was done by using laser line-scan techniques and various lines-of-sight to allow for minimal inference, correlation values were respectively 0.962 and 0.951. (Shi, et. al., 2013). The goal of this system is to "be ultimately integrated in a variable-rate-spraying system to improve real-time, high spatial resolution, variable rate nitrogen application (Shi, et. al., 2013)."

Mechanical crop sensing devices, such as John Deere AutoTrac™ RowSense™, have been successfully implemented on individual rows of a corn-head for additional machine guidance and productivity enhancements (Figure 14). Similar crop sensing devices had previous application as plant population monitors for research purposes. When controlled tests were conducted to evaluate performance of the mechanical crop sensing device it was found that correlation values were between 0.93 and 0.96 (Birrell, et. al., 2001). Several real-time harvest conditions produced significant amounts of error in this measurement. Examples included areas with weed infestations and stalks that were closer than 1.5 inches.

Figure 14: John Deere AutoTrac™ RowSense™ System
Photo Credit: (Deere & Company, 2015)

Each of these technologies has made an impact on precision agriculture and was capable of producing high correlation values in controlled environments. As discussed, several of these

systems have been implemented as productivity enhancements on machinery. Remote sensing has been the only system to show promise of being commercially adopted, but fails to give producers real-time information as fields are harvested. This research will investigate an additional on-machine method to produce secondary yield information. If successful, the research will provide producers with a tool to further evaluate site-specific management decisions at a higher resolution.

2.4 Patent Review

As an important step, a patent review was conducted to guide in the development of high-resolution yield maps. Patent reviews offer knowledge and provide useful insight into successful products or technologies in a similar area of interest. In this section, an overview of several patents is provided. More detailed descriptions of these patents can be found at the end of this thesis (Appendix A). Patented technology is broken into two sections: plant monitoring and yield estimation.

2.4.1 Plant Monitoring

In the patent, "Device to measure and provide data for plant population and spacing variability," inventors claim the development of a handheld device capable of monitoring: plant population, plant spacing and plant spacing variability. This device is a single wheel apparatus rolled along a crop row that gathers distance and plant location information that is used to generate estimated population and spacing data (Easton, et. al., 1998).

In the patent, "Sensing assembly for detection of one or more plants," inventors claim the development of a sensing assembly mounted to a crop divider of a row crop head. The device is capable of detecting plants and uses a minimum of one mounted arm that response to contact from plants in a field. A sensor measures the response of the arm to determine where plants were present (Wilcox et. al., 2010).

2.4.2 Yield Estimation

In the patent, "Crop yield prediction using piecewise linear regression with a break point and weather and agricultural parameters," inventors claim the development of a program of instructions to predict crop yield. The program uses agricultural and environmental information such as, weather, NDVI, soil moisture and surface temperature to predict crop yield data. The program instructions can be altered for different crops (Singh, et. al., 2010).

In the patent, “Evaluating commodity conditions using aerial image data,” inventors claim the development of a method to evaluate the condition and forecast the production of agricultural commodities in different regions of interest. The method uses aerial imagery data to perform the evaluation (Linville, 2015).

In the patent, “Multi-variable model for identifying crop response zones in a field,” inventors claim the development of a method to identify different crop response zones in a field. The method encompasses the processing of multiple aerial imagery data sets to determine a relative comparison of crop responses zones with similar vegetative growth characteristics in a field (McGuire, et. al., 2006).

2.5 Concepts of Momentum Transfer for Detection of Individual Ears

It was discussed in the combine operation section that stalk-rolls of a corn-head would accelerate and dislodge an ear of corn from its stalk as it made contact with a pair of deck-plates. This collision process which harvests ears of corn from a stalk has significant resemblance to many momentum transfer or collision examples found in elementary physics. Collisions can be thought of in two separate categories, elastic and inelastic.

In an elastic collision, momentum is conserved in the form of kinetic energy. A good example of an elastic collision is the collision between billiard balls. However, this collision is not a true elastic collision because some energy is dissipated during contact. Billiard balls are designed with a high coefficient of restitution value, which describes the ratio of final to initial velocities in a collision. This means that as two balls collide, both with the same mass and initial velocity, each ball will leave the collision in opposite directions with a velocity similar to its initial value.

In an inelastic collision considerable kinetic energy is dissipated in the form of heat, sound and deformation of material. Most collisions, such as an ear of corn that impacts a deck-plate, can be thought of as inelastic. An inelastic collision can be significantly complex to model and would need to take into consideration parameters such as, geometry of each object, initial velocities, material composition, angle of collision and friction coefficients. These models could be simplified, but estimation and variation in initial parameters can still lead to uncertainty in a calculation.

Several concepts behind inelastic collisions can still be used to assess difference between mechanical machine noise and impacts from crop material. One of these underlying concepts is

Newton's third law, for every action there is a reaction. This means that sum of forces that act on an object are equal to zero. This is a useful concept for collision analysis between an ear and a deck-plate. As an ear, with an unknown mass and height, is accelerated by a pair of stalk rolls it comes into contact with a stationary deck-plate(s). In an ideal case, a deck-plate will provide an opposite reaction force ($F_{deck\text{-}plate}$) that is equal to the sum of forces to de-accelerate the mass of an ear and the force required to dislodge the ear from its stalk (F_{ear}), (Figure 15).

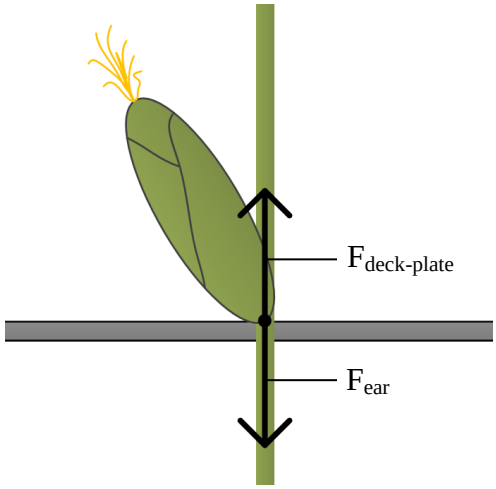

Figure 15: Free-body Diagram of a Collision between an Ear of Corn and a Deck-plate

Several variables and assumptions are needed to calculate the reaction force ($F_{deck\text{-}plate}$) of a deck-plate from a collision with an ear. Mass (m_{ear}), initial collision velocity ($v_{initial}$) and collision duration (Δt) for each ear would need to be known. Assumptions would include that kinetic energy is conserved as velocity of an ear after a collision (v_{final}) would achieve a zero state and the force required to dislodge an ear from its stalk is known. These variables summarize the reaction force of a deck-plate (Equation 1).

Equation 1: Reaction Force of a Deck-Plate

$$F_{deck-plate} = F_{ear} = m_{ear} * \frac{(v_{initial} - v_{final})}{\Delta t} + F_{dislodge}$$

As this model was developed and reviewed, researchers used best judgement practices to consider realistic measurement of variables and assumptions discussed above. It was concluded that as corn was harvested it was outside the scope of this research to accurately measure mass (m_{ear}), initial collision velocity ($v_{initial}$) and collision duration (Δt) for each ear. It was also believed that the dislodge force between an ear and a stalk would be highly dependent on hybrid

selection and moisture content of individual plants. This was also considered to be outside the scope of the research. For these reasons, this research focused on measuring changes in acceleration experienced during an ear/deck-plate collision. As the measurements shifted from force to acceleration, mass was neglected (Equation 3).

Equation 2: Force Experienced from an Impulse

$$Force\ from\ Impulse = m * a = m * \frac{\Delta v}{\Delta t}$$

Equation 3: Acceleration Experienced from an Impulse

$$Acceleration\ from\ Impulse = a = \frac{\Delta v}{\Delta t}$$

Accelerometers were chosen as an instrument to detect acceleration on deck-plates from shock impulses. A direct goal of this research was to quantify at what level acceleration data can predict a quantity of ears flowing through a single row unit of a corn head.

2.6 Concepts of Shock and Vibration for Detection of Individual Ears

This section is an overview of shock and vibration analysis and is a compilation of concepts found in the "Harris' Shock and Vibration Handbook" (Piersol, et. al, 2010). Shock and vibration are terms used to describe mechanical excitations that cause dynamic responses within physical systems. A shock or impulse is known as a mechanical excitation with a relatively short duration. Vibration is a mechanical excitation with an extend duration that encompasses the time for a physical system to respond. "Both shock and vibration excitations can appear either as an input motion or force at the mounting points or as a pressure field over the exterior surface of the physical system of interest" (Piersol, et. al., 2010).

Shock and vibration can be further categorized as deterministic or stochastic. Deterministic excitations are predictable in nature. They can be reproduced and measured in a control environment with calculations from fundamental principles of physics with minimal error. Deterministic shock is a step input of a controlled magnitude into a physical system. An example would include a drop test; similar to tests performed by electronic phone manufacturers. Here, products are submitted to known amount of shock, an estimate of the shock can be calculated with a known drop height and duration of collision. These tests ensures that products can withstand harsh environments that consumer may expose products too. Deterministic

vibration is generally the result of unbalanced rotational components. An example would include turbine blades; these blades are high-precision parts and can be further altered by removing material at each end of a blade to ensure the complete system is balanced. If not balanced appropriately, unbalanced blades can lead to accelerated wear in rotational components such as bearings and shafts. Additional wear on system components can lead to a decreased life expectancy or an eventual failure of equipment. Stochastic excitations can be classified as "one where neither analytical calculations nor previous observations of the excitation produced under identical circumstances will allow the prediction of the exact time history of the excitation in the future (Piersol, et. al., 2010)." Stochastic excitations are random as some component that caused the excitation is unknown, such as magnitude or duration. For any application, it should be taken into consideration which measures are known and unknown to decide if excitations are deterministic or stochastic.

Vibration of physical systems can be further classified as free or forced vibration. In free vibration, real systems are modeled as a mass and spring system with viscous damping, (Equation 4, Figure 16).

Equation 4: Differential Equation of Free Vibration with Viscous Damping

$$m\ddot{x} + c\dot{x} + kx = 0$$

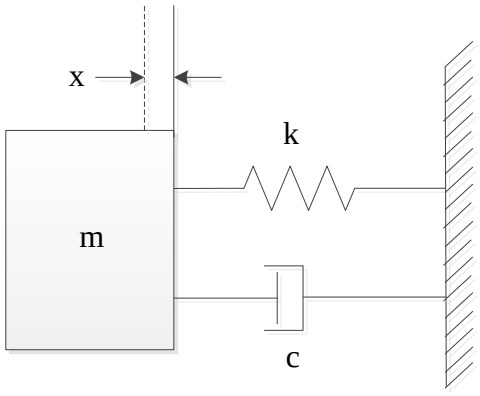

Figure 16: Free Vibration Model with Viscous Damping

In free vibration, energy from an initial motion or impulse force creates an oscillating response in the displacement of the mass. Energy introduced into the system is stored by inertia of the mass and potential energy of the spring. Once energy is stored by the system, it begins to move towards a previous stationary steady-state. This is done as oscillations in displacement of

the mass cause a respective exchange in kinetic and potential energy storage between the mass and spring. As oscillations occur, a damper dissipates energy in the form of heat to surroundings of the system. Interactions among these components cause a transient response which decays with time for a real physical system in free vibration. The rate at which this response decays is dependent on the frequency of oscillations and damping coefficients of the system.

In forced vibration, energy is continually added to a system by a forcing function which also creates a response in the displacement of a mass. Steady-state, forced vibration occurs when the energy that is being supplied equals the energy that is dissipated. Similar to free vibration, displacement (x) of the mass occurs and is different for given combinations of mass (m), force (F_0), damping coefficient (c) and spring constant (k), (Equation 5, Figure 17). Physically-damped systems with forced vibration achieve an oscillating, steady-state response in the displacement of the mass.

Equation 5: Differential Equation of Forced Vibration with Viscous Damping

$$m\ddot{x} + c\dot{x} + kx = F_0 \sin(\omega t)$$

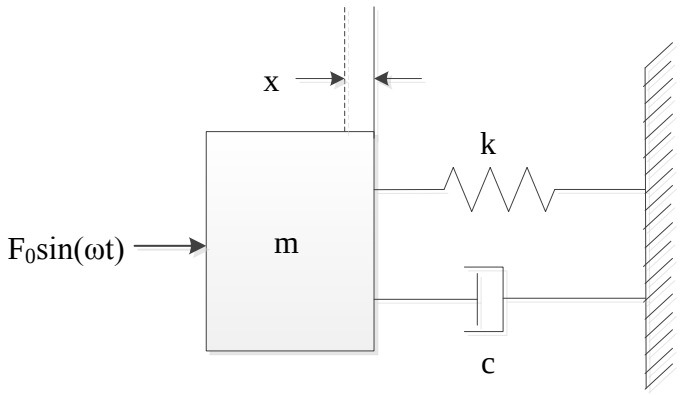

Figure 17: Forced Vibration Model with Viscous Damping

Deck-plates of a corn-head can be thought of as a mass in the forced vibration model (Figure 17). As a corn-head is engaged it supplies a forced vibration, $F_0\sin(\omega t)$, that is a function of the rotational speed (ω) of the corn-head. The model also includes: mass of the deck-plate (m), damping coefficient (c) and spring constant (k). Mass (m) determines the ability of the deck-plate to store potential energy in the form of inertia. Damping coefficient (c) determines the ability of a deck-plate to dissipate kinetic energy in the form of heat to the surrounding environment. Spring constant (k) determines the ability of a deck-plate to store potential energy

in the form of elastic strain. An oscillating, steady-state response in the displacement (x) of the deck-plate is achieved when forced vibration with a constant amplitude and frequency is applied.

The previous model is an accurate representation of a deck-plate when the corn-head is running and the combine has yet to start harvesting corn (Figure 17). As a combine begins to harvest, interactions between ears and deck-plate(s) generate shock impulses as ears are removed from respective stalks. Shock impulses should be considered an additional input into the previous model. If a shock impulse is large enough to disrupt the forced vibration of the deck-plate, a short period of free vibration would occur until the amplitude from the initial shock decays below the amplitude of the forced vibration. This will be the key concept in the rest of this thesis.

2.7 Conclusion

Grain yield monitoring technology provides the ability to collect yield information about a harvested area and displays it in the form of a yield map. Over the past 25 years, the swath width of corn-heads has grown significantly and resolution of yield maps has proportionally decreased due to an increase in pixel size created by larger corn-heads. Several methods have shown promise as solutions to these issues, but no solution has been fully tested or developed. Precision agriculture has shown a need for secondary information that can improve yield map resolution be redistributing grain mass flow data on a spatially reduced scale. This concept would allow for more yield pixels across the swath width of a corn-head, which would increase the resolution of yield maps. As an additional method, this research will investigate shock and vibration data caused by ears of corn striking deck-plates of a corn-head.

CHAPTER 3: OVERVIEW OF RESEARCH OBJECTIVES

3.1 Research Objectives

The long-term goal of this research is to give producers a tool that will provide an increase in spatial accuracy of yield data across a corn-head. The short-term goal of this research was to identify a method to produce secondary yield information across the swath width of a corn-head. Currently, yield monitor systems only generate a single pixel across the swath width of a corn-head over a harvested area. For an increase in spatial accuracy of yield data, secondary information must be generated to account for yield variation across the swath width of the corn-head. This secondary information could then be used to redistribute grain on a spatially reduced scale. For this reseach, ear detection will be the secondary information that is generated. Objectives to generate secondary information are listed below:

1. Develop and quantify the precision of a deck-plate mounted accelerometer ear detection algorithm on an individual row basis of a corn-head.
2. Develop and quantify a method to normalize predictive ear detection values across multiple rows of a corn-head.

CHAPTER 4: PRELIMINARY DESIGN CONCEPTS

4.1 Introduction

The short-term goal of this research was to identify a method to produce secondary yield information across the swath width of a corn-head. This information could then be used to redistribute grain mass flow data to more localized area of a field. Accelerometers were selected as a sensor to measure shock and vibration data as ears of corn collided with a deck-plate. These measurements were used to quantify how acceleration data could predict ear counts from an individual row of corn.

The objective of this section is to identify specifications of an accelerometer that will provide effective results for this application. An investigation of where an accelerometer should be placed to acquire such signals will also be discussed. This location must be able to keep an accelerometer safely out of the reach of other mechanically driven components. Requirements for the preliminary design process are listed below:

- Identify accelerometer specifications to ensure that signals from ear impacts can be measured.
- Identify an installation location for an accelerometer to detect a shock impulse as an ear impacts a deck-plate. Locations must be able to be exposed to harsh harvest environments.

4.2 Materials and Methods

4.2.1 Combine and Corn Head

For this research a John Deere S670 series combine and 616C, 16-row corn-head was used in lab tests for initial sensor selection and placement. Upon completion of these tests the corn-head and combine was instrumented for in-field harvest tests.

Figure 18: John Deere S670 Combine with a 616C Corn-head
Photo Credit: (Deere & Company, 2015)

4.2.2 Data Acquisition System

A National Instrument compactRIO-9024 with an 8 slot chassis was used to collect data. This instrument was able to handle up to 32 channels of accelerometer data at a limited sampling frequency. National Instrument module cards NI 9234 and NI 9853 were respectively used to collect accelerometer and CAN data. A sampling rate of 16.666 KHz was set for each channel. This frequency was the upper limit at which the system could collect data and was set as a standard throughout all in-field harvest tests.

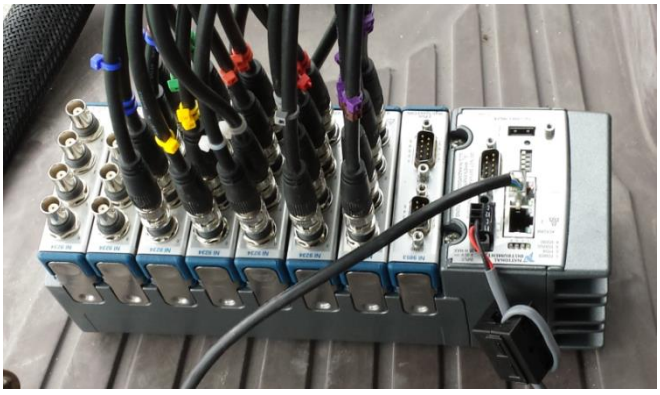

Figure 19: Data Acquisition System

4.2.3 Accelerometer Installation Considerations

For this application, several installation conditions were required to ensure shock signals from an ear/deck-plate collisions could be captured, these include:

- Accelerometers must be mounted to the surface of a deck-plate and in close proximity to the location of ear impacts
- Accelerometers must avoid contact with other mechanically driven components
- Minimal modifications to row-unit components should be made as accelerometers are installed

As described above an accelerometer must be mounted to the surface of a deck-plate and near the location of ear impacts. Best mounting locations found near ear impacts were towards the middle half of each deck-plate, based on video evidence from a previous harvest. This happened as ears were initially pulled downward by the stalk rolls before they would collide with a deck-plate. This constraint on location offers limited deck-plate surface area to successfully mount an accelerometer. Mechanically driven gathering-chains cover the majority of acceptable deck-plate surface area. The remaining surface area was covered by a plastic chain-guide that supports and directs the gathering-chain. These constraints left an area between the revolving gathering-chain as the only possible installation location for an accelerometer (Figure 20).

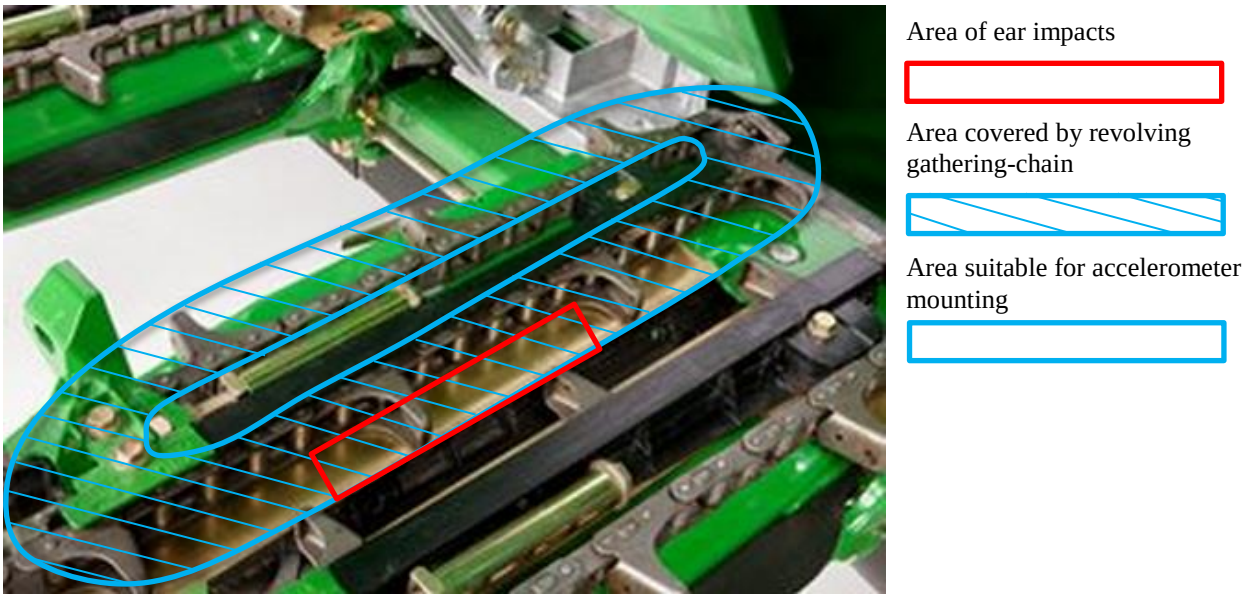

Figure 20: Suitable Installation Location for an Accelerometer
Photo Credit: (Deere & Company, 2015)

It was required that modifications be made to the plastic chain-guides of both fixed and adjustable deck-plates to adequately meet installation conditions. Plastic material was removed from the back-side of both chain-guides to uncover the surface area on each deck-plate. Cables could be routed through the plastic chain-guide and back to the data acquisition system in the combine cab, as accelerometers were installed.

Figure 21: Uncovered Deck-plate Surface Area for Accelerometer Installation

Additional material was removed from the base of each chain-guide to create a cavity where an accelerometer could be mounted on top of the deck-plate, but beneath the chain-guide. The cavity height was 0.75 of an inch off the surface of the deck-plate and is the reason the size specification of an accelerometer for this particular application was defined as 0.75 inch^3. This cavity would also allow accelerometers to translate beneath the chain-guide if deck-plate position was adjusted by an operator in the cab.

4.2.4 Accelerometer Mounting Methods

There are several mounting strategies that can be approached when collecting vibration and shock data with accelerometers. All methods have limitations in the frequency range of data that can be produced. Frequency range is a key specification to identify and makes mounting an important issue to be considered. These strategies range from: stud mounting, cement bonding, magnetic mounting and double-sided adhesives. Of all the mounting methods, stud mounting an accelerometer to a test surface provides the best contact. "Where stud mounting is practical, it is the best type to use for the following reasons:

1. It provides the highest resonance frequency (up to 100 kHz) of any of the mounting techniques and, therefore, the widest possible measurement frequency range (up to 50 kHz).

2. It permits measurements at very high vibration levels without the loosening of the transducer from the test surface.
3. It does not reduce the maximum permissible operating temperature at which measurements can be made.
4. It permits accurate and reproducible results since the measurement position can always be duplicated" (Harris, et. al., 2002).

It is important to note accelerometers were initially bonded to each deck-plate with a cement adhesive. This technique provided sufficient results for lab drop tests which are discussed in another section. As tests transitioned from lab-based tests to preliminary in-field harvest tests it was found that cement based mounting techniques could not withstand the harsh environments to which accelerometers were exposed. In a single test day it was common for several cement bonds between accelerometers and deck-plates to break. As accelerometers broke free they were allowed to jar back and forth. This motion produced useless data and a prolonged chance that accelerometers could be damaged. A mounting solution to resolve this issue was developed, which will be further discussed in the final accelerometer selection and installation section.

4.2.5 Accelerometer Amplitude Test

As discussed in the literature review section, when a corn stalk is pulled downward between deck-plates an ear attached to the stalk will become dislodged. Furthermore, the force required to remove an ear from its stalk is comprised of two forces. The two forces included a force to stop a moving ear and a force to tear an ear from its stalk. For this application it was important to find the amplitude or measurement range under consideration. As amplitude tests were conducted throughout the summer season, corn stalk with ear attached at appropriate moisture content were not readily available. For this reason, research focused on being able to identify and quantify shock impulses generated as an ear of corn was dropped on a deck-plate. Specific goals for this phase of the research were to quantify amplitude of an ear/deck-plate collision and estimate a measurement range so that an accelerometer could be selected for the harvest season.

4.2.5.1 Test Setup

For this test, a drop-shoot was mounted above an individual row-unit of the corn-head and was used to drop ears of corn on to the fixed deck-plate (Figure 22). The drop-shoot was capable dropping ears of corn on a deck-plate at various heights. An ear of corn could be loaded into the top of the drop-shoot and dropped as a stop pin was pulled from behind the corn-head. The ear could then free-fall until it collided with the deck-plate creating a shock impulse that was detected by a 500g accelerometer that was mounted to the fixed deck-plate between a revolving gathering-chain.

Figure 22: Drop-Shoot for Amplitude Test

4.2.5.2 Test Procedure

Tests were conducted at 5 different speeds of the corn-head. At each speed, 5 ears of corn were dropped on to the fixed deck-plate from a height of 3ft. A camera was mounted on top of the snout cover to capture the moment each ear struck the deck-plate. At the beginning and end of each test a wrench was used to tap the deck-plate to create a shock impulse in the accelerometer data file. This shock impulse could later be identified in the acceleration data and video evidence. Both time-series could then be synced. After an initial shock impulse was created the corn-head was turned on to a pre-selected speed. Individual ears were dropped with a short duration between each of them to reload the drop shoot. Synced acceleration and video

evidence could be used to determine if a shock impulse was created at the moment an ear made contact with the deck-plate. Impulses at each end of the signal were created by an initial tap on the deck-plate. After acceleration and video data were synced, red triangular markers were used to identify moments at which ears of corn made contact with the row-unit (Figure 23).

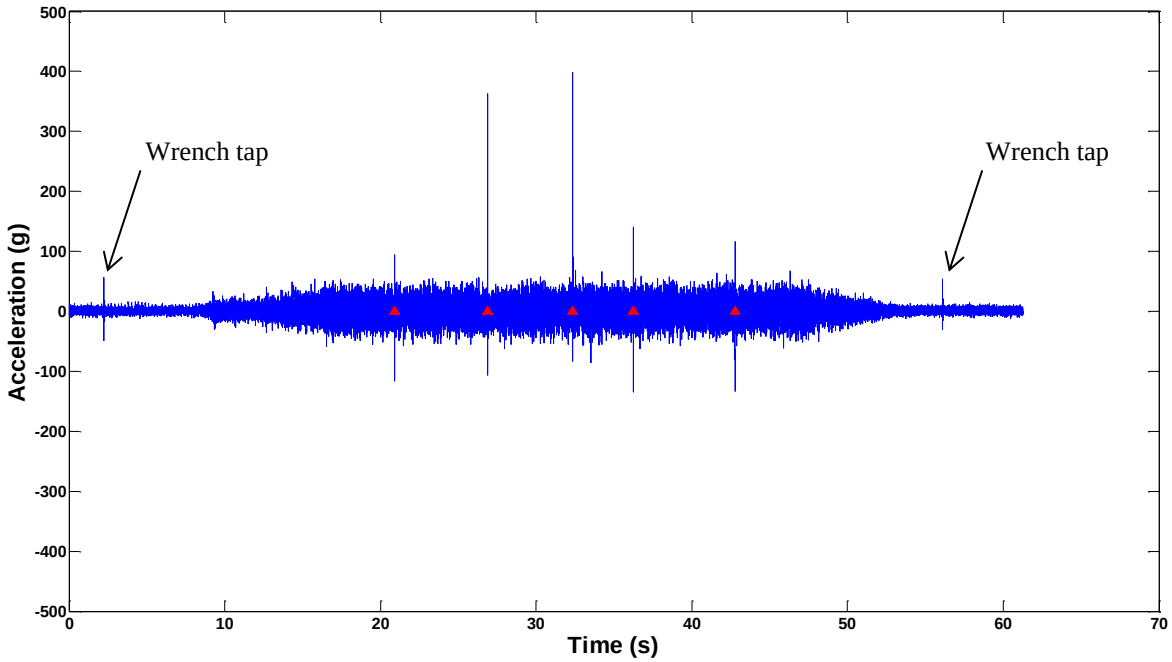

Figure 23: Individual Test Run from an Amplitude Drop Test

4.2.5.3 Test Results

From this information it was determined that 20 out of 25 ears impacted the fixed deck-plate (Table 1). Each of the amplitude from these shock impulses was determined and it was assumed that these impulse values were normal about a mean value for a 3ft drop height. A 95% confidence interval of the mean peak amplitude was calculated as an estimate for a range of values that an accelerometer may experience when exposed to these conditions. This confidence interval was used in a later section to identify an initial measurement range for an accelerometer. From video evidence, the 5 undetected ears did not make clear contact with the deck-plate. Each ear either engaged the snout-covers or gathering-chains before making contact with the deck-plate, which is not a desired form momentum transfer.

Table 1: Amplitude Drop Test Results

Corn Head Speed	Ear Drop Height	Number of Ears Detected	Measured Amplitude (g)
1	3 ft.	3 out of 5	344.7
	3 ft.		388.6
	3 ft.		Not detected
	3 ft.		Not detected
	3 ft.		243.8
2	3 ft.	4 out of 5	295.7
	3 ft.		332.1
	3 ft.		197.1
	3 ft.		457.7
	3 ft.		Not detected
3	3 ft.	3 out of 5	Not detected
	3 ft.		Not detected
	3 ft.		220.6
	3 ft.		105.6
	3 ft.		263
4	3 ft.	5 out of 5	170.8
	3 ft.		307.7
	3 ft.		109.9
	3 ft.		467.8
	3 ft.		89.54
5	3 ft.	5 out of 5	94.44
	3 ft.		362.7
	3 ft.		398.1
	3 ft.		140.5
	3 ft.		116.1
Mean		20 out of 25	255.3
Standard Deviation			121.5
95% Confidence Interval			255.3 ± 53.26

4.2.6 Determination of Accelerometer Specifications

In this section, required accelerometer specifications to capture an ear/deck-plate collision signal are presented. An overview of the required specifications and how each specification was determined will be discussed. In the results section of this chapter, accelerometer specifications will be consolidated into a suggest accelerometer specification sheet for this application. Accelerometer specifications can be classified into four categories,

performance, environmental, electrical and physical-based requirements. These categories will be broken into individual sections and discussed below.

4.2.6.1 Performance-Based Accelerometer Specifications

Goals for performance-based accelerometer specifications are to define a set of parameters that will capture a response of changes in acceleration for a specified application. Performance-based parameters are listed below. A discussion on identification or determination of each parameter will follow.

- Measurement Range
- Sensitivity
- Resonant Frequency
- Frequency Range
- Non-Linearity
- Transverse Sensitivity
- Broadband Resolution

Measurement Range

Measurement range is the effective range of amplitudes that an accelerometer can identify. Measurement range of an accelerometer should take into consideration expected acceleration levels of an application. An object drop tests was completed to estimate an initial measurement range from a known drop height. A 95% confidence interval of the mean peak amplitude was calculated for the drop test. The upper limit of 308.56g was used as an estimate for the measurement range of the selected accelerometer and an experienced customer support application engineer was consulted for the final accelerometer selection.

Sensitivity

For an accelerometer, sensitivity is the slope or ratio of voltage output of the sensor to acceleration input. A National Instrument module, NI 9234, was used for this research and had a full-scale voltage range of ±5V. Ideally, sensitivity will scale the full-scale voltage range of a data acquisition system over a measurement range of a sensor.

Resonant Frequency

Resonant frequency is a frequency at which the response amplitude of an accelerometer is at a relative maximum. As frequencies approach a resonant frequency the response amplitude becomes highly non-linear. For this reason, frequency ranges of an accelerometer are typically

set to 20% of the resonant frequency. As discussed later in the accelerometer mounting section, stud mounting offers the highest capabilities to capture resonance frequencies up to 100 kHz (Harris, et. al., 2002). From this information a resonant frequency equal to or less than 100 kHz was selected.

Frequency Range

Frequency range is a range of frequencies an accelerometer can capture and is typically cited with a percent tolerance. A rule-of-thumb suggests a frequency range that does not exceed 20% of the resonant frequency of an accelerometer. As discussed later in the accelerometer mounting section, stud mounting offers the highest capabilities to capture resonance frequencies up to 100 kHz (Harris, et. al., 2002). From this information a frequency range equal to or less than 20 kHz was selected.

Non-Linearity

Non-linearity is expressed as a percentage an actual measurement can shift from an ideal calibration curve. Non-linearity specification was selected as less than or equal to 1%, this value can typically be achieved by accelerometer manufacturers.

Transverse Sensitivity

Transverse sensitivity is the sensitivity in a direction that is not parallel to the normal axis of a mounting surface. A typical manufacturer range for this specification was selected as less than or equal to 5%.

Broadband Resolution

Broadband resolution is the lower limit of sensitivity when compared to white noise produced by a stationary accelerometer over a broad frequency range. This value is presented as a standard deviation of acceleration from zero over a specified frequency range. Since measurements of this research will be significantly greater than the range of white noise produced by a stationary accelerometer, this specification was neglected. Typical broadband resolutions from manufacturers should be sufficient.

4.2.6.2 Environmental-Based Accelerometer Specifications

Goals for environmental-based accelerometer specifications are to identify a range of environmental factors that could affect an accelerometer. Environmental-based parameters are listed below. A discussion on identification or determination of each parameter will follow.

- Shock Limit
- Temperature Operation Range

Shock Limit

The shock limit of an accelerometer is the maximum acceleration an accelerometer can experience before possible damage will occur. For this application, a shock limit was estimated by multiplying a factor-of-safety equal or greater than 10 with the amplitude range found during drop tests. From this information a shock limit of equal to or greater than 3085.6 g was selected.

Temperature Operation Range

Temperature operation range is the environmental temperature range an accelerometer will be exposed to for a specific application. For this application, an effective temperature operation range of -50 to +150 °F must be encompassed.

4.2.6.3 Electrical-Based Accelerometer Specifications

Goals for electrical-based specifications of an accelerometer are to ensure electrical parameters are compatible with the data acquisition system available. These parameters were taken into consideration for electrical compatibility and will not be further discussed in this thesis.

4.2.6.4 Physical-Based Accelerometer Specifications

Goals for physical-based specifications are to provide a range of physical parameters that will support the installation and functionality of an accelerometer. Physical-based parameters are listed below. A discussion on identification or determination of each parameter will follow.

- Sensing Element
- Sensing Geometry
- Housing Material
- Humidity Specification (Sealing)
- Mounting Method
- Size (Width & Height)

Sensing Element

A sensing element is the component in an accelerometer that produces an output signal as a mechanical excitation is provided. Piezoelectric accelerometers use a quartz crystal as a sensing element. An output charge is produced as a quartz crystal is subjected to flexural stress. Piezoelectric accelerometers are the most widely used accelerometers and offer a wide range of vibration and shock applications with broad frequency ranges, high sensitivity, and excellent linear responses. Specification ranges possible with quartz sensing elements are generally unrivaled by other sensing methods.

Sensing Geometry

Sensing geometry is determined by the selection of a sensing element. For this application the desired sensing element is a quartz crystal, which must be subjected to flexural stress to output a signal. Manufacturers typically complete this with shear type geometry which provides stress to the quartz crystal as changes in acceleration are experienced.

Housing Material

Housing material specifications for this application would require material properties such as high-strength, stiffness, toughness and good corrosion resistance to survive harsh field environment. A suggested material for this application would include titanium alloys.

Humidity Specification (Sealing)

Humidity specification is generally listed as a type of seal used in the manufacturing of accelerometers. It is recommended that if an accelerometer is subjected to high fluctuation in moisture and temperature that it uses a hermetic (air tight) seal to avoid degradation of the accelerometer.

Mounting Method

Mounting method is an important specification related to the frequency range an accelerometer can measure. It will be discussed in a later section that stud mounted accelerometers provide the best results in the collection of high frequency vibration data.

Size (Width & Height)

Size of an accelerometer is critical to the installation for any application. As discussed in the installation section of this chapter a maximum squared volume for this application was

specified as 0.75 in^3. The accelerometers width and height must remain inside the constraints of this volume.

4.3 Results

4.3.1 Suggested Accelerometer Specifications

From the previous section, a suggested accelerometer specification sheet was developed for this application and is presented below. This specification sheet was to act as a guide and not as absolute requirements for the accelerometer. An experienced customer support application engineer was consulted when a final accelerometer was selected.

Table 2: Suggested Accelerometer Specifications

Performance-Based	**English**	**SI**
Measurement Range	± 308.56 g pk	± 3,027 m/s^2 pk
Frequency Range	≤ 20,000 Hz	≤ 20,000 Hz
Resonant Frequency	≤ 100 kHz	≤ 100 kHz
Broadband Resolution	negligible	negligible
Non-Linearity	≤ 1%	≤ 1%
Transverse Sensitivity	≤ 5%	≤ 5%
Environmental-Based	**English**	**SI**
Shock Limit	± 3,085.6 g pk	± 30,269 m/s^2 pk
Temperature Operation Range	T ≤ -50 F° to T ≥ +150 F°	T ≤ -45 C° to T ≥ +66 C°
Physical-Based	**English**	**SI**
Sensing Element	quartz	quartz
Sensing Geometry	shear	shear
Housing Material	Titanium	Titanium
Humidity Specification	hermetic	hermetic
Mounting Method	stud	stud
Size (Wide & Height)	0.75 in^3	12.3 cm^3

4.3.2 Final Accelerometer Selection

A piezo-based accelerometer from PCB Piezotronics Inc. was selected as the final accelerometer for the 2014 harvest season, model number 353B11. The amplitude of this accelerometer has an operational range of ± 1000g and maintains a compact size of less than 11 mm^3. As the NI 9234 cards with a 24 bit analog-to-digital converter were paired with the selected PCB 353B11 accelerometers a resolution of 0.000119 g bit^{-1} was achieved.

Figure 24: PCB 353B11 Accelerometer

The PCB 353B11 accelerometer met or exceeded all performance, environmental, electrical and physical specifications. Key environmental and performance-based specifications of the accelerometer are identified (Table 3), and a detail specification sheet can be found at the end of this thesis (Appendix B). This accelerometer was further verified through an additional ear drop validation test, which will be discussed later in this chapter. As in-field tests were conducted it was noted that electrical connections on several accelerometers did become faulty. Data from these accelerometers will be identified, but not considered in the final analysis.

Table 3: PCB 353B11 Accelerometer Specifications

Performance-Based	**English**	**SI**
Sensitivity	5 mV/g	0.51 mV/(m/s^2)
Measurement Range	± 1000 g pk	± 9810 m/s^2 pk
Frequency Range (± 5 %)	1 to 10,000 Hz	1 to 10,000 Hz
Frequency Range (± 10 %)	1 to 18,000 Hz	1 to 18,000 Hz
Resonant Frequency	≥ 70 kHz	≥ 70 kHz
Environmental-Based	**English**	**SI**
Shock Limit	± 10,000 g pk	± 98,100 m/s^2 pk
Temperature Operation Range	-65 F° to +250 F°	-54 C° to +121 C°

4.3.3 Final Accelerometer Installation

In this section a discussion will present how an accelerometer was installed on an individual deck-plate. A section in the next chapter will cover how this installation method was applied across multiple row-units of a corn-head, so in-field tests could be conducted. As discussed in a previous section, an accelerometer was constrained by the following:

- Accelerometers must be mounted to the surface of a deck-plate and in close proximity to the location of ear impacts
- Accelerometers must avoid contact with other mechanically driven components
- Minimal modifications to row-unit components should be made as accelerometers are installed

To meet these constraints, small amounts of material from the plastic chain-guide were removed to undercover deck-plate surface area and create a cavity to successfully mount an accelerometer. Stud mounting was determined as the best possible method to mount an accelerometer. Each accelerometer had a threaded stud that extended from its base. Thread-orientation between accelerometers was inconsistent. This did not allow researchers to predict the final orientation of the electrical connection of the accelerometer, making it difficult to successfully route cables. A mechanical insert was designed to fit into a hole that was drilled in a predetermined installation location. Each insert could then be oriented in the correct direction to safely route cables back to the data acquisition system. As a mechanical insert was correctly oriented for a specific accelerometer the bottom of each insert was welded to the base of the deck-plate it was inserted in too. Accelerometer studs were threaded to each insert with a thread-locking agent as a specified install torque was applied. Stud mounting alleviated any failures of accelerometers becoming unattached for the fall 2014 harvest season.

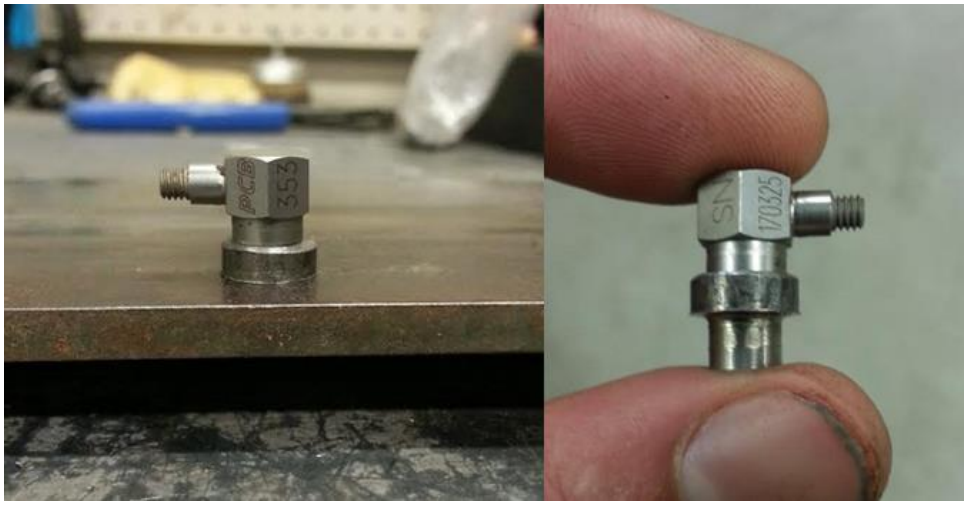

Figure 25: Stud Mounting Mechanical Insert with Accelerometer.

As accelerometers were mounted, deck-plates could then be reinstalled on the corn-head. Cables were routed inside protective polyvinyl tubing through the plastic chain-guide and back to the data acquisition system in the combine cab. Cables were secured to the surface of each deck-plate with adhesive pads and zip-ties, (Figure 26).

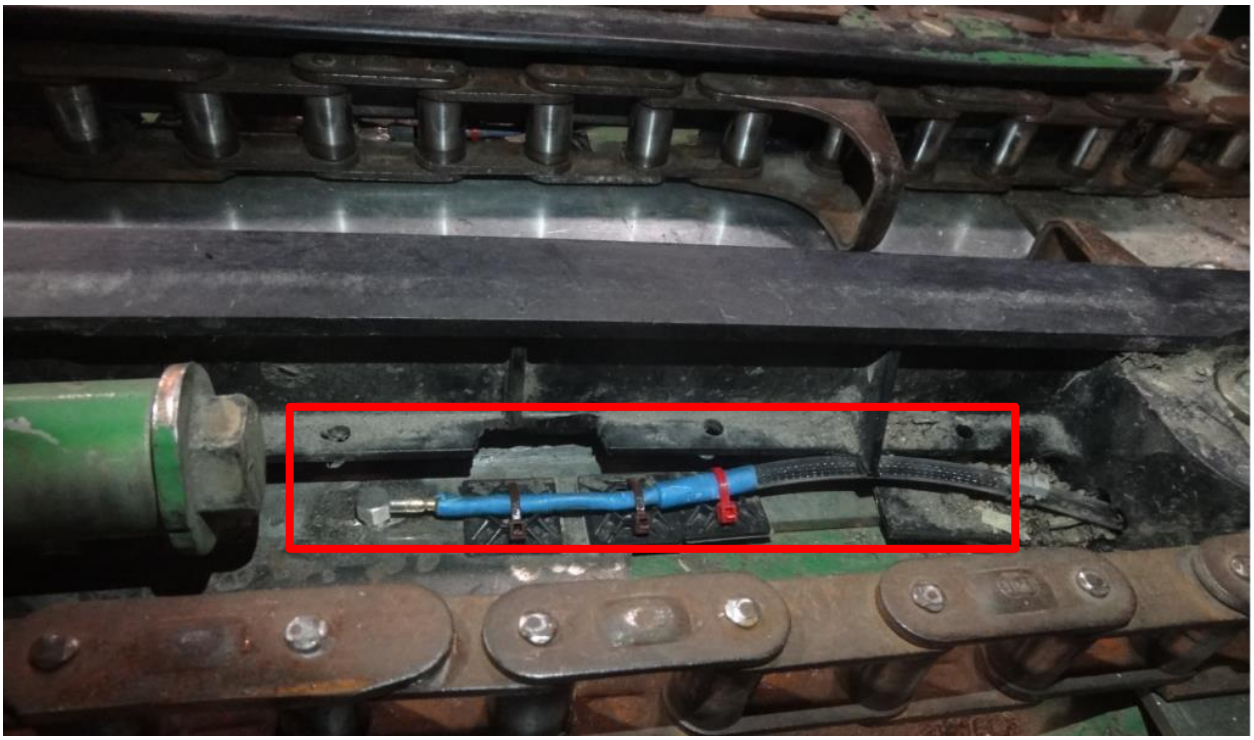

Figure 26: Final Accelerometer Installation

Final installation location for an accelerometer on a deck-plate depended on the row-unit the accelerometer was installed on. These locations will be further discussed in the full corn-head instrumentation section of the next chapter.

4.3.4 Accelerometer Validation Test

An accelerometer validation test was conducted to gain confidence in the preliminary design of the system. This test investigated if an accelerometer could predict a quantity of ears dropped on a row-unit at various speeds. It also helped to resolve other possible design issues that needed to be addressed for in-field harvest data sets.

4.3.4.1 Test Setup

The same drop-shoot used in the amplitude test was mounted above an individual row-unit of the corn-head. The drop-shoot was capable of dropping ears of corn on the deck-plates of

a row-unit at various heights. An ear of corn could be loaded into the top of the drop-shoot and dropped as a stop pin was pulled from behind the corn-head. The ear could then free-fall until it collided with the deck-plate(s) creating a shock impulse that was detected by one of the accelerometers mounted to either the fixed or adjustable deck-plates.

4.3.4.2 Test Procedure

Tests were conducted at 5 different speeds of the corn-head. At each speed, a random number of ears were dropped at a height of 3ft on to the deck-plates of a row-unit. A camera was mounted on top of the snout cover to capture the moment each ear struck the deck-plate(s). At the beginning and end of each test a wrench was used to tap the deck-plate to create a shock impulse in the accelerometer data file. This shock impulse could later be identified in the acceleration data and video evidence. Both time-series could then be synced. After an initial shock impulse was created the corn-head was turned on to a pre-selected speed. Individual ears were dropped with a short duration between each of them to reload the drop shoot. Once tests were completed synced acceleration and video data could be used to determine if a shock impulse was created at the moment an ear made contact with the deck-plate.

4.3.4.3 Results

Accelerometer data was used to predict the random number of ears dropped at each speed of the corn-head. A minimum amplitude of 60g was used to detect peaks in the acceleration data that exceeded this value. If multiple values exceeded 60g the highest of these values inside a 0.5 second window was taken as the peak amplitude. Peak detection parameters will be further discussed in the next chapter. Each identified peak in the acceleration data had a corresponding time-series value associated with it. Known time-series values from detected peaks at each speed of the corn-head were compared against synced video to determine if detected peaks were the results of an ear impact. Over the 5 different speeds, 37 ears of corn were dropped on the deck-plates of a row unit. Of the ears that were dropped, 33 out of 37 were successfully detected. Of the 33 that were successfully detected, 5 out of 33 were detected by both accelerometers mounted on fixed and adjustable deck-plates. The other 28 out of 33 were only detected by a single accelerometer on either a fixed or adjustable deck-plate. Similar to the previous drop test, video evidence showed that the 4 undetected ears either engaged the snout-covers or gathering-chains before they made contact with the deck-plate. The following figures are time-series plots

of the acceleration data from both fixed and adjustable deck-plates at various test speeds of the corn-head. For each figure, the following list of identification techniques were used to identify key events.

- Red triangles indicate the actual moment of an ear impact in the time-series
- Green boxes indicate that an ear impulse was only detected on a single deck plate
- Orange boxes indicate that an ear impulse was detected on both deck plates
- Impulses on each end of the fixed deck plate signal were created by tapping the deck plate to create a time stamp in the acceleration data

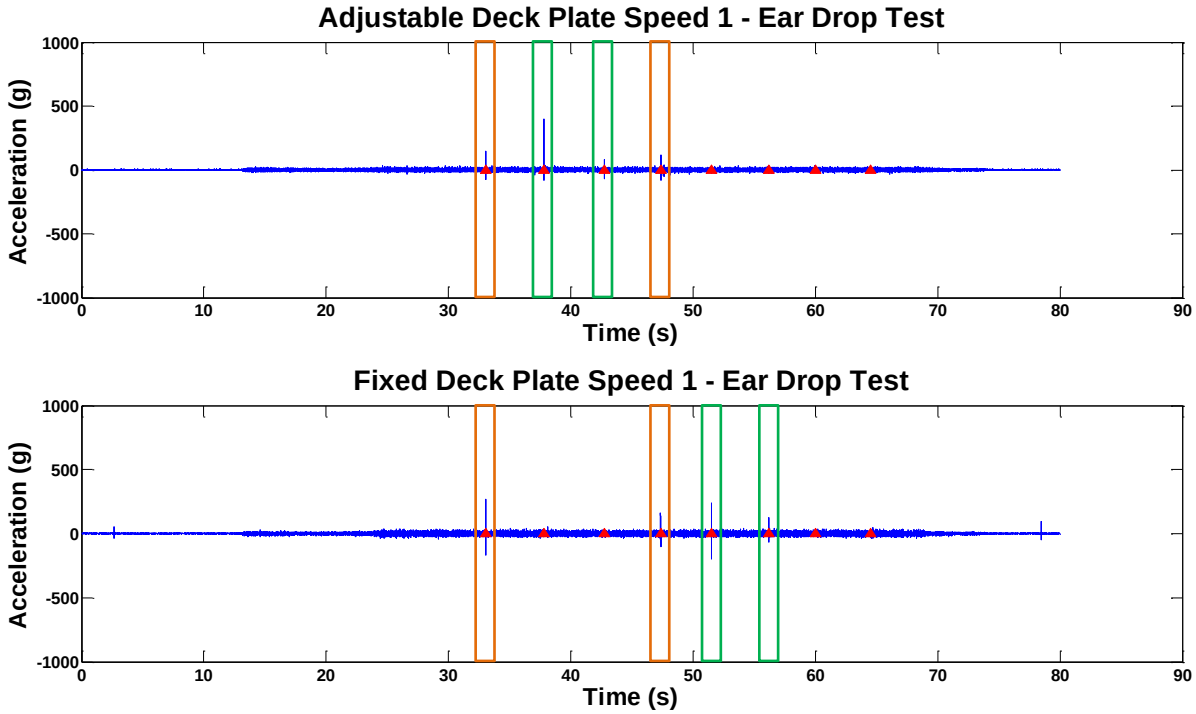

Figure 27: Accelerometer Validation Test - Speed 1 (6 out of 8 ears detected)

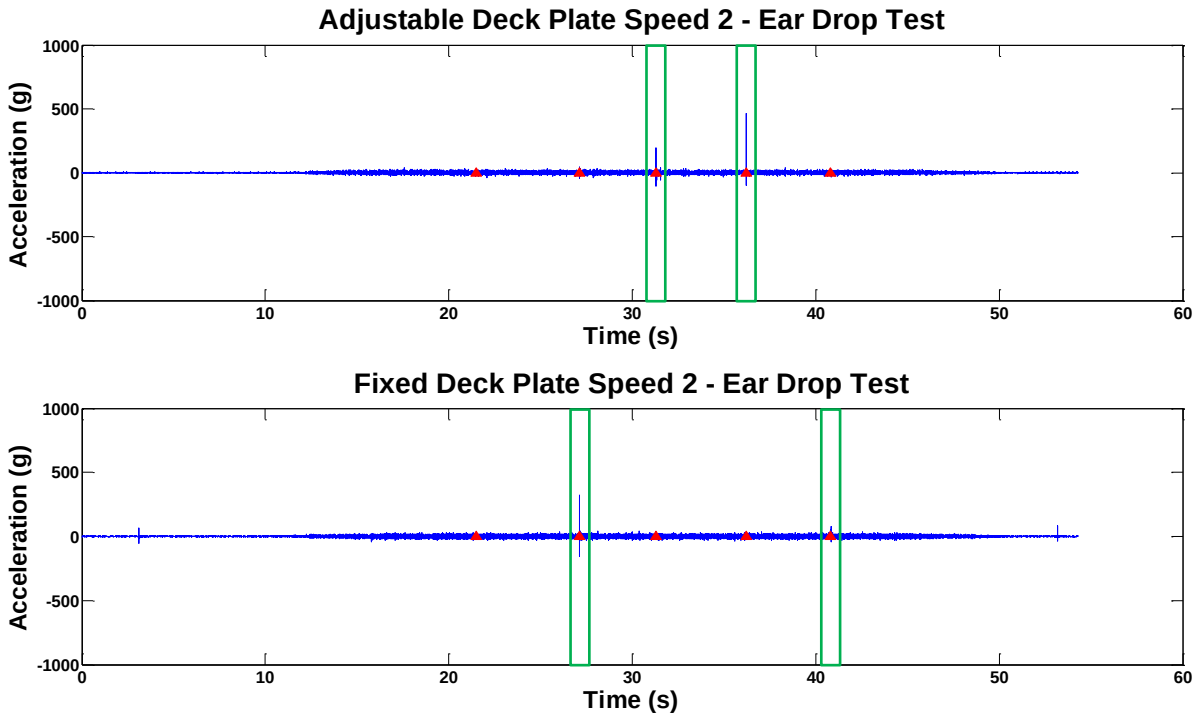

Figure 29: Accelerometer Validation Test - Speed 2 (4 out of 5 ears detected)

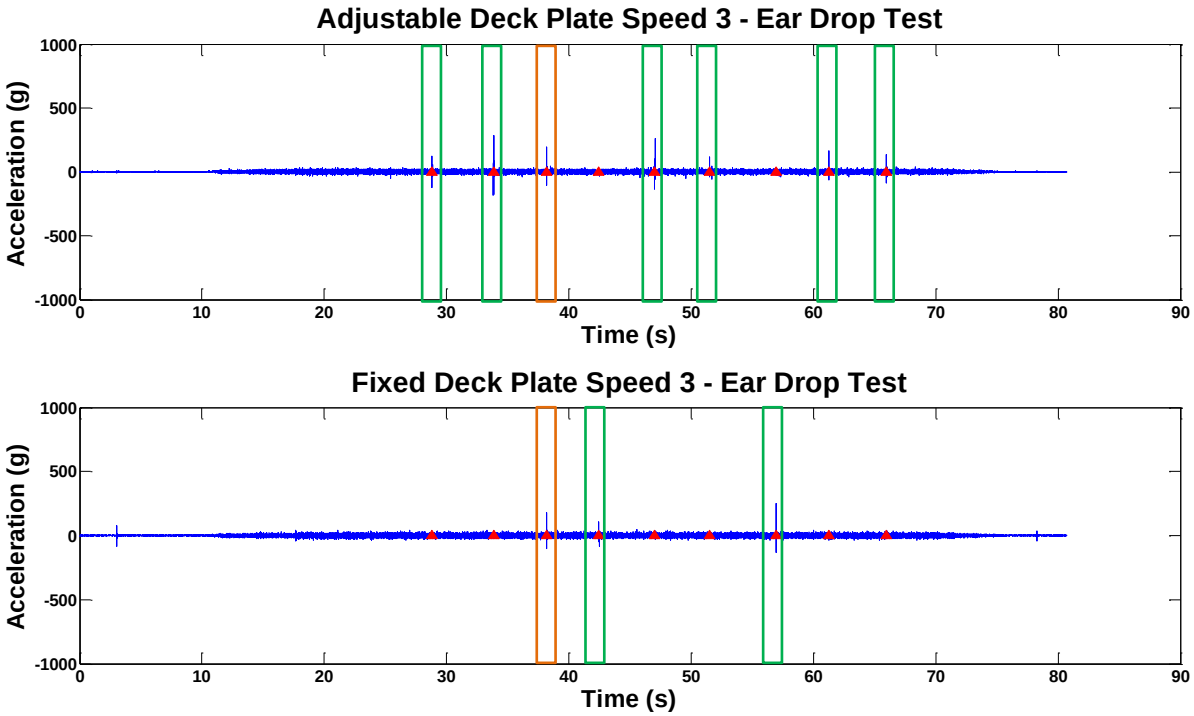

Figure 28: Accelerometer Validation Test - Speed 3 (9 out of 9 ears detected)

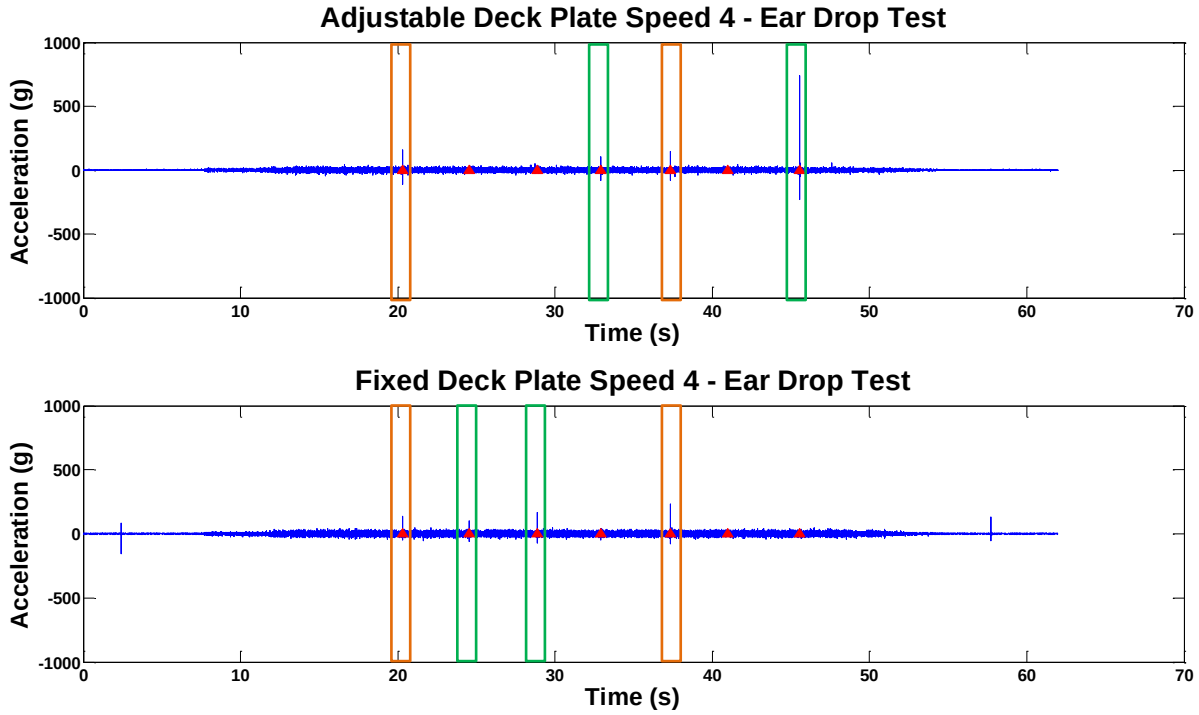

Figure 30: Accelerometer Validation Test - Speed 4 (7 out of 8 ears detected)

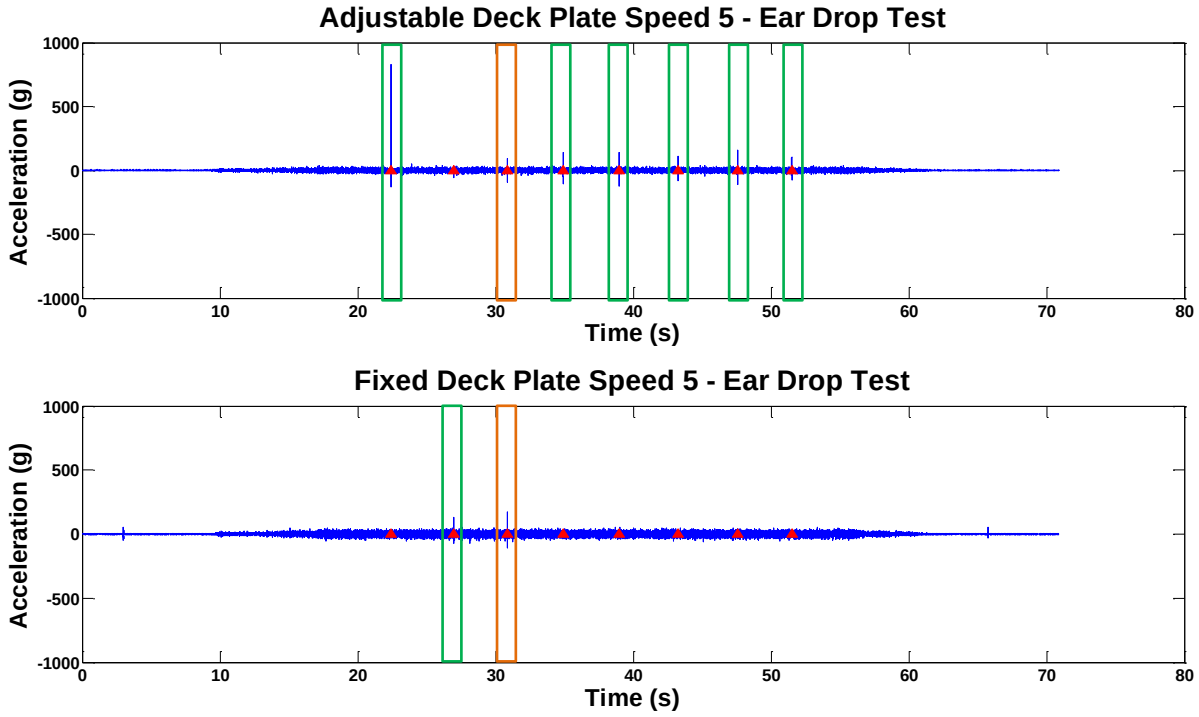

Figure 31: Accelerometer Validation Test - Speed 5 (9 out of 9 ears detected)

4.4 Conclusion

The preliminary design process was successful in identification of accelerometer specifications and an installation location. An accelerometer validation test generated confidence with several time-series plots. These time-series plots demonstrated that the selected, PCB 353B11, acclerometers could detect shock impulses as ears impacted a deck-plate. These tests further presented that predictive ear counts methods are possible with acceleration data and these methods will be further quantified in the next chapter. Additionally, it was seen that an ear impact could register a shock impulse on both deck plates. This will need to be taken into consideration when quantifying a predictive ear count for a single row. Overall, the preliminary design of system met the key requirements and identified other possible issues that need to be address in the next chapter.

CHAPTER 5: SECTIONAL HEADER CROP FLOW

5.1 Introduction

The long-term goal of this research was to identify a method to produce secondary yield information across the swath width of a corn-head. This information could then be used as a correction for current yield data. Accelerometers were selected as the sensor of choice for this project. They were used to detect the difference between the crop material and machine noise that engaged the deck-plates of a corn-head. The differences found between signals will be later quantified and discussed.

In this section, the setup, control and collection of in-field test data will be presented. Predictive algorithm concepts will be discussed and evaluated for performance. Results will quantify how well each algorithm can generate a predictive ear count value. The main objectives of this section are to:

- Quantify if accelerometer data can be used to predict ear count on an individual row basis
- Quantify and normalize variation of a predicted measurement across different rows of a corn-head

5.2 Materials and Methods

5.2.1 Full Corn-Head Instrumentation

For fall 2014 in-field harvest tests, a 16 row corn-head was instrumented with 20, PCB 353B11 accelerometers. These accelerometers were installed on 8 rows of a 16 row corn-head. Every other row was targeted, starting at the outside rows of the 16 row corn-head and moving inward. This was done to produce data across the entire swath width. The quantity of accelerometers installed on each row and deck-plates of that row are listed below:

- Two accelerometers were installed at two different locations (location A and B) on fixed and adjustable deck-plates of rows 1 and 16.
- One sensor was installed at the same location (location C) on fixed and adjustable deck-plates for rows 3, 5, 7, 10, 12 and 14.

As described above, accelerometers were placed in 1 of 3 locations depending on which row-unit they were installed on. These A, B and C locations are further dimensioned for an adjustable deck-plate (Figure 33). These same locations were mirror for a fixed deck-plate. The variation between installation locations A and B, for rows 1 and 16, were to quantify if location add an effect on ear count prediction.

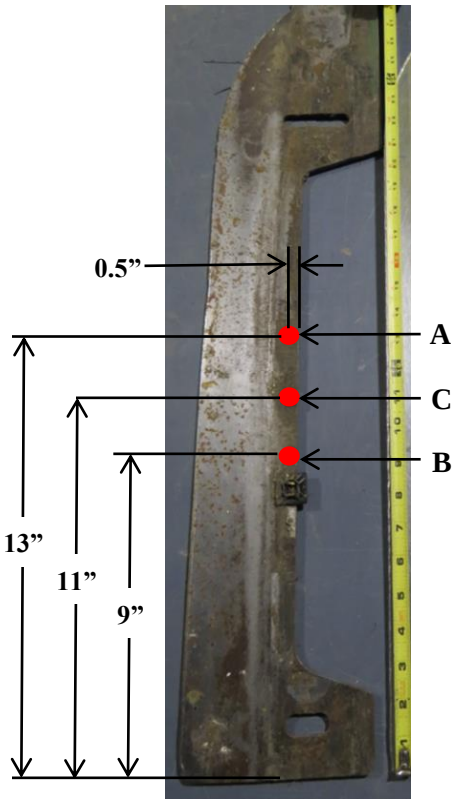

Figure 32: Sensor Locations on an Adjustable Deck-plate

A numerical value between 1 and 20 was assigned for each location an accelerometer was installed. Serial number of each accelerometer was tied to these values. Calibrated sensitivity factors from the manufacturer could be applied to data that each accelerometer produced (Figure 33, Table 4).

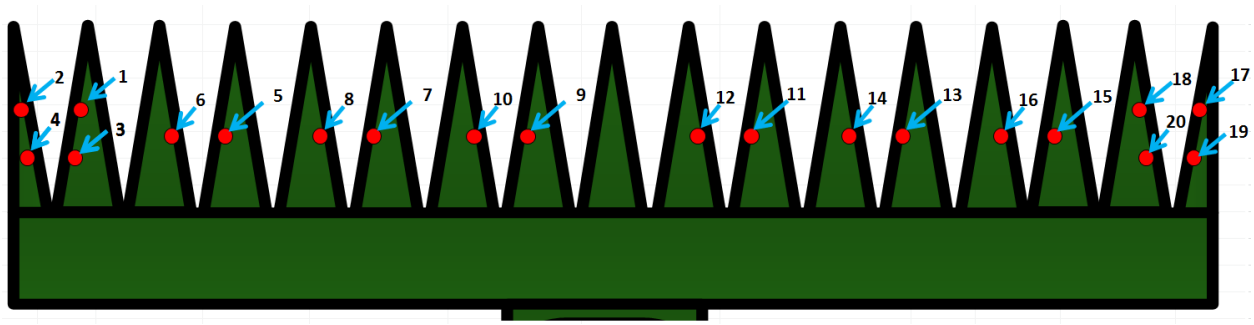

Figure 33: Corn Head Instrumentation Setup

Table 4: Corn Head Instrumentation Setup

Instrumentation Setup								
Sensor #	Row #	Deck-plate	Sensor Type	Sensor Position	CRIO Channel #	Sensor Serial Number	Sensor Sensitivity	
1	1	Fixed	Accelerometer	A	1	170651	5.10	mV/g
2	1	Adjustable	Accelerometer	A	2	166374	5.05	mV/g
3	1	Fixed	Accelerometer	B	3	166375	4.93	mV/g
4	1	Adjustable	Accelerometer	B	4	171016	4.61	mV/g
5	3	Fixed	Accelerometer	C	5	170324	4.97	mV/g
6	3	Adjustable	Accelerometer	C	6	170653	5.10	mV/g
7	5	Fixed	Accelerometer	C	7	170650	5.07	mV/g
8	5	Adjustable	Accelerometer	C	8	171017	4.66	mV/g
9	7	Fixed	Accelerometer	C	9	171015	5.43	mV/g
10	7	Adjustable	Accelerometer	C	10	170654	5.07	mV/g
11	10	Fixed	Accelerometer	C	11	170323	4.93	mV/g
12	10	Adjustable	Accelerometer	C	12	170325	5.05	mV/g
13	12	Fixed	Accelerometer	C	13	171013	5.42	mV/g
14	12	Adjustable	Accelerometer	C	14	171012	4.93	mV/g
15	14	Fixed	Accelerometer	C	15	171018	4.93	mV/g
16	14	Adjustable	Accelerometer	C	16	170648	5.10	mV/g
17	16	Fixed	Accelerometer	A	17	166373	5.08	mV/g
18	16	Adjustable	Accelerometer	A	18	179035	4.97	mV/g
19	16	Fixed	Accelerometer	B	19	171014	4.95	mV/g
20	16	Adjustable	Accelerometer	B	20	171019	4.98	mV/g

Once accelerometers were installed, appropriate cabling was routed from each accelerometer to the back of the corn-head. Cables were routed to a junction box which was attached to the feeder house of the combine. This junction box allowed cables to be disconnected when the corn-head was transported between fields.

Figure 34: Feeder House Junction Box

Additional cables were further routed from the junction box and into the cab of the combine. Once in the cab, specific accelerometers cables were attached to predefined channels of the data acquisition system. This allowed for data to be captured in an organized manner and manufacturer sensitivity factors to be correctly applied.

5.2.2 Fall 2014 Data Set

In this section a design of experiment of the controlled and uncontrolled in-field data will be presented. The first objective of this test plan was to gather controlled ground truth and accelerometer data that could be later analyzed and used in the development of a predictive algorithm. Controlled data consisted of in-field test plots of a predefined size and controlled treatment levels. A second objective was to gather uncontrolled data in real-harvest conditions that could later be used to test an algorithm for effectiveness when compared to other sources of known information, such as NDVI maps. Uncontrolled data consisted of selecting areas in a field with natural variation in ear counts. An example would include an area of underdeveloped corn from standing water in a field. Both types of data will be further discussed in respective sections.

5.2.2.1 Controlled Data Set

Controlled data was collected as a series of test plots were harvested with accelerometers mounted on a corn-head. A combination of NVDI images and in-field inspection were used to select an area of a field with minimal variation. A combine with a 16 row corn-head was used to layout grid-like pattern of 40ft wide and 50ft long test plots.

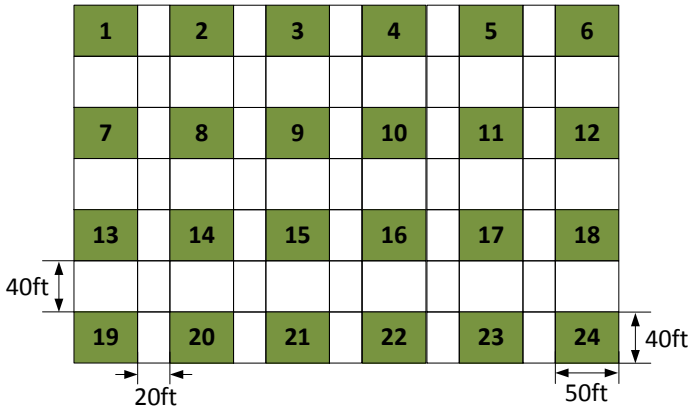

Figure 35: Example Diagram of a Controlled Test Plot

Once constructed, each test plot was assigned a unique number. Different treatment levels could then be applied across every instrumented row (1, 3, 5, 7, 10, 12, 14 and 16) of a test plot. Treatments were applied by removing plants from instrumented rows at 4 different rates, 75%, 50%, 25% and 0%, (Figure 36).

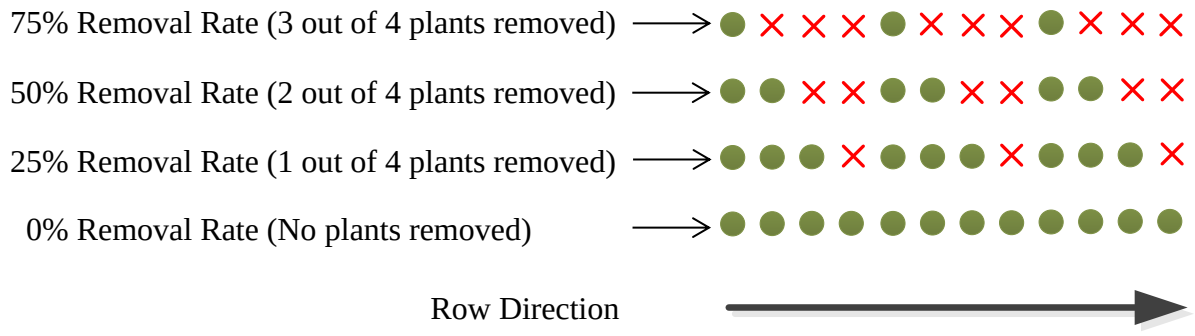

Figure 36: Treatments Levels of Controlled Test Plots

Each of the 4 treatments was randomly applied twice across the 8 instrumented rows of every test plot. This was done to minimize any effects in the data set that would result from applying the treatments. After treatments levels were applied, ears of corn in each instrumented row were hand-counted and recorded as ground truth data. Treated test plots were then harvested at a 2.5 mph travel speed with the instrumented corn-head operating at speed 1.

Figure 37: Removal of Corn Plants from Controlled Test Plots

Figure 38: Aerial View of Controlled Test Plots

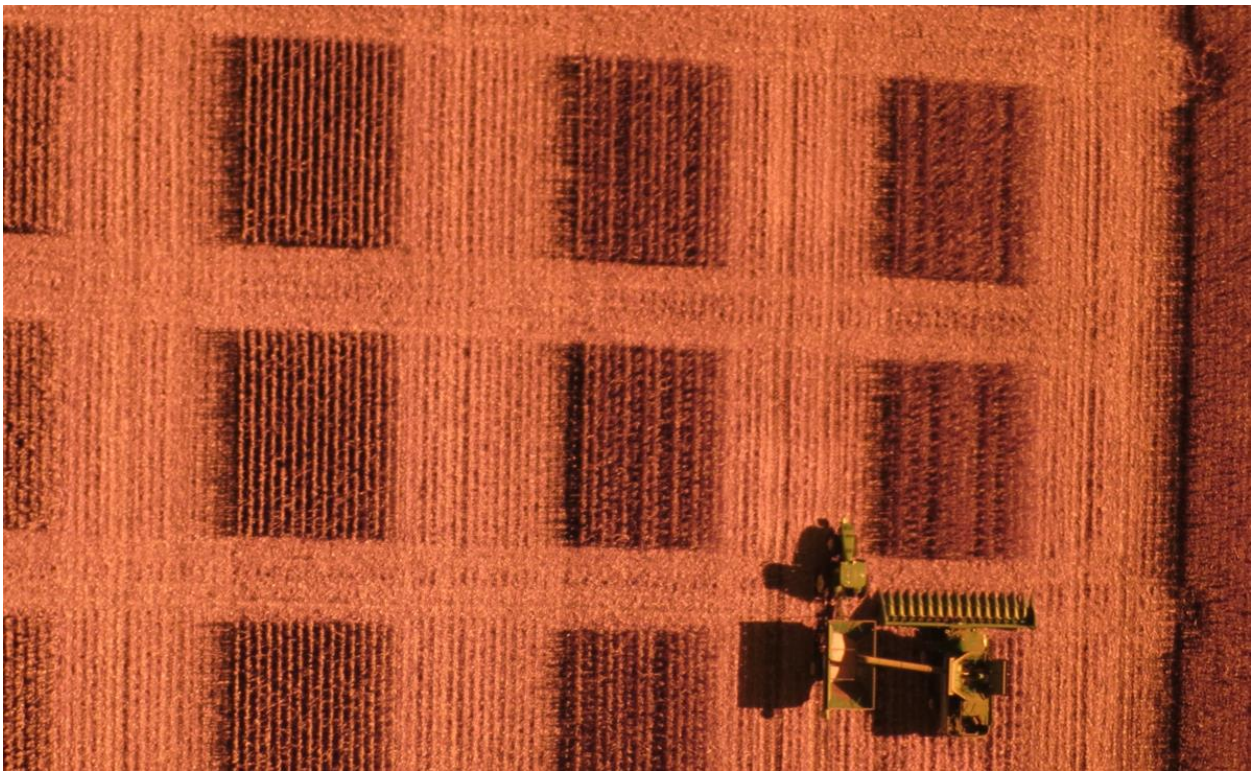

Figure 39: Harvest of Controlled Test Plots

From the controlled data that was collected, a set of 53 test plots were used in the algorithm development and results section of this chapter. Of these 53 test plots, it was found that data from rows 5, 10 and 16 had reoccurring issues with electrical connections. With data quality concerns these rows will not be considered in the results section of this thesis.

5.2.2.2 Uncontrolled Data Set

Uncontrolled data consisted of selecting areas in a field with natural variation in ear counts. An example would include an area of underdeveloped corn from standing water in a field. These areas were selected from NVDI images taken at different times throughout the growth season of the corn (Figure 40).

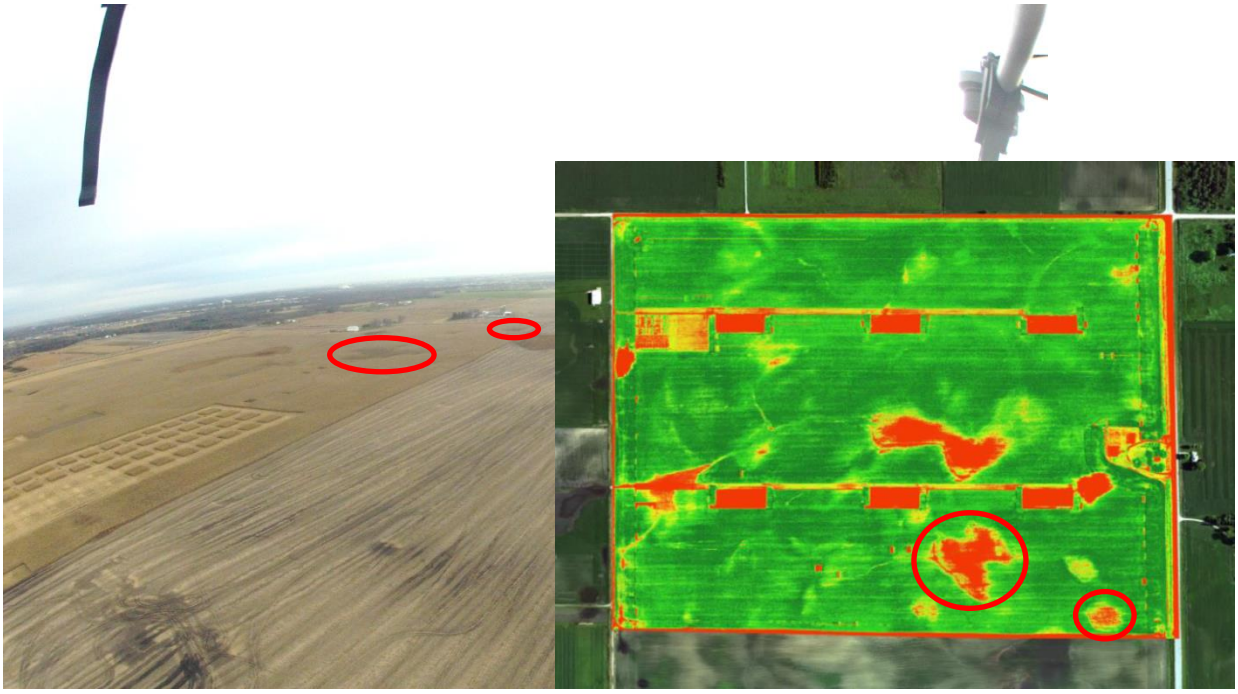

Figure 40: Identification of Uncontrolled Data Locations with Aerial and NVDI Imagery

Test plans were developed to collect pass-to-pass data as these areas were harvested. Ears were not counted as a ground truth in the instrumented rows of each pass. Video was collected in the travel direction of the combine as passes were harvested. Signals could then be compared with visual evidence from each pass. Multiple areas of uncontrolled data were collected through the fall 2014 harvest season. The goal with uncontrolled data was to gain confidence in the developed algorithm methods in real harvest conditions. These areas will be analyzed with developed algorithm and presented in the results section of this chapter.

5.2.3 Vibration Signal Theory

As mentioned in the literature review section there are two terms used to describe the mechanical excitation in a system, shock and vibration. Shock is a dynamic excitation with a short duration and vibration as a dynamic excitation with an extended duration. Shock can be considered deterministic when its amplitude can be predicted from an impulse with a known magnitude. Shock amplitudes generated by an impulse have a sharp rise in magnitude then decay shortly after an initial response. Deterministic vibrations are predictable and generally caused as small gaps in component tolerances allow a system to “wobble” or oscillate as an input force is provided. Mechanically driven systems can cause deterministic oscillations known as forced vibrations.

5.2.3.1 Forced Vibration from Gathering-Chain and Sprocket Assembly

Corn heads are large mechanically driven systems where forced vibration will undoubtedly occur. The largest of these vibrations came from gathering-chain and sprocket assemblies of a row unit. An assembly is comprised of a gathering-chain supported by two sprockets. The front sprocket is attached to a spring tensioner that provides support to the gathering-chain. The back sprocket is mechanically driven and provides power to the system (Figure 41).

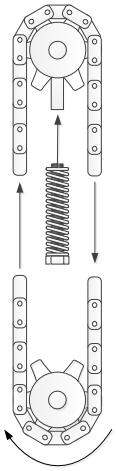

Figure 41: Gathering-Chain and Sprocket Assembly

As a gathering-chain revolves around a pair of sprockets it makes repetitive contact with multiple sprocket-teeth. A tachometer was used to find the rotational speed of a sprocket at each speed of the corn head. Contact frequency between chain-links and sprocket-teeth could then be calculated. This contact frequency coincided with a fundamental frequency from the frequency analysis of accelerometer data at each specific speed of the corn-head (Table 5).

Table 5: Frequency Analysis Gathering-Chain and Sprocket Vibration

Corn-head Speed	Sprocket Speed (RPM)	Contact Frequency of Chain-links and Sprocket-Teeth (Hz)	Fundamental Frequency of Accelerometer Data (Hz)
1	293	29.30	29.36
2	325	32.50	32.47
3	358	35.80	35.83
4	400	40.00	40.10
5	442	44.20	44.25

Periodograms were used for frequency analysis and are similar to a fast Fourier transform, as they identify key frequencies in a time-series. Periodograms detect the spectral power density of significant frequencies present in a time-series and are well equipped for time-sampled data. Frequency analysis was repeated after all gathering-chains were removed from the corn-head. Previous fundamental frequencies and harmonics were no longer invisible in each of the frequency spectrums (Figure 42). These observations made it evident that gathering-chain and sprocket assemblies were the primary source of forced vibration or noise found in accelerometer data (Figure 43).

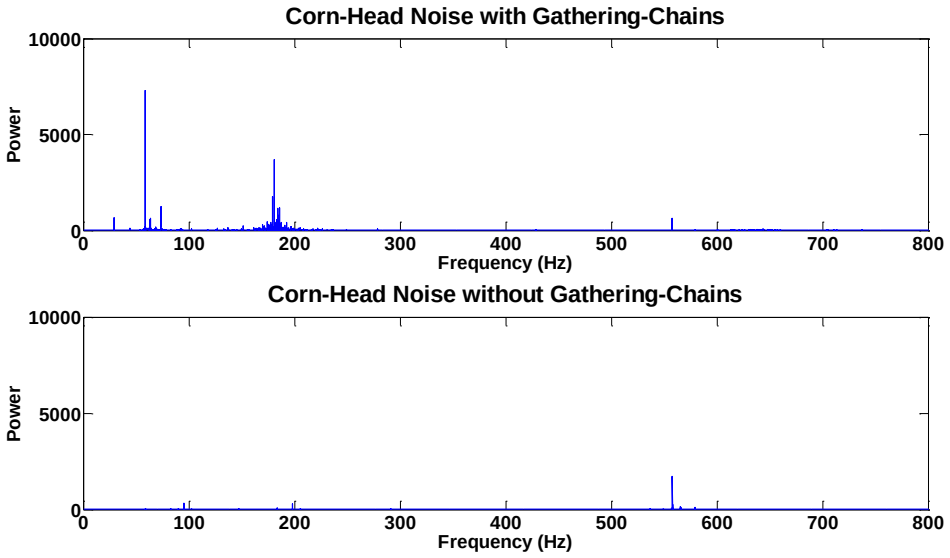

Figure 42: Frequency Spectrum of Corn Head Noise with and without Gathering Chains

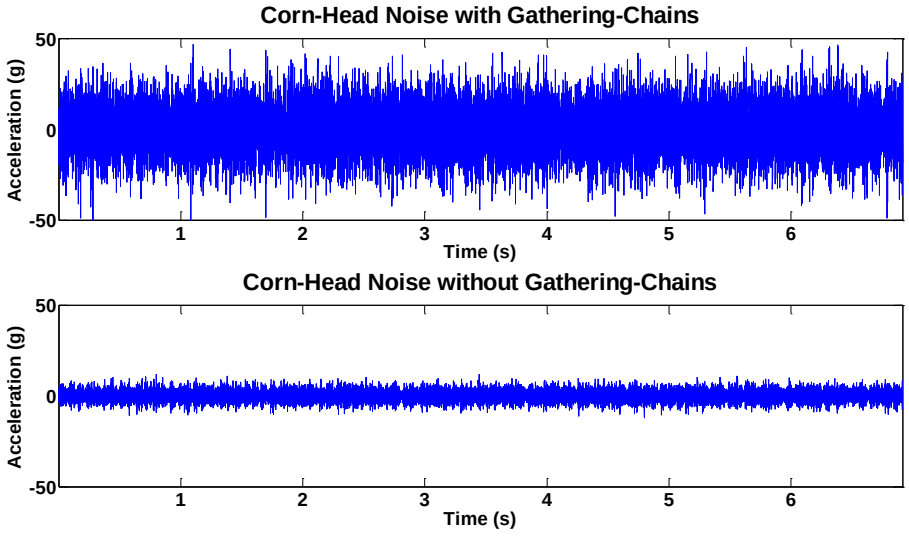

Figure 43: Time-series of Corn Head Noise with and without Gathering-Chains

Corn-head noise from the controlled data set was isolated and summarized in a cumulative distribution (Figure 44).

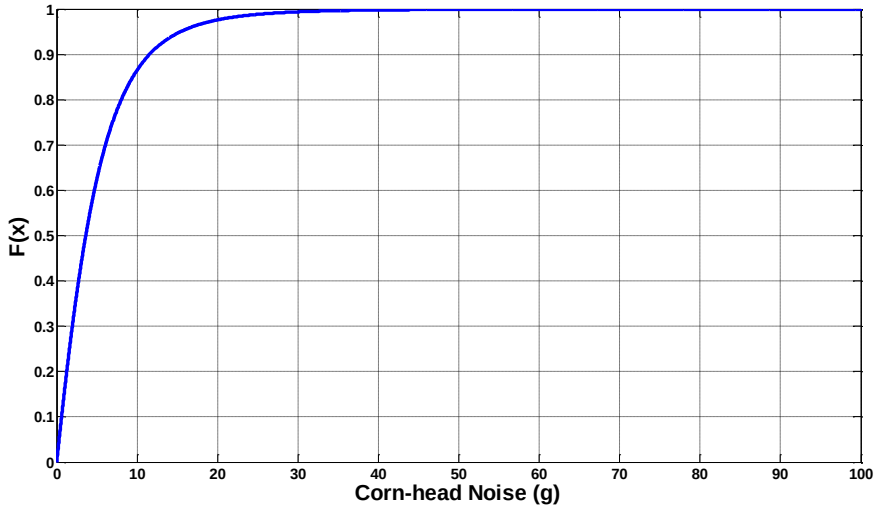

Figure 44: Cumulative Distribution of All Corn-head Noise

The cumulative distribution depicts an upper amplitude limit of corn-head noise across all rows in the controlled data set. Amplitude of the 99.9th percentile of corn-head noise was found as an approximate 48.95g. The amount of corn-head noise is an important factor with predictive ear count algorithms and will be further discussed later in this chapter.

5.2.3.2 Free Vibration from Ear Impacts

Forced vibrations are an inverse side-effect when a mechanical system is used to harvest corn. Mechanical corn-heads create a significant amount of background vibration, but are also used to generate useful vibration information related to the number of ears harvested. As stalks are pulled downward by stalk-rolls, ears attached to each stalk become dislodged as contact is made with a deck plate. The force needed to dislodge an ear from a stalk requires a deck-plate to provide an equal and opposite reaction force. Each reaction force generates a shock impulse which induces the deck-plate into free vibration with a sharp rise in magnitude that decays shortly after an initial response (Figure 45).

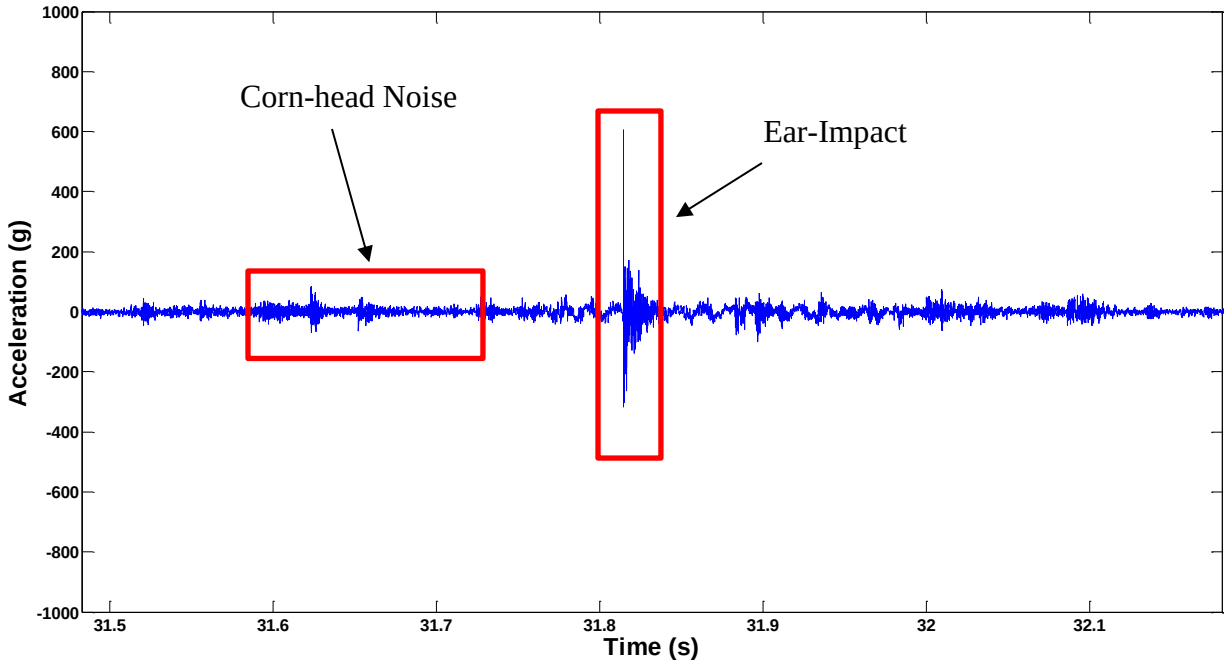

Figure 45: Ear Impact in Accelerometer Data Time-Series

Research will focus on generating ear count predictions from the differences in responses between ear impacts and forced vibrations of the corn-head.

5.2.3.3 Frequency Filtering

As previously discussed, the gathering-chain and sprocket assembly forced the deck-plate to vibrate with a known fundamental frequency related to the speed at which the corn-head was operated. Fundamental frequencies were determined at each speed of the corn-head. These frequencies and harmonics were targeted with low-pass and band-stop filters. Amplitudes from ears impacts and corn-head noise both experienced significant reductions when digital filters were applied. It was significantly difficult to target the corn-head noise without disruption of the short, transient impulse signals from ear impacts. For this reason, frequency filtering was not applied when results were analyzed.

5.2.4 Development of a Peak Detection Algorithm

5.2.4.1 Peak Detection Algorithm

Peak detection uses accelerometer data to monitor deck-plate shock impulses from ear impacts that are above the background noise of a corn-head. The peak detection algorithm was

developed in MATLAB and uses several input parameters to identify a shock impulse or peak in a time-series of acceleration data. These input parameters are defined and depicted in a graphical abstract of the peak detection algorithm (Figure 46).

Minimum Peak Height

– is the minimum amplitude a peak must obtain before it can be considered a peak.

Minimum Peak Threshold

– is the minimum difference in amplitude between neighboring values to be considered a peak.

Minimum Peak Window

– is the minimum amount of time required to elapse after one peak is detected and another can be considered.

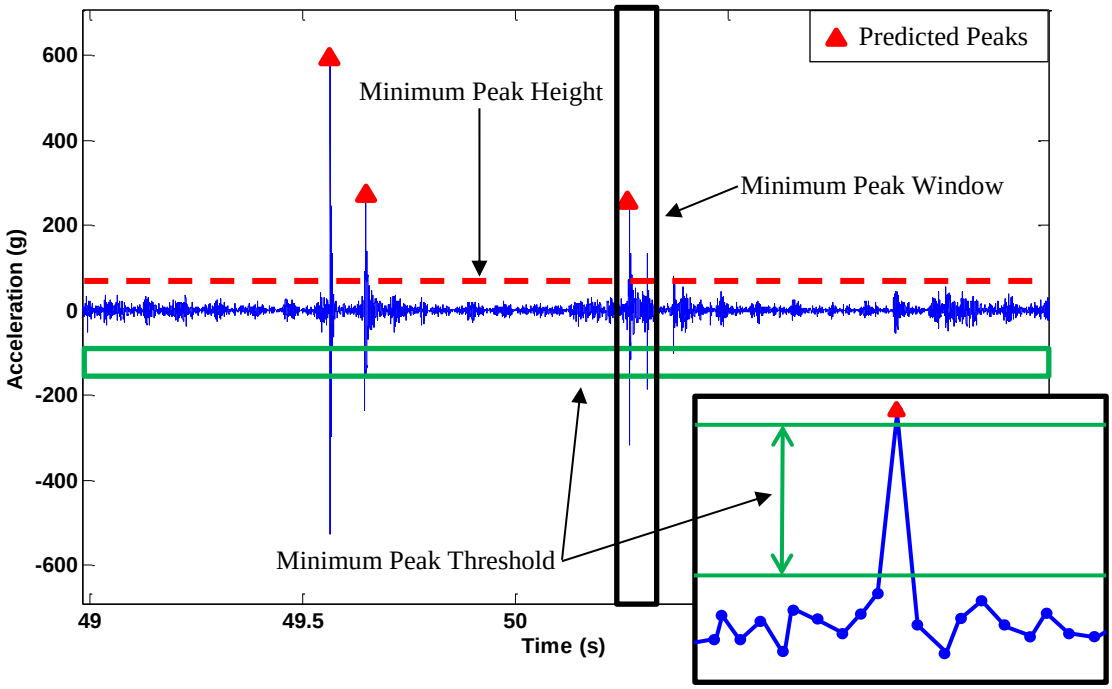

Figure 46: Graphical Abstract of Peak Detection Algorithm

Of the input parameters, the minimum peak window was the only initially set parameter at 50 milliseconds and allowed an individual row unit to detect up to 20 ears per a second. Most typical harvest applications would not exceed this value as row units are limited to a maximum throughput at different harvest speeds and plant populations (Table 6). For this research, harvest

speeds and plant populations kept the expected ear flow rate well within the 20 ears per a second limit. If higher rates were expected, the minimum peak window could be adjusted.

Table 6: Expected Ear Flow Rates for an Individual Row (Ears/s)

		Combine Speed (mph)							
		1	2	3	4	5	6	7	8
Plant Population	30000	2.5	5.1	7.6	10.1	12.6	15.2	17.7	20.2
	32000	2.7	5.4	8.1	10.8	13.5	16.2	18.9	21.5
	34000	2.9	5.7	8.6	11.4	14.3	17.2	20.0	22.9
	36000	3.0	6.1	9.1	12.1	15.2	18.2	21.2	24.2
	38000	3.2	6.4	9.6	12.8	16.0	19.2	22.4	25.6
	40000	3.4	6.7	10.1	13.5	16.8	20.2	23.6	26.9
	42000	3.5	7.1	10.6	14.1	17.7	21.2	24.7	28.3
	44000	3.7	7.4	11.1	14.8	18.5	22.2	25.9	29.6

As ears enter the row unit, the peak detection algorithm relies heavily on efficient energy transfer as an ear impacts the deck-plate(s). If ears do not make contact with the deck-plate(s) there will be no shock impulses to monitor in the accelerometer data. If an ear makes contact with both deck-plates a shock impulse could appear in accelerometer data from each deck-plate. When shock impulses are used to predict ear counts this can lead to double counting individual ears and an over-estimation in the predicted number of ears harvested. The final peak detection algorithm used accelerometer data from both fixed and adjustable deck-plates to generate a predictive ear count. Double counted shock impulses found inside the same minimum peak window of fixed and adjustable deck-plates were adjusted to represent a single ear in predicted ear counts. Double counting and optimal input parameters of the peak detection algorithm will be further discussed in the results section of this chapter.

Shock impulses were detected as the peak detection algorithm was implemented on individual row units (Figure 47). Amplitudes and locations of peaks are found in the acceleration time-series and marked with a red triangle to visually identify them. The red lines indicate the start and end of the crop zone.

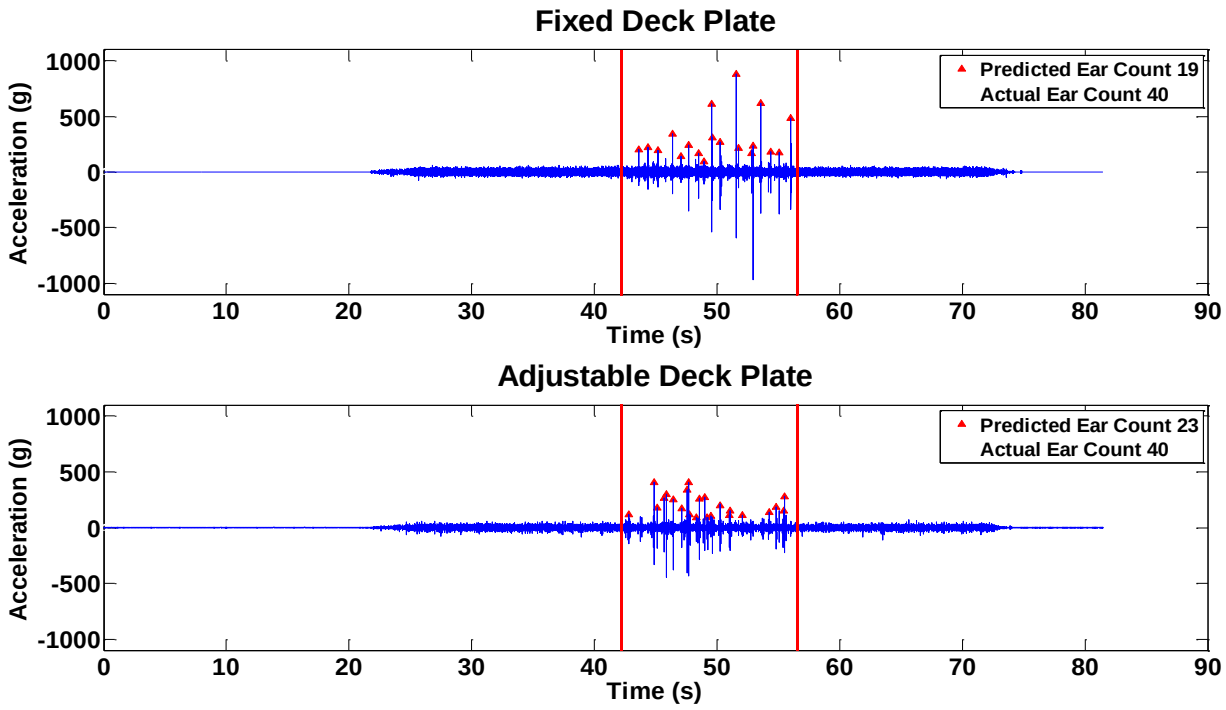

Figure 47: Peak Detection Algorithm Implemented on Deck-Plates of an Individual Row Unit

5.2.4.2 Normalization of Peak Detection Algorithm across Different Rows of a Corn Head

The objective of peak detection normalization is to have row units which generate similar ear count predictions across different rows of a corn-head. For the peak detection algorithm, predictions were normalized about the expected number of ears in a row for a predetermined distance. Estimation for this expected number of ears was calculated based off the number of ears found in the controlled test runs with a 0% plant removal rate. An expected ear count of 87.8 ears was calculated for the 50ft test plot increments.

For the controlled data set, a mean ear count prediction was produced for each row unit. Mean predictions used only individual 50ft rows with 0% plant removal rate from controlled test plot data. These were the rows without an applied treatment factor. Mean and expected ear count predictions were then used to normalize the rest of the treated 50ft test runs from the controlled data set. Original predictions were scaled to a normalized value by the ratio of expected ears to mean predicted ears of each row unit (Equation 6).

Equation 6: Normalization of a Row Unit Ear Count Prediction with a Scaled Factor

$$Normalized\ Prediction = Original\ Prediction * \left(\frac{Expected\ Ears}{Mean\ Predicted\ Ears}\right)$$

To illustrate this normalization process, assume that an expected 100 ears was calculated over a 50ft increment. Multiple 50ft increments were then harvested with an ear count prediction generated for each pass. The mean ear count prediction for these multiple passes is 125 ears. As the next 50ft pass is harvested, a prediction of 120 ears is produced; this original prediction would then be scaled to a normalized prediction of 96 ears (Equation 6).

Another normalization method was investigated to offset predictions by the difference between the expected and mean predicted ear counts. This method worked well in healthy crop with high and consistent ear counts. When crop began to deviate from these conditions the offset would cause an excessive shift in the normalized predictions. For this reason normalization with an offset was avoided.

5.2.5 Development of Crop Intensity Algorithms

5.2.5.1 Crop Intensity Algorithm

Crop intensity was an arbitrary value used to describe a discrete energy measurement of vibration data from a combination of fixed and adjustable deck-plates over a period of time. In an accelerometer data series, each acceleration term can be divided by the data sampling rate to produce a velocity term for each accelerometer sample (Equation 7).

Equation 7: Calculated Velocity Term from Acceleration Data

$$\boldsymbol{v = \int a * dt = \int a * \frac{1}{Fs}}$$

The absolute value of each velocity term is taken to create an absolute velocity term for each sample. Absolute velocity terms can then be summed over a period of time to find an absolute velocity summation of the accelerometers mass. This summation of absolute velocity terms over a period of time is known as a crop intensity value (CI), (Equation 8).

Equation 8: Crop Intensity from the Summation of Absolute Velocity Terms

$$CI = \sum_{i=0}^{t} |v_i|$$

Crop intensity is similar to a measurement that would be used in personal activity monitoring devices worn by individuals to monitor ones daily activity levels. Crop intensity

increases as shock impulses from ear impacts generate large amplitude changes in accelerometer vibration data. As discussed, crop intensity values are produced as absolute velocity terms are summed over a period of a time series (Figure 48). Red lines indicate the start and end of the crop zone.

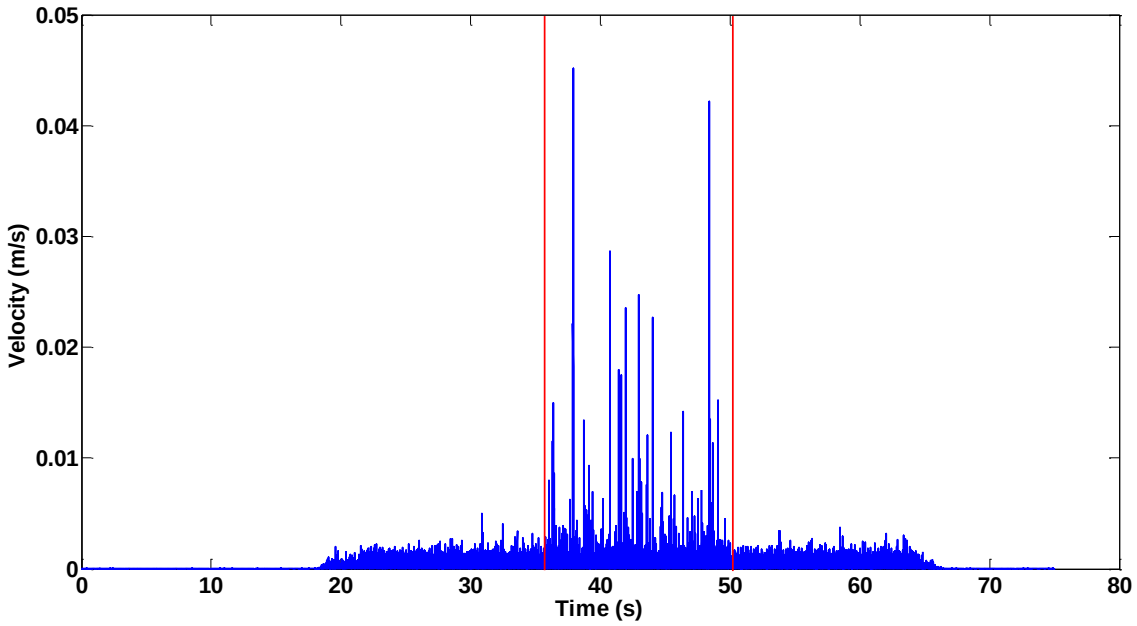

Figure 48: Time-Series Plot of Absolute Velocity Terms

Another method was investigated and is similar as it was the summation of velocity squared terms over a period of time. The method came from the kinetic energy equation and the constants of one half the mass were dropped from the equation (Equation 9).

Equation 9: Kinetic Energy Value from Summation of Squared Velocity Terms

$$KE = \sum_{i=0}^{t} v_i^2$$

As small velocity terms were squared, there was an increase in variation among kinetic energy summation measurements. This was due to the squaring of small velocity terms that were less than one. For this reason, this method was no longer considered and only crop intensity was used.

5.2.5.2 Normalization of Crop Intensity Algorithms across Different Rows of a Corn Head

The objective of crop intensity normalization is to have row units which generate similar predictions across different rows of a corn-head. For the crop intensity algorithm, there is not an expected crop intensity value that can be calculated for a set of given crop conditions. The crop intensity measurement is an arbitrary value that will remain relative and unit-less across different row units. Normalization must be done on a relative scale for the predictions of individual instrumented row units. From the controlled data set, test runs with the 0% plant removal rate were used to generate a mean crop intensity prediction for each individual row unit over a 50ft increment. An overall mean crop intensity prediction for the entire corn-head was found from the individual means of each row unit. Individual and overall means were then used to normalize the rest of the treated 50ft test runs from the controlled data set. These original crop intensity predictions from treated test plot data were then scaled to a normalized value by a ratio of the overall mean crop intensity for the entire corn-head to an individual mean crop intensity of a row unit (Equation 10).

Equation 10: Normalization of Crop Intensity Predictions

$$Normalized\ CI\ Prediction = Original\ CI\ Prediction * \left(\frac{Overall\ Mean\ CI}{Individal\ Mean\ CI}\right)$$

To illustrate this normalization process, assume that an overall mean crop intensity value of 400 was found for all 50ft increments at the 0% plant removal rate. Also assume that an individual mean crop intensity value of 500 was found with the 50ft increments at the 0% plant removal rate for a single row unit. As the next 50ft pass is harvested, a crop intensity prediction of 525 is produced; this original prediction would then be scaled to a normalized prediction of 420 (Equation 10).

5.2.6 Data Processing

Predictive algorithms were applied to accelerometer data from fixed and adjustable deck-plates of the instrumented row units. Peak detection and crop intensity algorithms respectively produced a predicted ear count or crop intensity value for each row of a treated test plots. Linear regression analysis was used to measure the performance of algorithm predictions for individual row units and the entire corn-head. For this analysis, linear regression models were produced for individual row units with ground truth ear counts versus predicted ear counts or crop intensity

predictions. Linear regression models provided several key parameters to allow comparison of algorithm predictions across different row units. A high coefficient of determination (R^2) is desired for all models. For the peak detection algorithm, it is desired to have a slope that would approach 1, as this would provide a model with a high sensitivity of expected input to predicted output. A numeric slope requirement was not identified for the crop intensity algorithm as an expected value for crop intensity is unknown. It is still desired to have a high slope for crop intensity. The last key parameter of the linear regression models is the variation or standard deviation in slope among row units. Minimum variation in slope among row units will allow a corn-head to produce similar prediction values from row to row. Initially, input parameters for the peak detection algorithm were used to minimize the standard deviation among row units. Normalization methods further address the minimization and control of the standard deviation of slope among row units. Residual analysis was conducted to analyze the before and after effects the normalization methods had on the original predictions of the controlled data set. Lastly, both algorithms used an uncontrolled training data set to normalize an uncontrolled test run over 5ft increments. Smaller increments and resolution limits will be discussed at the end of the results section. Uncontrolled test run data was further presented before and after normalization was applied for each algorithm. After normalization, uncontrolled test run data was plotted against the grain mass flow rate of the combine and response times of the different measurements were compared.

5.3 Results and Discussion

5.3.1 Analysis of Algorithm Predictions between Installation Locations A and B

As discussed in a previous section of this chapter, there were two possible accelerometer installation locations, A and B, on deck plates of row 1. Accelerometers were installed at these locations to investigate if a different installation location had an effect on algorithm predictions. Each prediction algorithm was applied across the controlled data set. For analysis, a null hypothesis of no difference in the predicted mean between location A and B was made. The null hypothesis was evaluated with a paired t-test by comparing the differences between algorithm predictions at each of the locations.

5.3.1.1 Paired T-Test for the Mean Predicted Ear Counts of the Peak Detection Algorithm

As described, a paired t-test was used to compare the mean predicted ear count produced at different accelerometer installation locations A and B. An alpha value of 0.05 was assumed to perform the statistical analysis in Minitab. Results presented a p-value of 0.398, which is much greater than 0.05. From this it can be concluded that there is no significant statistical difference between the mean predicted ear counts produced at accelerometer installation locations A and B with the peak detection algorithm. Statistical analysis performed in Minitab includes a summarization table, 95% confidence interval for the mean difference, T-statistic and P-value.

Table 7: Paired T-Test Results of the Mean Predicted Ear Counts from Accelerometer Installation Locations A and B

	N	Mean	St Dev	SE Mean
Difference	53	0.83	7.089	0.974
95% CI for mean difference: (-1.124, 2.784)				
T-Test of mean difference =0 (vs not = 0), T-statistic = 0.85, P-Value = 0.398				

The fundamental principle of this measurement is to detect the presence of shock impulses as it meets conditional criteria. It is known that a shock impulse excites the whole mass of the deck-plate not just a single part. If a minimum change in acceleration is the only conditional requirement, it should be clear how locations A and B can produce very similar ear count predictions.

5.3.1.2 Paired T-Test for the Mean Crop intensity Predictions of the Crop Intensity Algorithm

As described, a paired t-test was used to compare the mean crop intensity values produced at different accelerometer installation locations A and B. An alpha value of 0.05 was assumed to perform the statistical analysis in Minitab. Results presented a p-value of 0.000, which is much less than 0.05. From this it can be concluded that there is a significant statistical difference between the mean crop intensity values produced at accelerometer installation locations A and B with the crop intensity algorithm. Statistical analysis performed in Minitab includes a summarization table, 95% confidence interval for the mean difference, T-statistic and P-value.

Table 8: Paired T-Test Results of the Mean Crop Intensity Values from Accelerometer Installation Locations A and B

	N	Mean	St Dev	SE Mean
Difference	53	67.89	9.32	1.28
95% CI for mean difference: (65.32, 70.45)				
T-Test of mean difference =0 (vs not = 0), T-statistic = 53.03, P-Value = 0.000				

The fundamental principle of the crop intensity measurement is to sum all of the free deck-plate vibration generated from shock impulses. Deck-plates also experience a forced vibration cause by mechanically driven components of the corn-head. When a deck-plate is not in free vibration it will return to the forced vibration provided by the corn-head. The crop intensity algorithm does not distinguish between the two different types of vibration. A crop intensity measurement collects both forced and free vibration, unlike the peak detection algorithm which only monitors if a shock impulse meets conditional criteria. For this reason, it should be clear how deck-plate locations A and B could produce different crop intensity values. Furthermore, just because crop intensity measurements are different does not mean that they will not correlate with ground truth data.

5.3.2 Performance of the Peak Detection Algorithm

5.3.2.1 Definition of Performance Constraints for Peak Detection Algorithm

The main performance goal for the peak detection algorithm was to identify a set of optimal input parameters that would provide the greatest prediction capabilities across all instrumented rows of the corn-head. The next several paragraphs will focus on double counting of ears and performance constraints that will guided in the selection of an optimal set of input parameters. Prediction capabilities of a peak detection algorithm will be quantified once a set of parameters is identified.

Linear regression analysis was conducted with predicted and ground truth ear counts from 53 controlled test plots. This analysis produced a linear prediction model with R^2 and slope values for each of the instrumented row units. R^2 values measured how well predicted and ground truth ear counts correlated when the peak detection algorithm was used. Slope from linear regression models described the sensitivity of the peak detection algorithm. Sensitivity is the ratio of output of predicted ears detected by the algorithm, over the input of actual ears that entered the row unit. An ideal sensitivity of the peak detection algorithm would be a ratio of 1, a

predicted ear for every ear that entered a row unit. The accelerometer validation test in the preliminary design chapter showed that ears could be double counted if an ear made contact with both deck-plates. When predicted ear counts were adjusted for double counted ears, the slope of the regression lines shift from above 1 to below 1, (Figure 49).

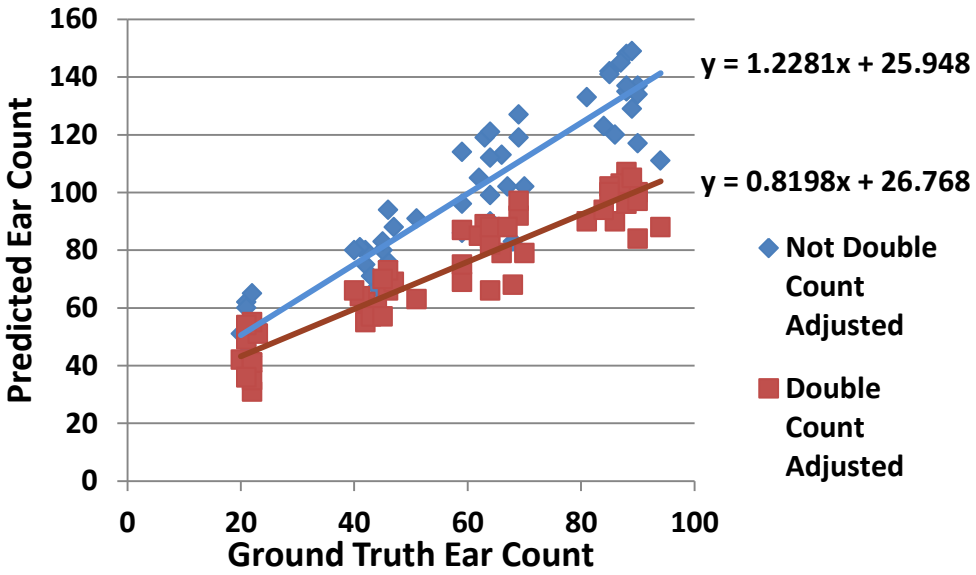

Figure 49: Linear Regression Model with Double Count Adjusted Ear Count Predictions

All instrumented row units experienced a similar shift in slopes as predicted ear counts were adjusted for double counted ears. If a linear regression model has an intercept of 0 and a slope greater than 1, the peak detection algorithm would consistently produces predictions higher than the number of ears that entered a row unit. As predicted ear count values were adjusted for double counted ears, slopes from the linear regression models fell below 1. As ears enter a row unit it was evident that every ear would not make contact with the deck-plates. For this reason, it does not make physical sense to have a slope greater than 1. Slope is more realistic as predictions are adjusted for double counted ears. All of the following results were analyzed with ear count predictions that were adjusted for double counting. Slope of a linear regression model for an individual row unit is an important factor in the design of a peak detection algorithm. An initial goal was to minimize standard deviation in slope among row units. This goal would help to control variation and provide similar algorithm predictions across different row units.

5.3.2.2 Selection of Peak Detection Input Parameters with the Controlled Data Set

In summarization, an optimal set of peak detection input parameters would achieve linear regression models with a high R^2, a slope which approached 1 and minimal variation in slope among different row units. For the input parameter selection process a range for each input parameter was identified. The minimum peak height ranged from 0 to 160g in increments of 10g. This range was identified as it swept from an initial state of 0g to amplitudes well above the background noise of the corn-head. The minimum peak threshold ranged from 0 to 50g in increments of 10g. This range was identified as it swept from an initial state of 0g to amplitudes which approached the noise limit. An initial maximum for this range was set at 80g, but with such similar results above 50g the range was restricted so plots were not as congested.

All of the possible combinations of peak detection input parameters were swept through to identify an optimal combination which would best meet the previously defined performance criteria for all instrumented row units of the corn-head. A mean R^2 value was calculated from the multiple R^2 values produced by linear regression models of each instrumented row unit for a specific combination of input parameters. The mean R^2 value summarizes all of the individual R^2 values produced by instrumented row units for a given combination of input parameters. Similarly, a mean slope value was calculated with the multiple slope values produced by linear regression models of each instrumented row unit for a specific combination of input parameters. The mean slope value summarizes all individual slope values produced by instrumented row units for a given combination of input parameters. Lastly, the standard deviation of slope was calculated with the multiple slope values produced by linear regression models of each instrumented row unit for a specific input parameter combination. The standard deviation of slope summarizes the variation in all individual slopes from instrumented row units for a given combination of input parameters. Standard deviation in slope is an important parameter which controls how similar predictions are across different instrumented row units of a corn-head.

Mean Coefficient of Determination

Mean R^2 values were determined for all combinations of input parameters of the peak detection algorithm (Figure 50). A 95% confidence interval was applied to each mean R^2 value to determine if there was a level of significances among different combinations of input parameters. From this information, effective combinations of input parameters that produced high mean R^2 values could be identified.

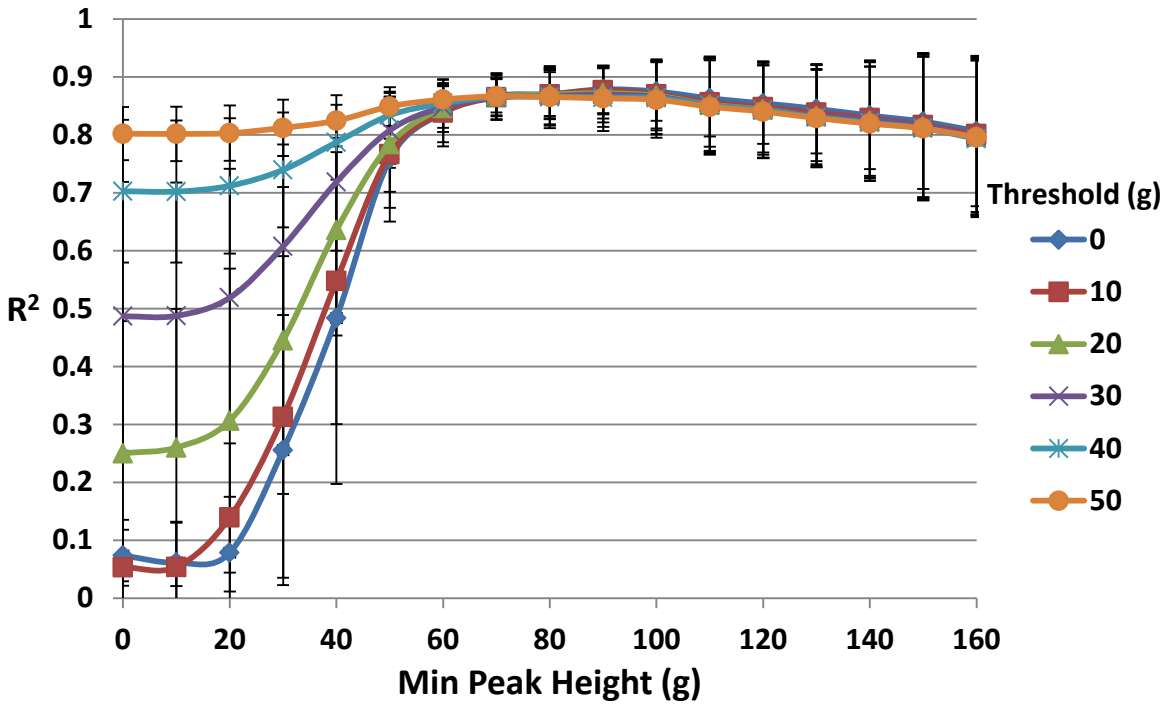

Figure 50: Mean R^2 Values from Different Combinations of Minimum Peak Height and Threshold

In a previous section, 48.95g was identified as the 99.9th percentile of corn-head noise. It can be seen that combinations of input parameters with a minimum peak height greater than this value begin to produce stronger R^2 values around this point (Figure 50). This circumstantial evidence re-enforces that peak detection must happen above the amplitude produced by forced vibrations of the corn-head. As shown, minimum peak height values of 50g or greater have no significant difference in mean R^2 values when thresholds are compared (Figure 50). Mean R^2 values from 0.758 to 0.877 were produced as the minimum peak height ranged from 50 to 160g, across all threshold values.

Minimum peak height is a driving factor of the peak detection algorithm. However, it should not be concluded that the minimum peak threshold does not have an effect on the predictions of the peak detection algorithm. Minimum peak threshold is effective at increasing the mean R^2 in the lower range of the minimum peak height, where corn-head noise is present. For an example, if the amplitude of the corn-head noise was to increase from 50 to 80g and minimum peak threshold was set to 0g and minimum peak height to 60g. The correlation between ground truth and predicted ears would decrease as the algorithm would find it difficult to distinguish the difference between corn-head noise and shock impulses. For the same situation, if the minimum peak threshold was to increase it would generate another conditional

statement for the corn-head noise to meet before it could be falsely identified as a shock impulse. For a peak detection algorithm with a high R^2 value, shock impulse detection must happen just above the background noise of the corn-head and requires an appropriate balance of both input parameters.

Mean Slope

Mean slope values were determined for all combinations of input parameters of the peak detection algorithm (Figure 51). A 95% confidence interval was applied to each mean slope values to determine if there was a level of significances among different combinations of input parameters. From this information, effective combinations of input parameters that produced mean slope values that approached 1 could be identified.

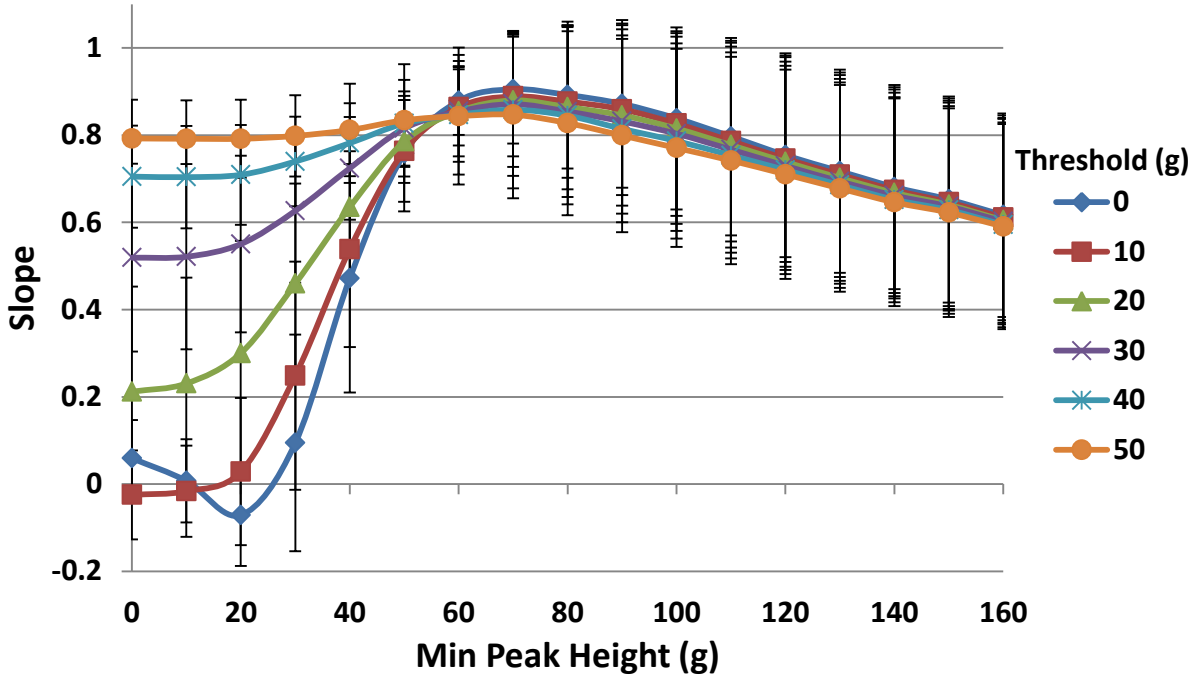

Figure 51: Mean Slope Values from Different Combinations of Minimum Peak Height and Threshold

Again, 48.95g was identified as the 99.9th percentile of corn-head noise. It can be seen that combinations of input parameters with a minimum peak height greater than this value begin to produce mean slope values that approach 1 around this point (Figure 51). This circumstantial evidence re-enforces that peak detection must happen above the amplitude produced by forced vibrations of the corn-head. Furthermore, minimum peak height values of 50g or greater have no significant difference in mean slope when thresholds are compared (Figure 50). Mean slope

values from 0.591 to 0.905 were produced in the minimum peak height range from 50 to 160g, across all threshold values.

Mean slope values are highest when input parameters are just above the background noise of the corn-head. As minimum peak height continued to increase the mean slope values start to deviate further away from 1. This should not be surprising; as minimum peak height increases the shock impulses just above the background noise of the corn-head no longer meet the conditions of the peak detection algorithm. Minimum peak threshold is effective at increasing the mean slope in the lower range of the minimum peak height, where corn-head noise is present. For a peak detection algorithm with a mean slope value that approaches 1, shock impulse detection must happen just above the background noise of the corn-head and requires an appropriate balance of both input parameters.

Standard Deviation of Slope

Standard deviation of slope was determined for all combinations of input parameters of the peak detection algorithm (Figure 52). From this information, effective combinations of input parameters that produced minimized variation in slope could be identified.

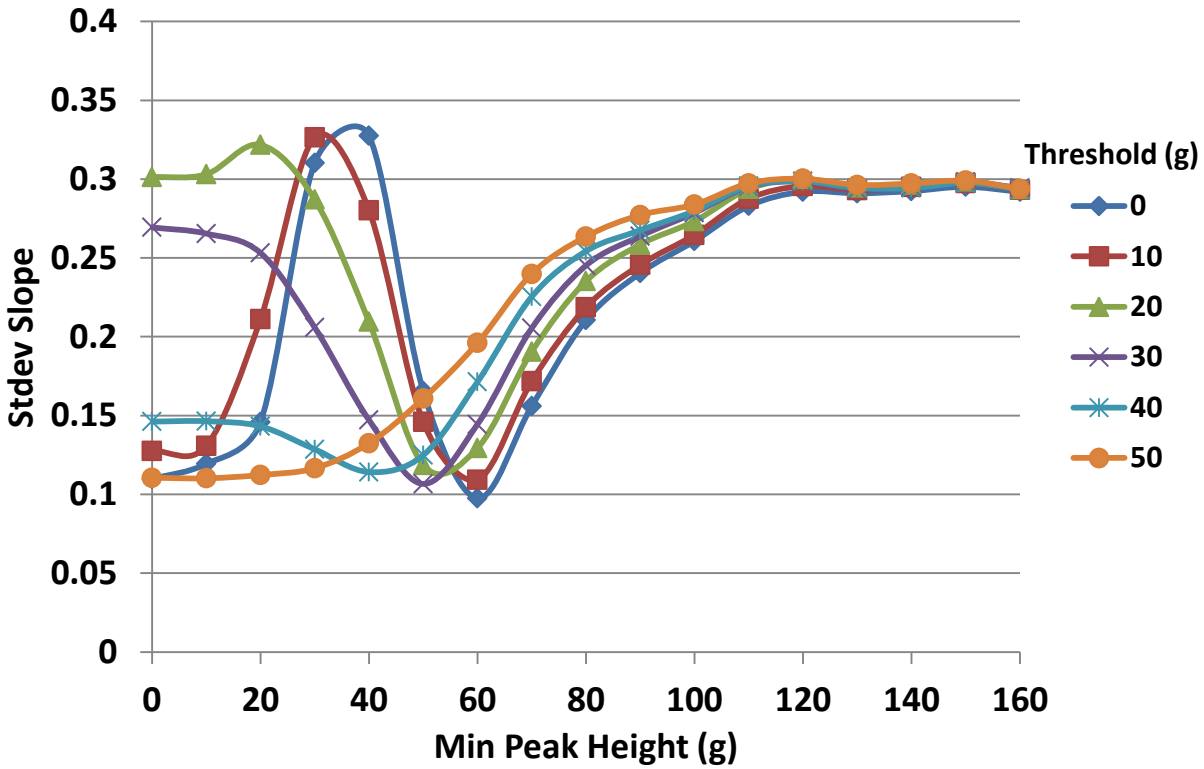

Figure 52: Standard Deviations of Slope from Different Combinations of Minimum Peak Height and Threshold

Standard deviation of slope is minimized when the minimum peak height is just above the background noise of the corn-head. As minimum peak height increases the shock impulses just above the background noise of the corn-head no longer meet the conditions of the peak detection algorithm. This limits the number of peaks that can be detected and causes excess variation in peak detection predictions. To minimize standard deviation of slope, a minimum peak height between 50 to 70g and a minimum threshold between 0 to 30g should be selected.

Input Parameter Selection

By inspection of previous data, it should be evident that the minimum peak height should be set above the background noise of the corn-head. From the defined performance constraints, an optimal combination of input parameters for the peak detection algorithm was selected as: minimum peak height of 60g, minimum peak threshold of 20g and the predefined minimum peak window of 50 milliseconds. This combination of input parameters achieved a linear regression model with a mean R^2 value of 0.854 and a mean slope of 0.844. The standard deviation in slope across all row units was limited to 0.129. Performance of the peak detection algorithm will be addressed with this combination of input parameters for the remainder of this thesis.

5.3.2.3 Peak Detection Performance with Controlled Data

In this section, controlled data was processed by the peak detection algorithm to produce linear regression models for each row unit. The peak detection algorithm was first applied without a normalization method to demonstrate how original predictions may initially vary between instrumented row units (Figure 53). Afterwards, the algorithm was reapplied with the normalization method (Figure 54). This method used the expected ear count of 87.8 ears per a row for the 50ft controlled test plots. The method also used rows of test plot data with a 0% plant removal rate to generate a mean predicted ear count for each row unit over the 50ft increment. The ratio of expected to predicted ear counts for each row unit was used to normalize the ear count predictions of the entire controlled data set (Equation 6). Residuals were plotted against ground truth ear counts to investigate the before and after effects of the normalization method (Figures 55 and 56).

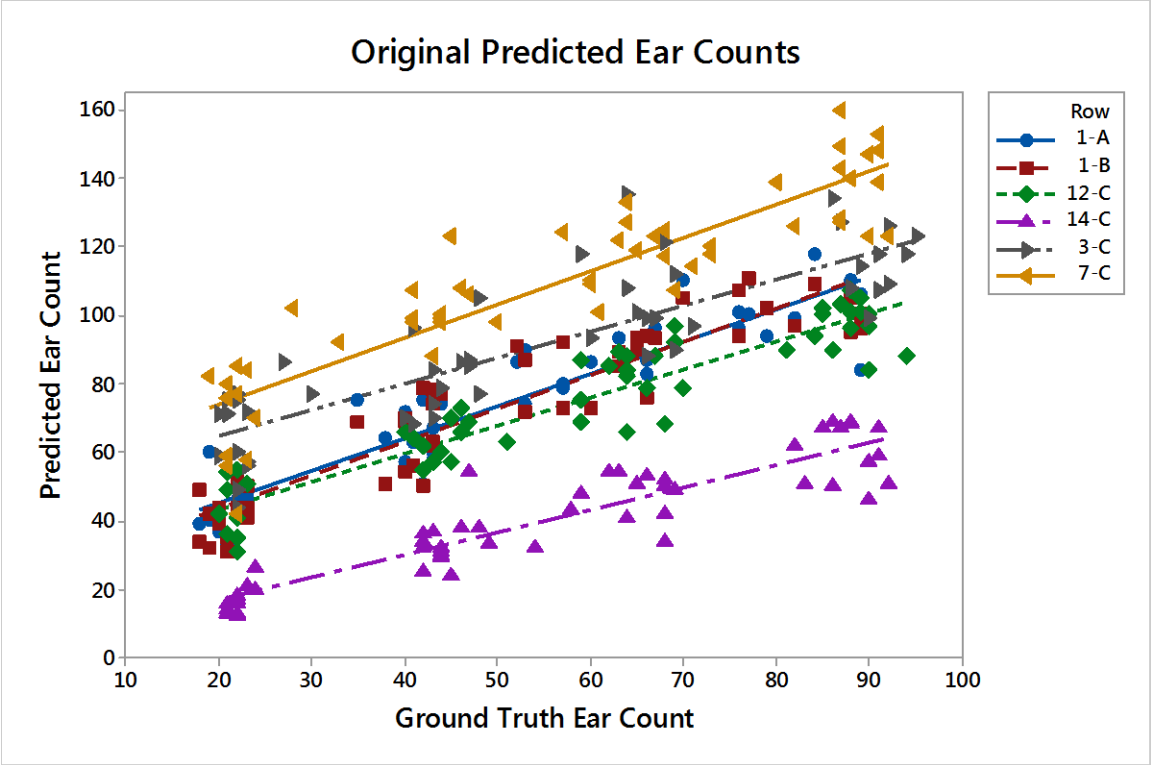

Figure 53: Predicted Ear Counts without Normalization Applied and Grouped by Row Unit

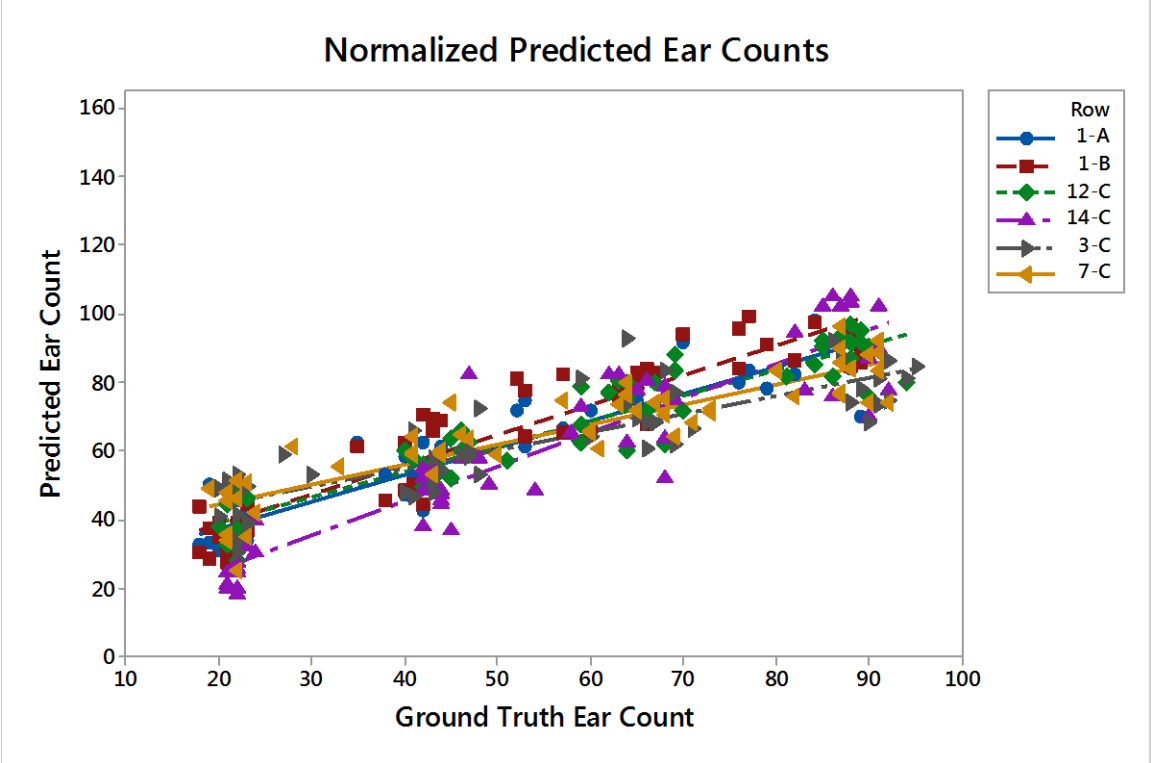

Figure 54: Predicted Ear Counts with Normalization Applied and Grouped by Row Unit

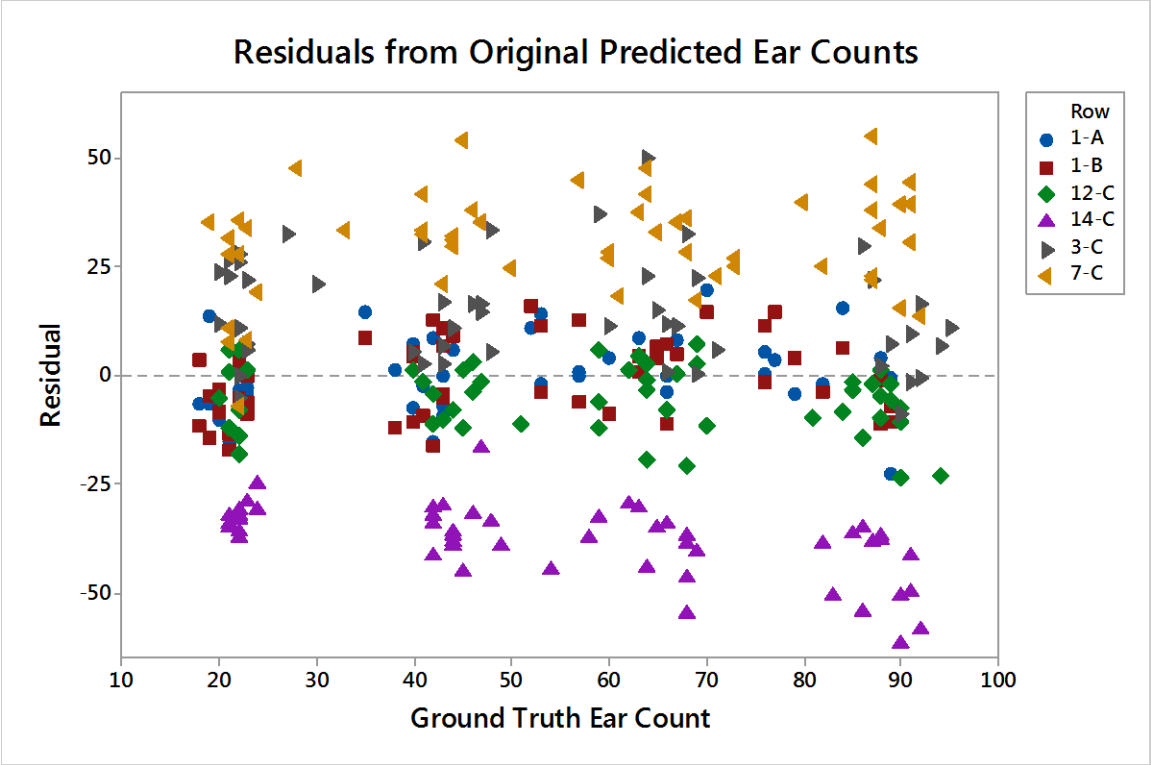

Figure 55: Residuals from Original Predicted Ear Counts and Grouped by Row Unit

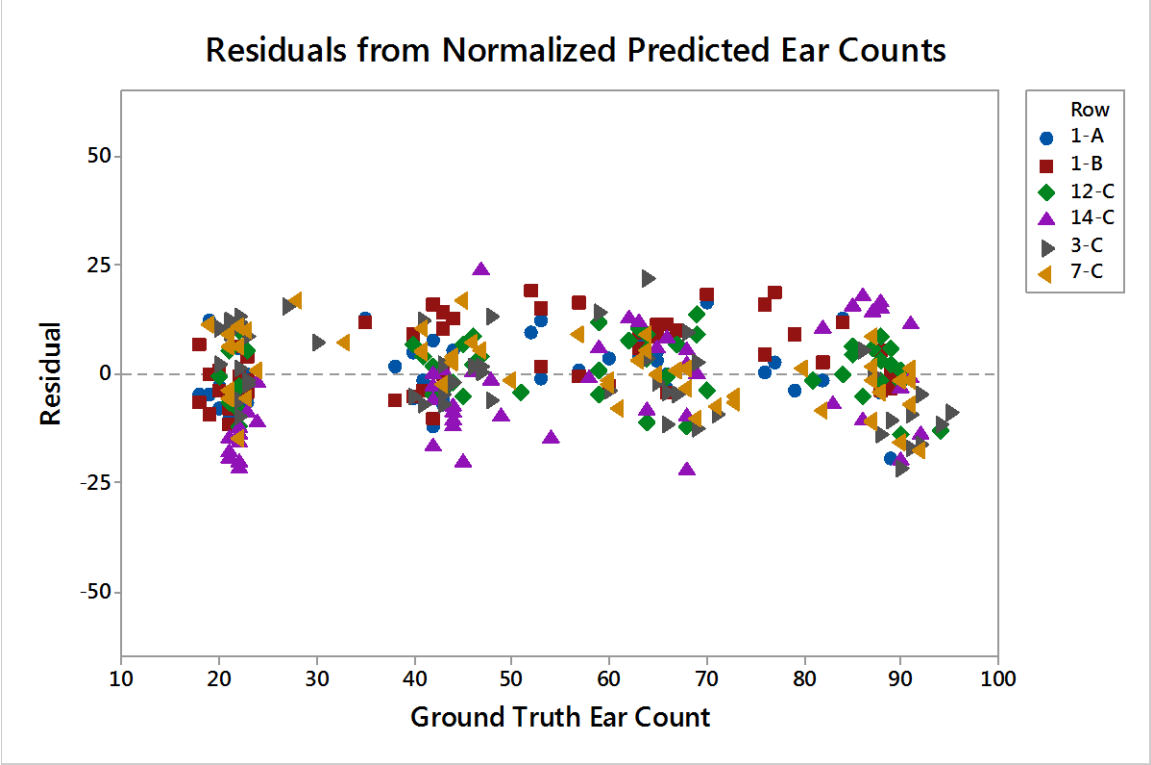

Figure 56: Residuals from Normalized Predicted Ear Counts and Grouped by Row Unit

From the original and normalized linear regression models, it is visually evident that the normalization method had a positive effect on the prediction model of each row unit. After the normalization method was applied, prediction models were capable of producing similar results for a given crop condition. Additional conformation of this conclusion can be seen as a controlled reduction in the size of the residuals is demonstrated before and after the normalization method was applied (Figure 55 and 56). The random pattern of the residuals from the normalized predictions further supports the linear models.

5.3.2.4 Peak Detection Performance with Uncontrolled Data

Expected and predicted ear counts over 50ft increments were used to normalize the controlled data set. In this section, the peak detection algorithm and normalization method used a training data set to normalize an uncontrolled test run over 5ft increments in an effort to validate both the algorithm and normalization process. It is believed that with a higher sampling frequency of combine velocity an increment of 2.5ft could possibly be achieved. Due to limitations in sampling frequency of CAN (controller area network) data this is outside the scope of this research.

For validation of the peak detection algorithm, video evidence and NVDI images were used to select a 400ft length of crop in a field with a relatively high expected ear count. Accelerometer data from this area was used as a training set to calibrate ear count predictions for each row unit. It was assumed that the actual mean ear count prediction for 5ft increments would be normal about a value for each row unit. Velocity and time vectors from the combine CAN data were used to identify the 400ft length of crop. Total predicted ear counts for each row unit were divided by the number of 5ft increments to fit in the 400ft length of crop. This produced an estimate of the mean ear count prediction for each row unit over a 5ft increment (Table 9). Accelerometer pairs 1B, 3 and 14 were not included in this process due to signal quality issues.

Table 9: Estimated Mean Ear Count Predictions for a 5ft Increment

	Estimated Mean for Ear Count Predictions
Row 1	10.32
Row 7	12.44
Row 12	9.12

Controlled test data was again used to calculate an expected ear count of 8.78 ears for every 5ft increment. Mean and expected ear counts could then be used to normalize future ear count predictions from each row unit over 5ft increments (Equation 6).

A near-infrared (NIR) image was used to select an uncontrolled test run to evaluate this normalization process with uncontrolled data. The uncontrolled test run included a harvest pass with several different types of crop conditions (Figure 59). In the NIR image, red represents areas of healthy crop and gray is areas of either underdeveloped or no crop. From video evidence, the large area of gray is underdeveloped crop and the two smaller areas of gray have no crop as a result of planter skips. This pass was harvested from left to right and the planter skips are towards the end of the time-series.

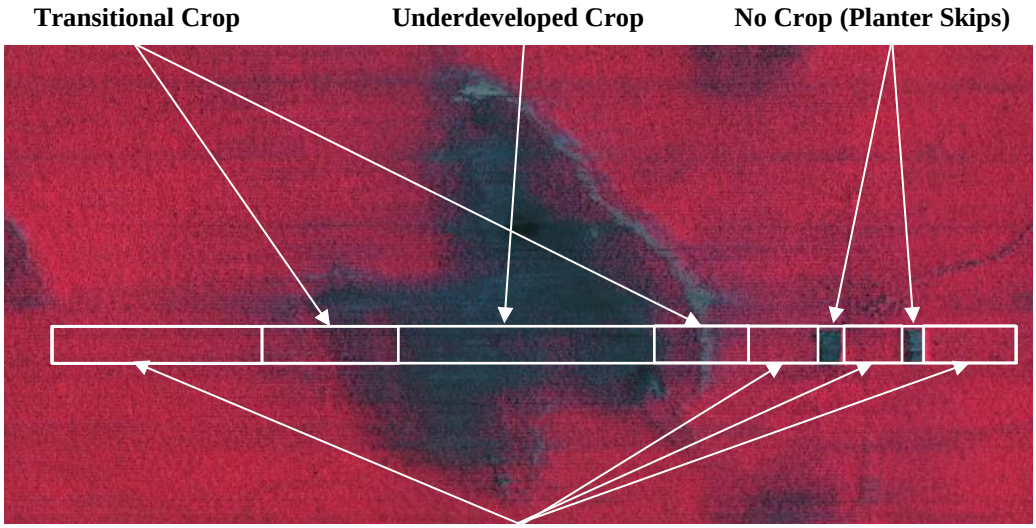

Figure 57: Uncontrolled Harvest Test Run

As discussed, mean and expected ear count predictions were used to normalize the unrelated 5ft ear count predictions of the uncontrolled test run (Figure 58). The expected ear count of 8.78 ears per a 5ft increment is presented as a black horizontal line.

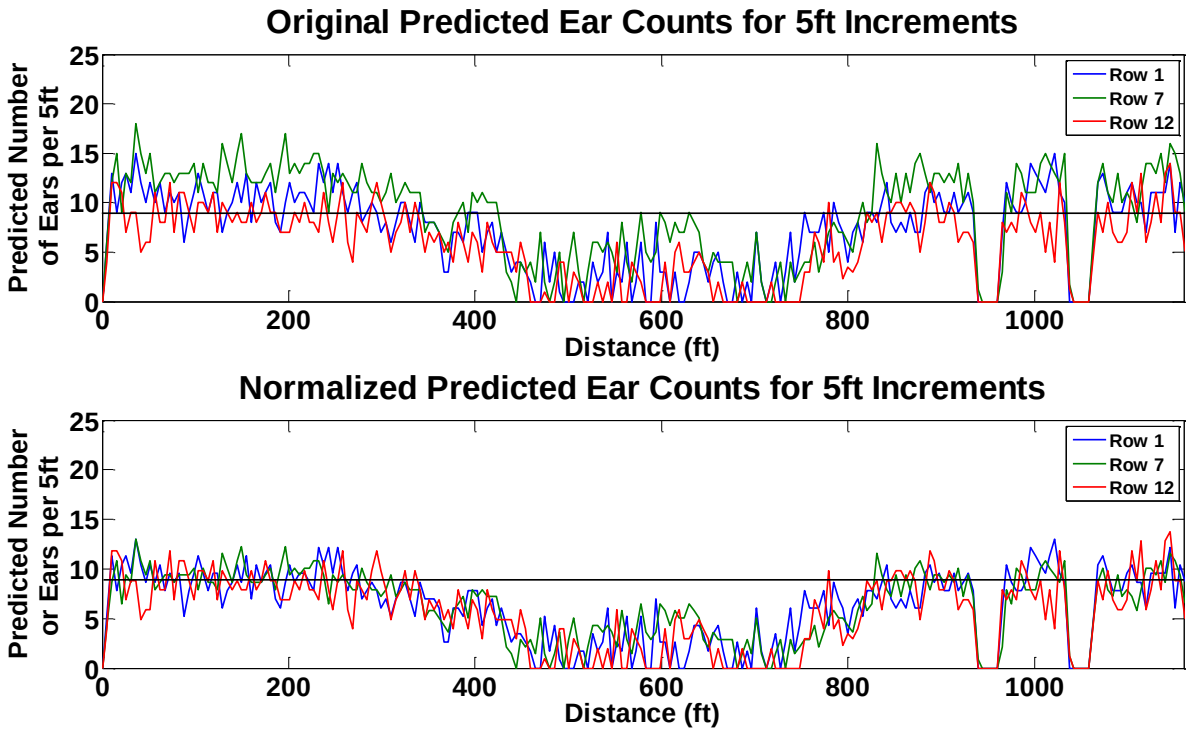

Figure 58: Normalization of Ear Count Predictions with Uncontrolled Data

Overall, original and normalized ear count predictions both follow an accurate field trend for the uncontrolled test run. As both predictions are further compared it can be seen that the normalized ear count predictions more closely follow the expected ear count of healthy crop for the first 300ft, as it should. Original ear count predictions are not as controlled, row 7 can be routinely seen over predicting the expected ear count and other row units. For an additional comparison, the normalized ear count predictions and grain mass flow rate of the combine were then plotted as a function of distance (Figure 59). The grain mass flow rate signal was offset by the distance traveled before grain reached the impact plate to generate an initial response.

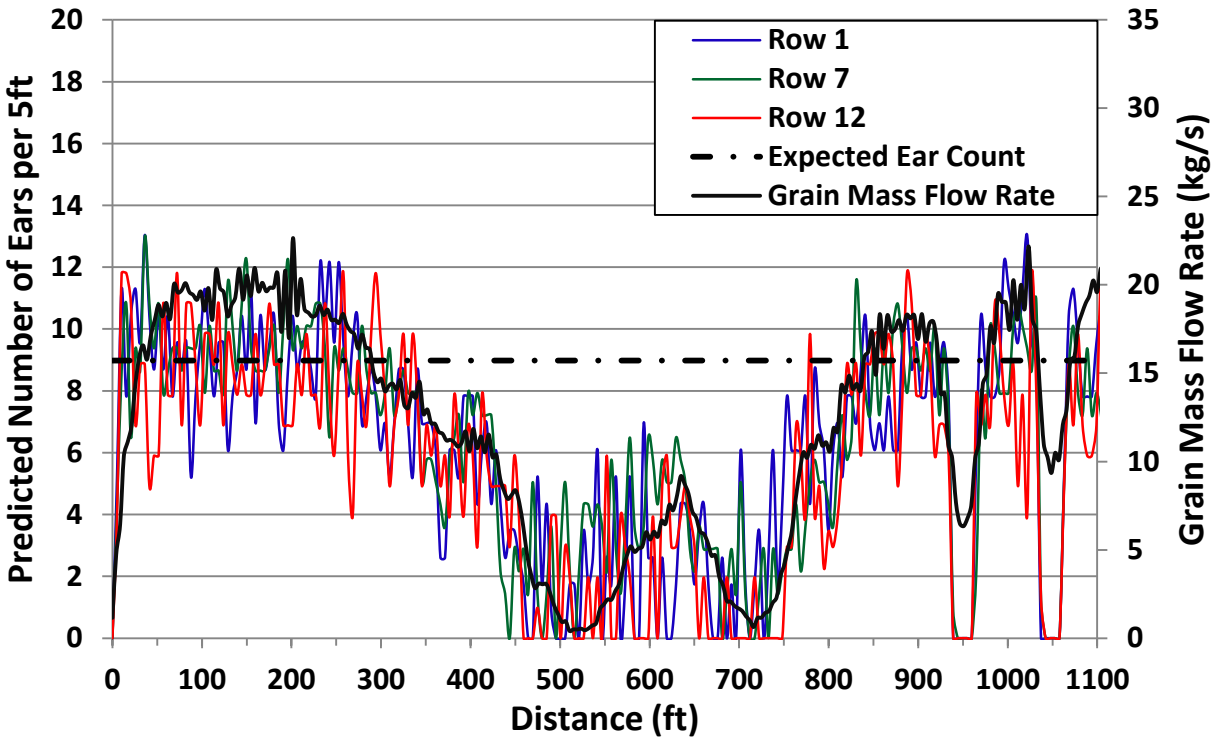

Figure 59: Normalized Ear Count Predictions vs. Grain Mass Flow Rate Measurement

It is evident that the response of the ear detection system is significantly faster than the grain mass flow rate measurement. Ear detection and grain mass flow rate are respectively, direct and indirect measurements. The ear detection system began to predict an ear quantity as soon as ears were harvested. This can be seen as it only takes 10 feet for the ear detection system to fully respond, and includes the several feet for the combine to initially engage the crop. Once the combine was in crop for a full 5ft increment, the system output an ear count prediction similar to the expected ear count. Adversely, grain mass flow rate required a significant amount of grain to be harvested before a measurement was collected. The grain mass flow rate measurement is typically model as a 1^{st} order response with an initial time delay. Approximately 45 feet of crop was harvest before the grain mass flow rate measurement had responded, which was applied as an initial offset. Another 55 feet was harvested before the measurement reached steady-state. These distances corresponded to an initial 13 second time delay once the combine entered crop and another 11 seconds to reach a steady-state flow rate.

A decrease in system response times allows for more accurate identification of areas with little to no crop. As the combine harvested through the planter skips there was a transition from healthy crop to no crop and back. At an approximate harvest speed of 4.28 feet $second^{-1}$, the ear

detection system was able to respond within a 5ft increment, less than 1.17 seconds. The grain mass flow rate measurement took an approximate 25ft or 5.84 seconds to respond, despite the initial system delay. With fast ear detection response times, spatial management software was used to cross-reference geospatial information from NIR images to place the location of the planter skips within a single 5ft increment of where the predicted ear counts transitioned from healthy crop to no crop. Furthermore, the grain mass flow rate was used to quantify the amount of grain misrepresented in the area of each planter skip, by using the response of the ear detection system. Grain was spatially misrepresented at approximately 66 and 105 bushels $acre^{-1}$ for the two planter skips.

5.3.3 Performance of the Crop Intensity Algorithm

5.3.3.1 Crop Intensity Performance with Controlled Data

In this section, controlled data was processed by the crop intensity algorithm to produce linear regression models for each row unit. The crop intensity algorithm was first applied without a normalization method to demonstrate how original crop intensity predictions may initially vary between instrumented row units (Figure 60). Afterwards, the algorithm was reapplied with the normalization method (Figure 61). The 0% plant removal rate of the controlled data set was used to generate a mean crop intensity prediction for each individual row unit over a 50ft increment. It should be noted that the control test plots were harvested at approximately 2.5mph. This is important as crop intensity is a time dependent function which sums all deck-plate vibration including corn-head noise and shock impulses. For this reason, the normalization parameters generated are specific to that harvest speed. An overall mean crop intensity prediction for the entire corn-head was found from the individual mean crop intensities of each row unit. The ratio of overall to individual mean crop intensity for each row unit was used to normalize the crop intensity predictions of the entire controlled data set (Equation 10). From the linear regression models, residuals were plotted against fitted values to investigate the before and after effects of the normalization method (Figures 62 and 63).

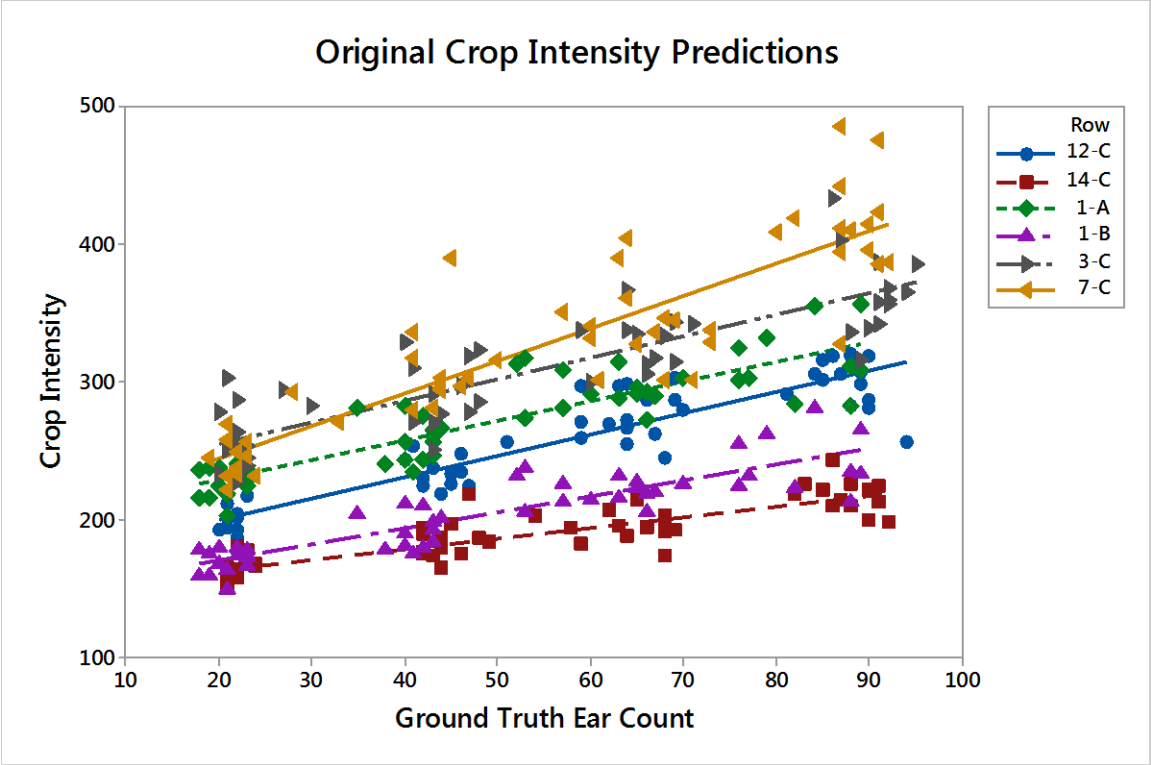

Figure 60: Crop Intensity Values without Normalization Applied and Grouped by Row Unit

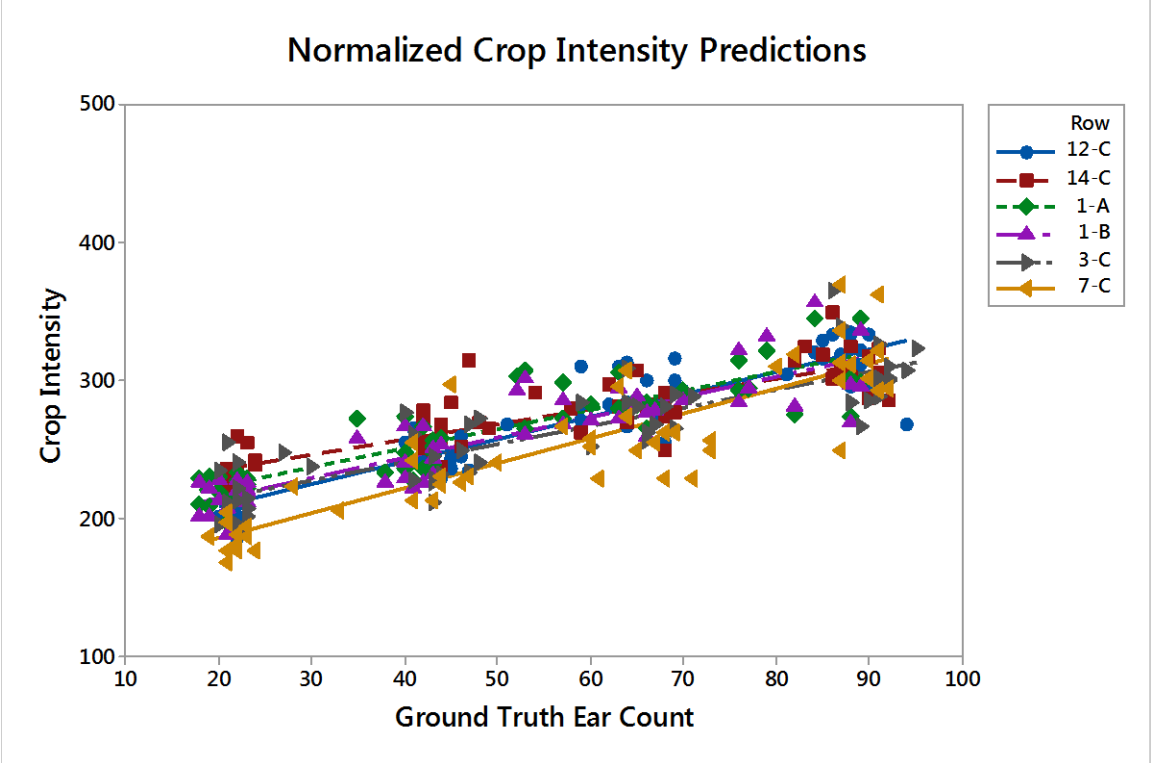

Figure 61: Crop Intensity Values with Normalization Applied and Grouped by Row Unit

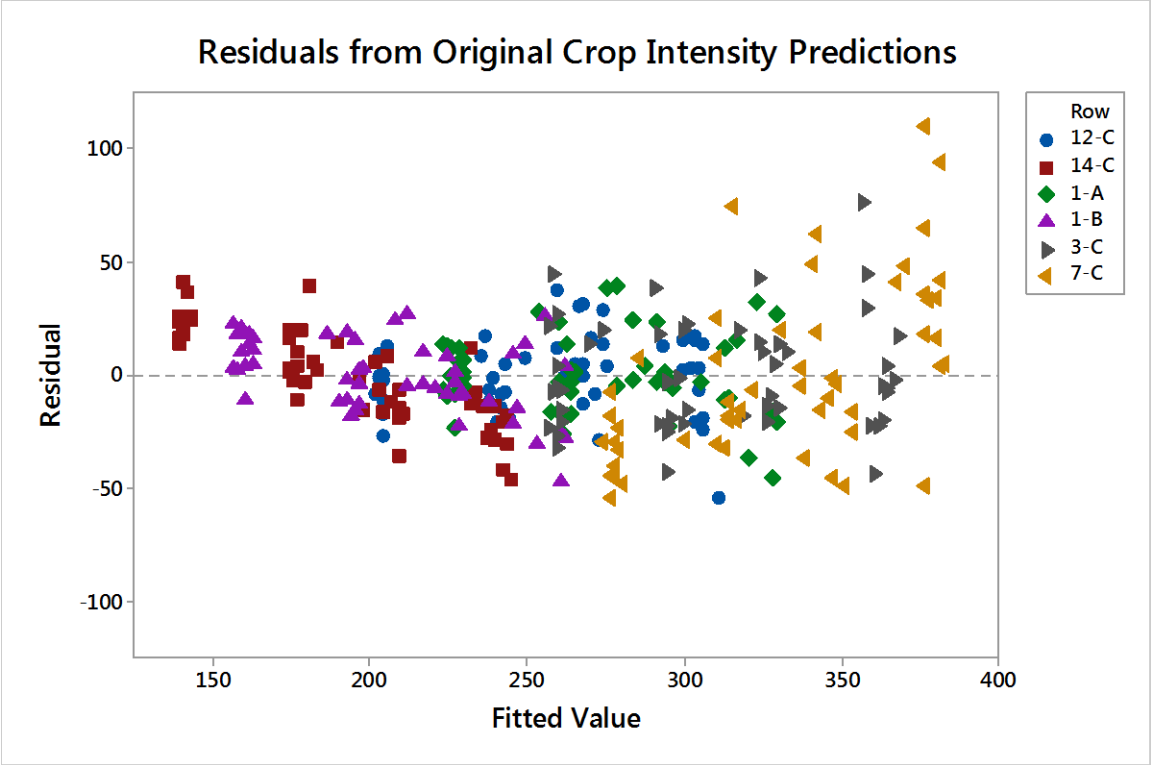

Figure 62: Residuals from Original Crop Intensity Predictions and Grouped by Row Unit

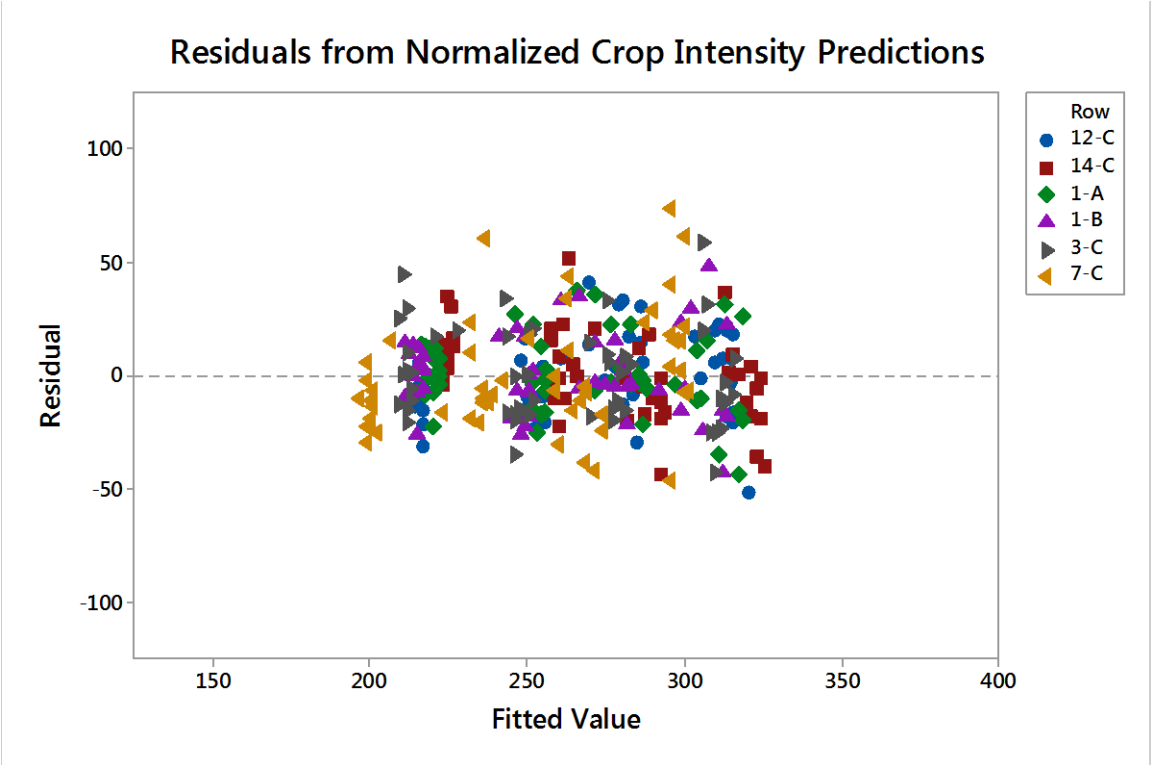

Figure 63: Residuals from Normalized Crop Intensity Predictions and Grouped by Row Unit

Similar to peak detection, the normalization method had a positive effect on the prediction model of each row unit. The desired outcome was to control the variation among the prediction models of row units. After the normalization method was applied it was evident the prediction models were capable of producing similar results for a given crop condition (Figure 62). Additional conformation of this conclusion can be seen as a controlled reduction in the size of the residuals is demonstrated before and after the normalization method was applied (Figure 62 and 63). The random pattern of the residuals from the normalized predictions further supports the linear models. Lastly, with the crop intensity algorithm and normalization method applied to the controlled data set, a mean R^2 of 0.766 was produced across all instrumented row units.

5.3.3.2 Crop Intensity Performance with Uncontrolled Data

As previously mentioned crop intensity is a time-dependent function and requires predictions to be summed over similar time increments and at a consistent harvest speed to ensure predictions can be relatively compared. If harvest speeds vary, different amounts of the corn-head noise will be summed into crop intensity predictions. The effect of shock impulses on the corn-head noise that is produced while crop is harvested is unknown. As a result, summation of corn-head noise produced while stationary cannot be subtracted from crop intensity predictions for an increment of time. Crop intensity normalization parameters must be determined at the harvest speed they will be applied at to remain effective. For this reason, the 400ft training data set could not be used to normalize the previous uncontrolled test run, as both were harvested at different speeds. For simplicity, a new training data set was taken from a healthy section of the same uncontrolled test run. This test run was harvested at an approximate steady-state harvest speed of 4.28 feet $second^{-1}$. The initial and final de-acceleration periods were neglected for the analysis.

The selected training data set was a 200ft length of healthy crop that was used to generate overall and individual mean crop intensity predictions for the entire corn-head and individual row units. As crop was harvested at a consistent speed, crop intensity normalization parameters could be found for a 5ft increment, similar to the peak detection algorithm. It was assumed that the actual mean crop intensity prediction for 5ft increments would be normal about a value for each row unit. Velocity and time vectors from the combine CAN data were used to find the total crop intensity predictions for each row unit over the 200ft training set. Total crop intensity predictions were divided by the number of 5ft increments to fit in the 200ft length of crop. This

produced an individual crop intensity prediction for each row unit over a 5ft increment (Table 10).

Table 10: Mean Crop Intensity Predictions for a 5ft Increment

	Mean for Crop Intensity Predictions
Row 1	22.11
Row 7	30.23
Row 12	20.98

An overall mean crop intensity of 24.44 was found from the mean crop intensities of individual row units. Overall and individual mean crop intensities were then be used to normalize crop intensity predictions of the previous uncontrolled test run over 5ft increments (Figure 64). The overall mean crop intensity for a 5ft increment is presented as a black horizontal line. As previously mentioned, initial and final periods of acceleration and de-acceleration were not analyzed in the uncontrolled test run.

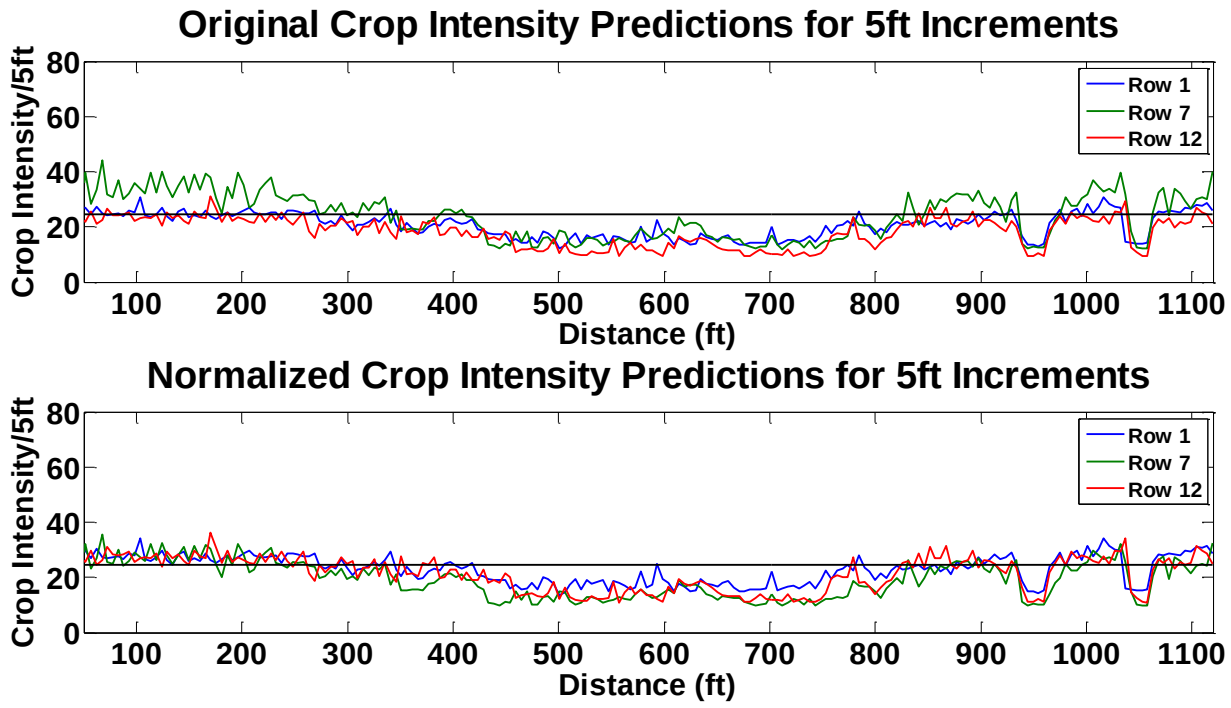

Figure 64: Normalization of Crop Intensity Predictions with Uncontrolled Data

Overall, original and normalized crop intensity predictions both follow an accurate field trend for the uncontrolled test run (Figure 64). The normalized crop intensity predictions more

closely follow the overall mean crop intensity of healthy crop for the first 300ft, as it should. Original ear count predictions are not as controlled, row 7 can be routinely seen over predicting other row units. Both original and normalized crop intensity prediction series were offset by an unknown value, likely related to the corn-head noise. When comparing the area of underdeveloped crop (460ft to 760ft) to the two planter skips, it can be seen that the planter skips produced a relatively consistent lower prediction. For an additional comparison, the normalized crop intensity predictions and grain mass flow rate of the combine were then plotted as a function of distance (Figure 65). The grain mass flow rate signal was offset by the distance traveled before grain reached the impact plate to generate an initial response.

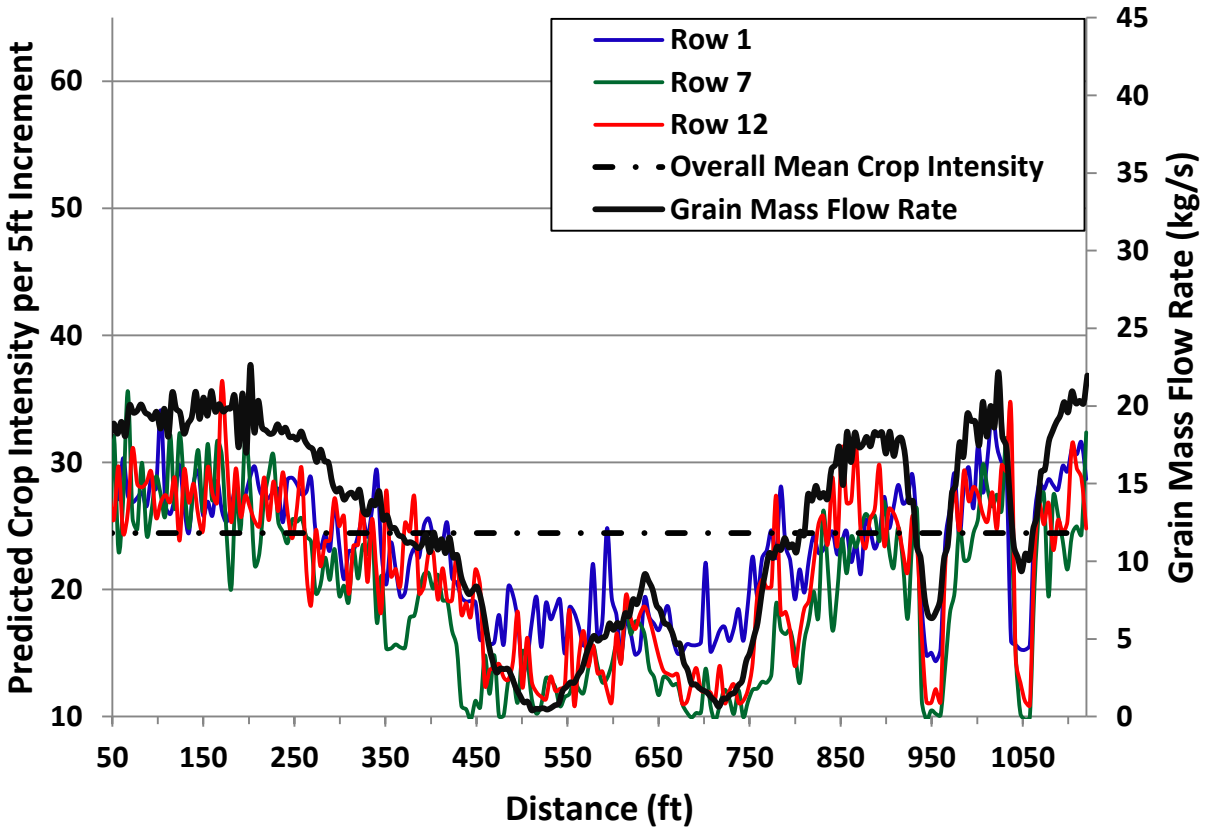

Figure 65: Normalized Crop Intensity Predictions vs. Grain Mass Flow Rate Measurement

Visually it can be seen that both crop intensity and grain mass flow rate signals follow the trend of the uncontrolled test run. After normalization, row 1 seems to be still over predicting areas with little to no crop. The response time of crop intensity predictions could be investigated as the planter skips were harvested at a consistent speed. Both planter skips responded within a

10ft increment, less than 2.34 seconds. With known planter skip locations, spatial management software was used to cross-reference geospatial information from an NIR image. Planter skips could then be placed within a 10ft increment of where the predicted ear counts transitioned from healthy crop to no crop. The grain mass flow rate was not used to estimate the amount misrepresented grain due to inconsistent crop intensity predictions for the planter skips.

5.4 Conclusion

Both peak detection and crop intensity algorithms produced results that demonstrated control of predictions when normalized methods were applied to the controlled data set. This improved confidence in the ability of both algorithms to make similar predictions across multiple row units for a given crop condition. Both algorithms also demonstrated reasonable enhancements in responses times in transitions from healthy crop to no crop. Between the algorithms, peak detection showed superior functionality with uncontrolled data due to its ability to distinguish between shock impulses and corn-head noise. Peak detection allowed for reasonable prediction and placement for groups of ears. Crop intensity struggled as it relied heavily on consistent harvest speeds to normalize data. After crop intensity predictions of the uncontrolled test run were normalized relative displacement between row units data series were still visible for similar crop conditions.

CHAPTER 6: CONCLUSIONS

The developed ear detection system allowed researchers to predict the number of ears that enter different row units of a corn-head. Additionally, individual row unit predictions were normalized across the corn-head to produce similar values. This provided the ability to generate comparable ear count prediction values across the swath width of the corn-head. The functionality of this system is an advantage over a traditional yield monitor. It generates additional yield attributes for different sections of a corn-head instead of a single average yield pixel for the covered area. The predictive ear detection system was also more responsive than the conventional mass flow rate sensor of a combine. When compared, the predictive ear detection system showed significant improvements in response to short bursts in area where no crop was present.

6.1 Suggestions for Future Testing

As the system relies highly on efficient energy transfer from an impact, further testing should investigate the effects on the predictive ear detection system at different operator and crop conditions.

6.2 Suggestions for Future Development

Further design work on system reliability is needed. Electrical connections between the accelerometer and data acquisition system were an issue for the data integrity of several row units. Production style electrical hardware should be considered to ensure signal reliability. An additional study on the redesign of deck-plates to generate amplified shock impulse signals from ear and deck-plate collisions could be investigated. Future development should focus on repeatability and reliability of generated data.

Development of machine learning calibration processes should be a considered. A first calibration should focus on gathering information on corn-head noise to set input parameters of predictive algorithms for individual row units. An additional calibration would collect mean ear count predictions for each individual row units. This calibration should collect predictions in an area of a field with the highest expected ear counts. Mean ear count predictions should be compared against expected ear counts calculated from operator inputs of planted population and survival rates. Both expected and predicted ear counts should then be used to normalize future predictions across multiple row units of the corn-head.

REFERENCES

Ag Leader Technology Corporation. (2015). *The Evolution of Ag Leader Technology*. Retrieved March 18, 2015, from Ag Leader Technology Web Site: http://www.agleader.com/about/history/

Barnes, E. M., Moran, M. S., Pinter, P. J., & Clarke, T. R. (1996). Multispectral Remote Sensing and Site-Specific Agriculture:. *Proceedings of the 3rd International Conference on Precision Agriculture* (pp. 843-854). Minneapolis, Minnesota: International Conference on Precision Agriculture.

Birrell, S., Hummel, J., Lobdell, B., & Sudduth, K. (2001). Sensing Corn Population-Another Variable in the Yield Equation. *InfoAg Conference.*

Casady, W., Pfost, D., Ellis, C., & Shannon, K. (n.d.). Precision Agriculture: Yield Monitors. *Water Quality*. Retrieved from http://extension.missouri.edu/p/wq451

Claas of America Inc. (2010). *Lexion 500 Series.* Retrieved March 20, 2015, from Claas of America Corporation WebSite: http://www.classofamerica.com

CNH Industrial. (2015, June 6). *New Holland Agriculture*. Retrieved from newholland.com: http://agriculture.newholland.com/PublishingImages/cnhimg/PLM/CROP-MAN/Yield-Moisture_Sensing/Moisture%20Sensor.jpg

Deere & Company. (2015, May 20). *600C Series Corn Head*. Retrieved from deere.com: https://www.deere.com/en_US/products/equipment/grain_harvesting/headers/600c_series_corn_heads/600c_series_corn_heads.page

Deere & Company. (2015, May 19). *616C Corn Head*. Retrieved from deere.com: https://www.deere.com/en_US/products/equipment/grain_harvesting/headers/600c_series_corn_heads/616c_corn_head/616c_corn_head.page

Deere & Company. (2015, May 14). *AutoTrac RowSense*. Retrieved from Deere.com: https://www.deere.com/en_US/products/equipment/ag_management_solutions/guidance/autotrac_rowsense_sf2/autotrac_rowsense_sf2.page

Dobermann, A., & Ping, J. (2004). Geostatistical Integration of Yield Monitor Data and Remote Sensing Improves Yield Maps. *Precision Agriculture*, 285-297.

Easton, D. T., & Easton, D. J. (1998, August 4). *Patent No. US5790428 A.* US.

Edgerton, M. D. (2009). Increasing Crop Productivity to Meet Global Needs for Feed, Food and Fuel. Retrieved March 18, 2015, from http://www.ncbi.nlm.nih.gov/pmc/articles/PMC2613695/

Farnham, D. (2015, June 6). *Corn Planting Guide.* Retrieved from Iowa State University Extension and Outreach: https://store.extension.iastate.edu/Product/pm1885-pdf

Fulton, J., Sobolik, C., Shearer, S. A., Higgins, S. F., & Burks, T. (2009). Grain yield monitor flow sensor accuracy for simulated varying field slopes. *Applied Engineering in Agriculture*, 15-21.

Gitelson, A., Vina, A., Arkebauer, T., Rundquist, D., Keydan, G., & Leavitt, B. (2003). Remote estimation of leaf area index and green leaf biomass in maize canopies. *Geophysical Research letters*, Lett. 30:1248,doi 10.1029/2002 GL016450.

Grisso, R., Alley, M., & McClellan, P. (2009). Precision Farming Tools: Yield Monitor. *Virginia Cooperative Extension*. Retrieved March 18, 2015, from http://pubs.ext.vt.edu/442/442-502/442-502_pdf.pdf

Harris, C. M., & Piersol, A. G. (2002). Harris' Shock and Vibration Handbook. In C. M. Harris, *Measurement Techniques* (5th ed., pp. 5-13). New York, New York: McGraw-Hill.

Iowa Corn Organization. (2015, June). *FAQ.* Retrieved from Iowa Corn: http://www.iowacorn.org/en/corn_use_education/faq/

Linville, C. (2015, Feb 24). *Patent No. US8965812 B2.* US.

McGuire, J. D., & Pearson, R. S. (2006, June 6). *Patent No. US7058197 B1.* US.

Myers, A. (1991, June 17). *Patent No. 5343761.* United States of America. Retrieved March 20, 2015

Nielsen, R. (2010, August). *Yield Monitor Calibration: Garbage In, Garbage Out.* Retrieved from Purdue Agriculture, Department of Agronomy: https://www.agry.purdue.edu/ext/corn/news/timeless/yldmoncalibr.html

PCB Piezotronics. (2015, May 21). *Model: 353B11*. Retrieved from www.pcb.com: http://www.pcb.com/Products.aspx?m=353B11

Piersol, A. G., & Peaz, T. L. (2010). *Harris' Shock and Vibration Handbook.* McGraw-Hill.

Senay, G., Ward, A., Lyon, J., Fausey, N., & Nokes, S. (1998). Manipulation of high spatial resolution aircraft remote sensing data for use in site-specific farming. *American Society of Agricultural Engineers*, 489-495.

Shanahan, J., Schepers, J., D.D, F., G.E., V., Wilhelm, W. W., Tringe, J. M., . . . Major, D. J. (2001). Use of Remote-Sensing Imagery to Estimate Corn Grain Yield. *Agronomy & Horticulture*, 583-589.

Shearer, S., Fulton, J., McNeil, S., Higgins, S., & Mueller, T. (1999). Elements of Precision Agriculture: Basics of Yield Monitor Installion and Operation. *Kentucky Cooperative Extension Service*. Retrieved March 18, 2015, from http://www.bae.uky.edu/precag/PrecisionAg/Exten_pubs/pa1.pdf

Shi, Y., Wang, N., Taylor, T. R., Raun, W. R., & Hardin, J. A. (2013). Automatic corn plant location and spacing measurement using laser line-scan technique. *Precision Agriculture*, 474-494.

Shrestha, D. S., & Steward, B. L. (2003). Automatic Corn Plant Population Measurement Using Machine Vision. *American Society of Agricultural Engineers*, 559-565.

Singh, R. P., Prasad, A. K., Tare, V., & Kafatos, M. (2010). *Patent No. US7702597 B2.* US.

Thomison, P. (2010, August). *C.O.R.N. Newsletter.* Retrieved from The Ohio State University Extension: http://corn.osu.edu/newsletters/2010/2010-08-4-13/corn-seeding-rates-vs.-final-stands

Whelan, B. M., & McBratney, A. B. (2000). An Approach to Deconvoluting Grain-Flow within a Conventional Combine Harvester using a Parametric Transfer Function. *Precision Agriculture*, 389-398.

Wilcox, T. A., & Nelson, F. W. (2010). *Patent No. US7716905 B2.* US.

Zhang, M., Hendley, P., Drost, D., O' Neill, M., & Ustin, S. (1998). Corn and soybean yield indicators using remotely sensed vegetation index. *International Conference on Precision Agriculture* (pp. 1475-1481). St. Paul, Minnesota: Proceedings of the 3rd International Conference on Precision Agriculture.

APPENDIX A: PATENT REVIEW

Plant Monitoring Patents

Patent Title: "Device to measure and provide data for plant population and spacing variability"

Patent Number: US5790428 A

Patent Inventor(s): Dan T. Easton, David J. Easton

Patent Assignee: Easton Goers, Inc.

Patent Abstract: "An apparatus and method for determining plant population, plant spacing, plant spacing variability, and other information regarding row-planted crops. The apparatus senses the presence of a plant. The sensing can be adjusted to ignore such things as leaves, weeds, or other irrelevant items. The apparatus also concurrently measures the distance between each sensed plant. The information regarding location and distance between plants is used to derive plant population and plant spacing data. The method senses the location and distance between plants for a given area to derive the population and spacing data."

Patent Claims:

1. "An apparatus for use with a field implement for determining plant population and other information regarding row-planted crops in a field."
2. "A method of determining plant population and other information regarding row-planted crops in a field."

For more detailed information see reference (Easton, et. al., 1998).

Patent Title: “Sensing assembly for detection of one or more plants”

Patent Number: US7716905 B2

Patent Inventor(s): Timothy Amos Wilcox, Frederick William Nelson

Patent Assignee: Deere & Company

Patent Abstract: “A sensing assembly comprises a forward point for mounting on a crop divider associated with a header. At least one movable arm is capable of interacting with one or more plants standing in a field. A sensor detects a position of the movable arm. A mounting assembly operably supports the movable arm and the forward point, where a rear portion of the forward point is spaced apart from a forward edge of the crop divider and the at least one movable arm is located above a bottom portion of the forward point when the mounting assembly is secured to the crop divider.”

Patent Claims:

1. “A sensing assembly for a header for harvesting a crop.”
2. “A header for harvesting stalk crops, the header comprising a frame, a plurality of row-units mounted to the frame, crop dividers provided between adjacent row-units and a sensing assembly mounted to the forward end of one of said crop dividers.”

For more detailed information see reference (Wilcox, et. al., 2010).

Yield Estimation Patents

Patent Title: "Crop yield prediction using piecewise linear regression with a break point and weather and agricultural parameters"

Patent Number: US7702597 B2

Patent Inventor(s): Ramesh P. Singh, Anup Krishna Prasad,Vinod Tare, Menas Kafatos

Patent Assignee: George Mason Intellectual Properties, Inc.

Patent Abstract: "Crop yield may be assessed and predicted using a piecewise linear regression method with break point and various weather and agricultural parameters, such as NDVI, surface parameters (soil moisture and surface temperature) and rainfall data. These parameters may help aid in estimating and predicting crop conditions. The overall crop production environment can include inherent sources of heterogeneity and their nonlinear behavior. A non-linear multivariate optimization method may be used to derive an empirical crop yield prediction equation. Quasi-Newton method may be used in optimization for minimizing inconsistencies and errors in yield prediction. Minimization of least square loss function through iterative convergence of pre-defined empirical equation can be based on piecewise linear regression method with break point. This non-linear method can achieve acceptable lower residual values with predicted values very close to the observed values. The present invention can be modified and tailored for different crops worldwide."

Patent Claims:

1. "A computer readable storage medium, embodying a program of instructions executable by a machine to perform a method for predicting crop yield."
2. "A crop yield predicting device."

For more detailed information see reference (Singh, et. al., 2010)

Patent Title: “Evaluating commodity conditions using aerial image data”

Patent Number: US8965812 B2

Patent Inventor(s): Charles Linville

Patent Assignee: Archer Daniels Midland Company

Patent Abstract: “Various tools, strategies and techniques are provided for evaluating the condition of one or more commodities in one or more regions of interest. Collection of image data associated with the commodities can be facilitated through use of an aircraft traveling a predetermined travel route over the regions of interest. The collected image data may be analyzed to evaluate the condition of the commodities, forecast commodity production, and/or to perform other tasks.”

Patent Claims:

1. “A method for evaluating the condition of an agricultural commodity and forecasting the production thereof in a geographical region of interest.”

For more detailed information see reference (Linville, 2015).

Patent Title: “Multi-variable model for identifying crop response zones in a field"

Patent Number: US7058197 B1

Patent Inventor(s): John Dennis McGuire, Randall Scott Pearson

Patent Assignee: Board Of Trustees Of The University Of Illinois

Patent Abstract: “An computer implemented apparatus and method are disclosed for defining areas of a field in which a crop or other vegetation is grown based on their selective ability to grow such vegetation through a growing season, or some shorter preselected time period. The method includes making a number of temporally separated measurements through air borne imaging of a field, registering the data to the geography of the field and each other, normalizing the data including converting the data to a vegetative index indicative to the presence of vegetation in the field, comparing the data to identify clusters of like value, and classifying the clusters and images to learn how the different field areas responded in growing vegetation through the season. With this method, the field may be segregated into a number of like areas called crop response zones which exhibit similar vegetative growth characteristics as an aid to a grower in his decision making regarding how to maximize yield in his field.”

Patent Claims:

1. “A method for processing multiple initial data sets of unclassified pixel values to enable their comparison on a relative basis, each of said data sets being representative of the vegetative growth in a field.”
2. “A method for scaling multiple data sets of pixel values to enable their comparison on a relative basis, each of said data sets being representative of the vegetative growth in a field.”
3. “A method for defining a plurality of crop response zones in a field used for growing vegetation, each of said crop response zones being characterized by having similar temporal growth characteristics.”
4. “A pre-programmed digital electronic device for defining a plurality of crop response zones in a field used for growing vegetation, each of said crop response zones being characterized by having similar temporal vegetative growth characteristics.”

5. “A pre-programmed digital electronic device for processing multiple initial data sets of unclassified pixel values to enable their comparison on a relative basis, each of said data sets being representative of the vegetative growth in a field.”
6. “A method for defining areas in a field which perform substantially alike in growing vegetation over the course of at least a portion of a growing season.”
7. “A method for processing multiple data sets of unclassified pixel values to enable their comparison on a relative basis, at least one of said data sets being representative of the agronomic variability in a field.”
8. “A method of scaling multiple data sets of unclassified pixel values to enable their comparison on a relative basis, at least one of said data sets being representative of the agronomic variability in a field.”
9. “A method for characterizing different areas of a field used for growing vegetation according to the presence of vegetation in said areas over time.”
10. “A method for characterizing different areas of a field used for growing vegetation according to the presence of vegetation in said areas over time.”
11. “A method for defining a plurality of crop response zones in a field used for growing vegetation, each of said crop response zones being characterized by having similar temporal vegetative growth characteristics.”
12. “A method for defining areas in a field which perform substantially alike in growing vegetation over the course of time.”

For more detailed information see reference (McGuire, et. al., 2006).

APPENDIX B: INSTRUMENTATION

500g – ICP 625B00 Accelerometer

Model Number 625B00	INDUSTRIAL ICP® ACCELEROMETER	Revision: A ECN #: 14824

Performance	ENGLISH	SI	
Sensitivity (±5 %)	10 mV/g	1.0 mV/(m/s²)	[2]
Measurement Range	±500 g	±4905 m/s²	
Frequency Range (±5 %)	30 to 390000 cpm	0.5 to 6500 Hz	[3]
Frequency Range (±10 %)	22 to 450000 cpm	0.37 to 7500 Hz	
Frequency Range (±3 dB)	12 to 630000 cpm	0.2 to 10500 Hz	
Resonant Frequency	1500 kcpm	25 kHz	[1]
Broadband Resolution (1 to 10000 Hz)	350 µg	3434 µm/s²	[1]
Non-Linearity	±1 %	±1 %	[4]
Transverse Sensitivity	≤5 %	≤5 %	
Environmental			
Overload Limit (Shock)	5000 g pk	49050 m/s² pk	
Temperature Range	-65 to +250 °F	-54 to +121 °C	
Temperature Response	See Graph	See Graph	
Enclosure Rating	IP68	IP68	
Electrical			
Settling Time (within 1% of bias)	≤8 sec	≤8 sec	
Discharge Time Constant	≥1.0 sec	≥1.0 sec	
Excitation Voltage	18 to 28 VDC	18 to 28 VDC	
Constant Current Excitation	2 to 20 mA	2 to 20 mA	
Output Impedance	<100 ohms	<100 ohms	
Output Bias Voltage	8 to 12 VDC	8 to 12 VDC	
Spectral Noise (10 Hz)	15 µg/√Hz	147 (µm/s²)/√Hz	[1]
Spectral Noise (100 Hz)	7 µg/√Hz	69 (µm/s²)/√Hz	[1]
Spectral Noise (1 kHz)	4 µg/√Hz	39 (µm/s²)/√Hz	[1]
Electrical Isolation (Case)	>10^8 ohms	>10^8 ohms	
Electrical Protection	RFI/ESD	RFI/ESD	
Physical			
Size (Diameter x Height)	1.38 in x 1.13 in	35.1 mm x 28.7 mm	
Weight	5.1 oz	145 gm	
Mounting	Through Hole	Through Hole	
Mounting Thread	1/4-28 Male	Not Applicable	[5]
Mounting Torque	2 to 5 ft-lb	2.7 to 6.8 N-m	
Sensing Element	Ceramic	Ceramic	
Sensing Geometry	Shear	Shear	
Housing Material	Stainless Steel	Stainless Steel	
Sealing	Welded Hermetic	Welded Hermetic	
Electrical Connector	2-Pin MIL-C-5015	2-Pin MIL-C-5015	
Electrical Connection Position	Side	Side	

Typical Sensitivity Deviation vs Temperature

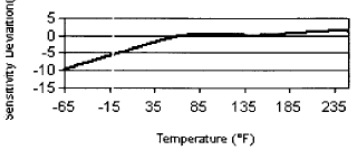

All specifications are at room temperature unless otherwise specified.
In the interest of constant product improvement, we reserve the right to change specifications without notice.
ICP® is a registered trademark of PCB Group, Inc.

OPTIONAL VERSIONS
Optional versions have identical specifications and accessories as listed for the standard model except where noted below. More than one option may be used.

LB - Low Bias Voltage		
Output Bias Voltage	6 to 8 VDC	6 to 8 VDC
Excitation Voltage	12 to 28 VDC	12 to 28 VDC
Measurement Range	±350 g	±3434 m/s²
M - Metric Mount		
Supplied Accessory : Model M081A73 Mounting Bolt M6 x 1.00 (1)		
TO - Temperature Output		
Temperature Output Range	+36 to +250 °F	+2 to +121 °C
Temperature Scale Factor	5.56 mV/°F + 32	+10 mV/°C
Electrical Connector	3-Pin	3-Pin
Electrical Connections (Pin A)	Acceleration Output	Acceleration Output
Electrical Connections (Pin B)	Ground	Ground
Electrical Connections (Pin C)	Temperature Output	Temperature Output

NOTES:
[1] Typical.
[2] Conversion Factor: 1g = 9.81 m/s².
[3] The high frequency tolerance is accurate within ±10% of the specified frequency.
[4] Zero-based, least-squares, straight line method.
[5] 1/4-28 has no equivalent in S.I. units.

SUPPLIED ACCESSORIES:
Model 081B45 Thermal Boot (1)
Model 081A73 Captive mounting bolt 1/4-28 x 1.34" (1)
Model ICS-1 NIST-traceable single-axis amplitude response calibration from 600 cpm (10 Hz) to upper 5% frequency

Entered: MK	Engineer: MK	Sales: BG	Approved: N.F	Spec Number:
Date: 11.1.02	Date: 11.1.02	Date: 11/5/02	Date: 11/4/02	16284

IMI SENSORS
A PCB PIEZOTRONICS DIV.
3425 Walden Avenue, Depew, NY 14043
Phone: 800-959-4464
Fax: 716-684-3823
E-Mail: imi@pcb.com

1000g – PCB 353B11 Accelerometer

Model Number	ICP® ACCELEROMETER	Revision: J
353B11		ECN #: 26810

Performance	ENGLISH	SI	
Sensitivity(± 10 %)	5 mV/g	0.51 mV/(m/s²)	
Measurement Range	± 1000 g pk	± 9810 m/s² pk	
Frequency Range(± 5 %)	1 to 10,000 Hz	1 to 10,000 Hz	
Frequency Range(± 10 %)	0.7 to 18,000 Hz	0.7 to 18,000 Hz	
Frequency Range(± 3 dB)	0.35 to 30,000 Hz	0.35 to 30,000 Hz	
Resonant Frequency	≥ 70 kHz	≥ 70 kHz	
Broadband Resolution(1 to 10,000 Hz)	0.01 g rms	0.1 m/s² rms	[1]
Non-Linearity	≤ 1 %	≤ 1 %	[2]
Transverse Sensitivity	≤ 5 %	≤ 5 %	[3]
Environmental			
Overload Limit(Shock)	± 10,000 g pk	± 98,100 m/s² pk	
Temperature Range(Operating)	-65 to +250 °F	-54 to +121 °C	
Temperature Response	See Graph	See Graph	[1]
Base Strain Sensitivity	≤ 0.005 g/με	≤ 0.05 (m/s²)/με	[1]
Electrical			
Excitation Voltage	18 to 30 VDC	18 to 30 VDC	
Constant Current Excitation	2 to 20 mA	2 to 20 mA	
Output Impedance	≤ 100 ohm	≤ 100 ohm	
Output Bias Voltage	8 to 12 VDC	8 to 12 VDC	
Discharge Time Constant	0.5 to 2.0 sec	0.5 to 2.0 sec	
Settling Time(within 10% of bias)	<5 sec	<5 sec	
Spectral Noise(1 Hz)	6400 µg/√Hz	62,784 (µm/s²)/√Hz	[1]
Spectral Noise(10 Hz)	1400 µg/√Hz	13,734 (µm/s²)/√Hz	[1]
Spectral Noise(100 Hz)	360 µg/√Hz	3532 (µm/s²)/√Hz	[1]
Spectral Noise(1 kHz)	128 µg/√Hz	1256 (µm/s²)/√Hz	[1]
Physical			
Sensing Element	Quartz	Quartz	
Sensing Geometry	Shear	Shear	
Housing Material	Titanium	Titanium	
Sealing	Hermetic	Hermetic	
Size (Hex x Height)	0.31 in x 0.43 in	7.9 mm x 10.9 mm	
Weight	0.07 oz	2.0 gm	[1]
Electrical Connector	5-44 Coaxial	5-44 Coaxial	
Electrical Connection Position	Side	Side	
Mounting Thread	5-40 Male	5-40 Male	
Mounting Torque	8 to 12 in-lb	90 to 135 N-cm	

CE [4]

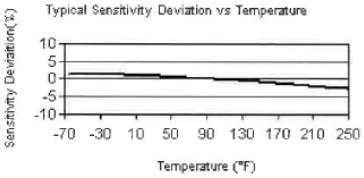

All specifications are at room temperature unless otherwise specified.
In the interest of constant product improvement, we reserve the right to change specifications without notice.

ICP® is a registered trademark of PCB Group, Inc.

OPTIONAL VERSIONS

Optional versions have identical specifications and accessories as listed for the standard model except where noted below. More than one option may be used.

A - Adhesive Mount [5]
Supplied Accessory : Model 080A90 Quick Bonding Gel (1)

B - Low bias electronics

Output Bias Voltage	4.5 to 7.5 VDC	4.5 to 7.5 VDC
Excitation Voltage	12 to 30 VDC	12 to 30 VDC
Constant Current Excitation	1 to 20 mA	1 to 20 mA
Measurement Range	± 600 g pk	± 5886 m/s² pk

J - Ground Isolated

Frequency Range(± 5 %)	1 to 8000 Hz	1 to 8000 Hz
Frequency Range(± 10 %)	0.7 to 15,000 Hz	0.7 to 15,000 Hz
Resonant Frequency	≥ 56 kHz	≥ 56 kHz
Electrical Isolation(Base)	≥ 10^8 ohm	≥ 10^8 ohm
Size - Hex x Height	0.37 in x 0.57 in	9.5 mm x 14.5 mm
Weight	0.11 oz	3.2 gm

M - Metric Mount

Mounting Thread	M3 x 0.50 Male	M3 x 0.50 Male

Supplied Accessory : Model M080A15 Adhesive Mounting Base (1) replaces Model 080A15

Q - Extended discharge time constant [6]

Frequency Range(± 5 %)	0.15 to 10,000 Hz	0.15 to 10,000 Hz
Frequency Range(± 10 %)	0.1 to 20,000 Hz	0.1 to 20,000 Hz
Discharge Time Constant	>5 sec	>5 sec
Settling Time(within 10% of bias)	<45 sec	<45 sec

Supplied Accessory : Model ACS-4 Single-axis, low frequency phase and amplitude response calibration. (1)

W - Water Resistant Cable

Electrical Connector	Sealed Integral Cable	Sealed Integral Cable
Electrical Connection Position	Side	Side

NOTES:
[1] Typical.
[2] Zero-based, least-squares, straight line method.
[3] Transverse sensitivity is typically ≤ 3%.
[4] See PCB Declaration of Conformance PS023 for details.
[5] Adhesive mounting base is not required. "Quick Bonding Gel" has maximum temperature range of 180 ° F (82°C).
[6] ACS-4 starts at 1 Hz for sensitivities <20 mV/g.

SUPPLIED ACCESSORIES:
Model 080A109 Petro Wax (1)
Model 080A15 Adhesive Mounting Base (1)
Model ACS-1 NIST traceable frequency response (10 Hz to upper 5% point). (1)

Entered: BLS	Engineer: BAM	Sales: WDC	Approved: EB	Spec Number:
Date: 7-10-07	Date: 7-2-07	Date: 7-2-07	Date: 7-5-07	353-2110-80

PCB PIEZOTRONICS
VIBRATION DIVISION
3425 Walden Avenue, Depew, NY 14043
Phone: 716-684-0001
Fax: 716-685-3886
E-Mail: vibration@pcb.com